Marius Skagen Elvestad
Remi André Andersen Fosse

Fatigue capacity of partially loaded areas for fiber reinforced concrete structures submerged in water

Master's thesis in Bygg og miljøteknikk
Supervisor: Jan Arve Øverli & Paola Mayorca
June 2019

Master's thesis

NTNU
Norwegian University of Science and Technology
Faculty of Engineering
Department of Structural Engineering

NTNU
Kunnskap for ei betre verd

DNV·GL

Marius Skagen Elvestad
Remi André Andersen Fosse

Fatigue capacity of partially loaded areas for fiber reinforced concrete structures submerged in water

Master's thesis in Bygg og miljøteknikk
Supervisor: Jan Arve Øverli & Paola Mayorca
June 2019

Norwegian University of Science and Technology
Faculty of Engineering
Department of Structural Engineering

NTNU
Kunnskap for ei betre verd

Department of Structural Engineering
Faculty of Engineering
NTNU- Norwegian University of Science and Technology

ACCESSIBILITY
OPEN

MASTER THESIS 2019

SUBJECT AREA:	DATE:	NO. OF PAGES:
Concrete structures	11.06.2019	75+21(Appendix)

TITLE:

Fatigue capacity of partially loaded areas for fiber reinforced concrete structures submerged in water.

Utmattingskapasitet til partielt belastede fiberarmerte betongkonstruksjoner nedsunket i vann.

BY:

Marius Skagen Elvestad and Remi André Andersen Fosse

SUMMARY:

Wind-turbines are subjected to large cyclic loads and will therefore suffer from problems related to fatigue. This thesis will therefore try to give further understanding of the behavior of foundations for wind-turbines subjected to fatigue loading. The thesis will analyze the effect of steel fiber reinforced concrete compared to a minimum reinforced cross-section and unreinforced cross-section. The analysis will be of foundations submerged in water.

Three different specimen types have been tested and analyzed for this thesis, with 3 specimens subjected to static loading and 3 specimens subjected to dynamic loading within each specimen type. Specimen type A represents the minimum reinforced cross-section. Specimen type B represents the unreinforced cross section has no reinforcement in the top of the specimen and specimen type C represents the steel fiber reinforced cross-section. The dynamic results show that the formula from DNV-OS-C502, with C_1=10 gives an accurate prediction of fatigue life for unreinforced concrete subjected to cyclic compressive forces submerged in water. Partially loaded areas with minimum reinforcement also gives a higher fatigue life than unreinforced concrete, with a suggested C_1-factor of 11.4 (± 0.65), and steel fiber reinforced concrete show almost identical results with a C_1- factor of 11.22 (± 1.02).

RESPONSIBLE TEACHER: Jan Arve Øverli

SUPERVISOR(S): Jan Arve Øverli and Paola Mayorca

CARRIED OUT AT: Department of Structural Engineering at NTNU, and at DNV GL

Preface and acknowledgements

This thesis is submitted for the master`s degree in Structural engineering at Norwegian University of Science and Technology (NTNU) in spring 2019. This report is made in cooperation with NTNU and DNV GL.

The main focus of this thesis is to analyze the effect of steel fiber reinforced concrete used in partially loaded areas subjected to fatigue loading. The analysis is made by use of specimens submerged in water. The report will compare the results with minimum reinforced and unreinforced specimens.

This thesis is divided into four main parts. The first part is a literature review giving an introduction to the theoretical background of partially loaded areas, fatigue and fiber reinforced concrete. The two following parts describes the test setup and the testing procedure. In the fourth and final part, both the static and dynamic results are presented, analyzed and discussed.

We would like to direct special thanks to our supervisor at NTNU Professor Jan Arve Øverli for all the help and guidance during this period. Our sincere thanks to staff engineer Steinar Seehus for all assistance provided in the lab at NTNU. We would also like to express our utmost gratitude to DNV GL and their wonderful staff at Høvik for their extended hospitality and the opportunity to conduct this study in collaboration with them. We would like to specifically thank Paola Mayorca and Ole Martin Hauge as our external supervisors at Høvik as their expertise and guidance have been instrumental for this thesis. We would also like to thank Knut Palme Hansen and Anette Hage Ripe for their invaluable help during the laboratory testing at DNV GL.

Abstract

Wind-turbines are subjected to large cyclic loads and will therefore suffer from problems related to fatigue. This thesis will try to give further understanding of the behavior of foundations for wind-turbines. The main scope of this thesis is to give further insight to the concrete capacity directly under the loaded area for these foundations subjected to fatigue loading. The thesis will analyze the effect of steel fiber reinforced concrete compared to a minimum reinforced cross-section and unreinforced cross-section. The analysis will be of foundations submerged in water.

This thesis could be considered an extension of the work previously done in collaboration between NTNU and DNV GL. This collaboration is the result of two theses, the first written by Furnes and Hauge in 2011 and the second in 2014 by Bognøy et.al. Furnes and Hauge looked at the validity of design code factors used to increase the concrete strength under partially loaded areas subjected to fatigue loading. In other words, their main focus was the role of splitting reinforcement in concrete under dynamic loading. Bognøy et.al. looked at how submerging the specimens in water would affect the validity of the same design code factors for partially loaded areas subjected to dynamic loading.

Three different specimen types have been tested and analyzed for this thesis, with 3 specimens subjected to static loading and 3 specimens subjected to dynamic loading within each specimen type. All test specimens are of dimensions 210x210x525mm (LxWxH) with a loaded surface of 70x210mm. Specimen type A representing the minimum reinforced cross-section contains two ø8mm in both horizontal directions with a cover of 40mm from the top of the specimen. Specimen type B representing the unreinforced cross section has no reinforcement in the top of the specimen and specimen type C representing steel fiber reinforced cross-section has no reinforcement in the top of the specimen, but the concrete mix contains 20kg/m^3 of steel fibers.

The unreinforced specimens show that the confinement effect of the partially loaded area combined with the boundary conditions for these specimens gives a 6% increase of the static capacity, though the standard deviation is fairly high (± 7%). The minimum reinforced specimens show a further increase to approximately 11% (± 4%), and the fiber reinforced specimen show a capacity 20% (± 5%) higher than the capacity of the loaded area.

As concluded by Bognøy et.al. the environmental effect of submerging the specimen in water significantly reduces the fatigue life of the specimens. However, few design codes take this into account. Results from this investigation show that the formula from DNV-OS-C502 given below, with C_1=10 gives an accurate prediction of fatigue life for unreinforced concrete subjected to cyclic compressive forces submerged in water.

$$logN = C_1 \frac{\left(1 - \frac{\sigma_{c.max}}{f_{rd}}\right)}{\left(1 - \frac{\sigma_{c.min}}{f_{rd}}\right)}$$

Partially loaded areas with minimum reinforcement gives a higher fatigue life than unreinforced concrete, with a suggested C_1 factor of 11.4 (± 0.65), and steel fiber reinforced concrete show almost identical results with a C_1 factor of 11.22 (± 1.02). This indicates that partially loaded areas with minimum cover reinforcement and partially loaded areas with steel fiber reinforced concrete give the same increase of fatigue life, though the steel fiber reinforced concrete gives a higher increase of static capacity.

Sammendrag

Vind-turbiner et utsatt for store sykliske laster og vil derfor ha problemer med utmatting. Denne avhandlingen vil prøve å gi en videre forståelse av vind-turbiners fundamenter. Hovedfokuset til denne avhandlingen er å gi en bedre innsikt på betongens kapasitet under last arealet når disse fundamentene blir utsatt for utmattingslaster. Denne avhandlingen vil analysere effekten av stål fiber armert betong sammenlignet med et minimums armert tverrsnitt og uarmert tverrsnitt. Analysen til være av fundamenter nedsunket i vann.

Denne avhandlingen kan sees på som en fortsettelse av tidligere arbeid gjort i samarbeid med NTNU og DNV GL. Denne fortsettelsen er et resultat av to avhandlinger, den første av Furnes og Hauge i 2011 and den andre i 2014 av Bogøy m.fl. Furnes og Hauge så på gyldighetsområdet til forskjellige dimensjonerings-faktorer brukt i diverse regelverk til å øke betongstyrken under partielt belastede flater utsatt for utmattingslaster. Med andre ord, deres hovedfokus var å studere rollen til spaltestrekkarmering i betong under dynamiske last. Mens Bognøy m.fl. så på hvordan nedsynking i vann ville påvirke gyldigheten til de samme dimensjoneringsfaktorene for partielt belastede flater utsatt for dynamiske laster.

I denne avhandlingen er 3 forskjellige typer prøvestykker blitt testet og analysert, med 3 prøvestykker utsatt for statisk last og 3 utsatt for dynamisk last innad i hver type. Alle prøvestykkene hadde dimensjoner 210x210x525mm (LxBxH) med et lastareal på 70x210mm. Prøvestykke type A representerer minimumsarmering med 2 stk. ø8mm i begge horisontale-retninger med en overdekning på 40mm fra toppen av prøvestykket. Prøvestykke type B, som representerer det uarmerte tverrsnittet, hadde ingen armering i toppen og prøvestykke type C hadde heller ingen armering i toppen men er utstøpt med fiberarmert betong. Disse prøvestykkene hadde en betongblanding som inneholdt 20kg/m^3 med stålfiber.

De uarmerte prøvestykkene viste at fastholdingseffekten av partielt belastede flater kombinert med randbetingelsene for disse prøvestykkene gir en 6% økning av statisk kapasitet, selv om standardavviket er relativt høyt (± 7%). Prøvestykkene med minimumsarmering viste en videre økning til 11% (± 4%), og de fiberarmerte prøvestykkene viste en kapasitet på 20% (± 5%) høyere enn kapasiteten til last arealet.

Som Bognøy m.fl. konkludere med vil miljøeffekten av nedsynking av prøvestykker i vann gi en betydelig reduksjon i utmattingskapasiteten til prøvestykkene. Allikevel, er det få regelverk som tar dette i betraktning. Resultatet av denne undersøkelsen viser at formelen til DNV-OS-C502, gitt under, med C_1=10, gir en presis beskrivelse av utmattingskapasiteten til uarmert betong nedsunket i vann utsatt for sykliske trykk laster.

$$logN = C_1 \frac{\left(1 - \frac{\sigma_{c.max}}{f_{rd}}\right)}{\left(1 - \frac{\sigma_{c.min}}{f_{rd}}\right)}$$

Partielt belastede flater med minimumsarmering gir en høyere utmattingskapasitet enn uarmert betong, med et foreslått C_1-faktor på 11.4 (± 0.65). I tillegg viste stålfiber armert betong nesten identiske resultater med en C_1-faktor på 11.22 (± 1.02). Dette indikerer at partielt belastede flater med minimumsarmering og partielt belastede flater med stål fiber gir samme økning av utmattingskapasiteten, selv om fiber armert betong gir en større økning av statisk kapasitet.

Table of Contents

Symbols and abbreviations

Latin upper-case letters:

A_c	Cross-section area of concrete.
A_f	Cross-section area of one steel fiber.
A_{sa}, A_{sb}	Reinforcement in the two perpendicular directions in a partially loaded specimen.
A_s	Cross-section area of reinforcement.
A_1	The loaded area at the top of a partially loaded specimen.
A_2	The maximum design distribution area of a partially loaded specimen with a similar shape as A_1.
C_1	Climate factor for structures subjected to dynamic loading according to Equation (26)
F_{Aco}	Capacity of loaded area of partially loaded concrete.
F_{Rk}	Tension force capacity of fiber reinforced concrete.
N	Number of resisting stress cycles until failure occurs.
N^*	Number of resisting stress cycles until failure occurs for $\Delta\sigma_{Rsk,N^*}$ according to Table 2.
$S_{cd.\ max}$	Maximum design compressive stress level for concrete.
$S_{cd.\ min}$	Minimum design compressive stress level for concrete.
$S_{td.\ max}$	Maximum design tension stress level for concrete.

Latin lower-case letters:

a_1, a_2	Dimension of the loaded area, dimension of the maximum distribution area of a partially loaded specimen.
b_1, b_2	Dimension of the loaded area, dimension of the maximum distribution area of a partially loaded specimen.
b	Width.
$f_{cd.fat}$	Design fatigue reference strength for concrete in compression.
f_{cd}	Design strength for concrete in compression.
$f_{ck.fat}$	Characteristic fatigue reference strength for concrete in compression.
$f_{ctd.fat}$	Design fatigue reference strength for concrete in tension.
$f_{ctk.0.05}$	5^{th} percentile of the tensile strength of concrete.
$f_{ftk.res.2,5.norm}$	Normalized characteristic residual tensile strength.
$f_{ftk.res.2,5}$	Characteristic residual tensile strength of concrete.
f_L	Stress at the limit of proportionality of the F-CMOD curve.

$f_{Rk.3}$	Residual flexural tensile strength with CMOD = 2,5mm.
f_{rd}	Compressive reference strength for the type of failure in question.
$f_{R.d}$	Residual flexural strength corresponding to CMOD.
f_{yk}	Characteristic yield stress for reinforcement.
h_{sp}	Distance between the notch tip and the top of the specimen.
h	Height.
l	Length.
n	Foreseen number of cycles during the required design service life, number of fibers.

Greek upper-case letters:

$\Delta\sigma_{Es}$	stress range under the frequent combination of loads.
$\Delta\sigma_{Rsk.n}$	Stress range relevant to n cycles.
$\Delta\sigma_{Rsk,N*}$	Stress range relevant to N* cycles.

Greek lower-case letters:

α_{struct}	Fiber orientation factor.
α	Averaging factor of concrete stress; Fiber orientation factor.
$\beta_{cc}(t)$	Coefficient compensating for the age of the concrete at the beginning of loading.
$\beta_{c.sus}(t, t_0)$	Coefficient compensating for high mean stresses during loading.
δ	Displacement.
$\gamma_{c.fat}$	Partial safety factor for concrete material properties under fatigue loading. $\gamma_{c.fat}$=1.5.
γ_{Ed}	Partial safety factor at the loading side.
$\gamma_{s,fat}$	Partial safety factor for steel under fatigue loading.
η_c	Averaging factor of concrete stress.
η_0	Capacity factor for calculation of theoretical residual tensile strength.
η	Cumulative damage ratio.
$\sigma_{fk,mid}$	Middle stress in all the fibers crossing a crack. This parameter is used for calculating a theoretical residual tensile strength.
$v_{f,norm}$	Nominal volume ratio of the fibers.
$v_{f,struct}$	Volume ratio of fibers in a part of a structure.
v_f	Volume ratio of the fibers.
$\sigma_{c.max}$	Maximum compressive stress in concrete in MPa.
$\sigma_{c.min}$	Minimum compressive stress in concrete in MPa.
$\sigma_{ct.max}$	Maximum tension stress in concrete in MPa.

σ_{c1}	Minimum absolute value of the compressive stress within a distance of 300 mm from the surface.
σ_{c2}	Maximum absolute value of the compressive stress within a distance of 300 mm from the surface.
φ	Diameter for a reinforcing bar.

Abbreviations:

CEB	Comite Euro-International du Beton
CMOD	Crack mouth opening
Fib	Federation for Structural Concrete
FRC	Fiber reinforced concrete
LVDT	Lateral variable displacement transformer
SFRC	Steel fiber reinforced concrete
SLS	Serviceability limit state
ULS	Ultimate limit state

1 Introduction

1.1 General

As the worlds global economy keeps growing, the demand for energy rapidly increases. The increased focus on environmental effects has dictated a shift away from fossil dependent energy sources towards renewable energy (Leung & Yang, 2011). To minimize the global climate changes, production of renewable energy is the future. Therefor the development of wind as an energy source is already playing an important role in the future. From the first wind turbine to generate electricity in 1887 up until today, wind turbines have come a long way with respect to both performance and size, as shown in Figure 1.

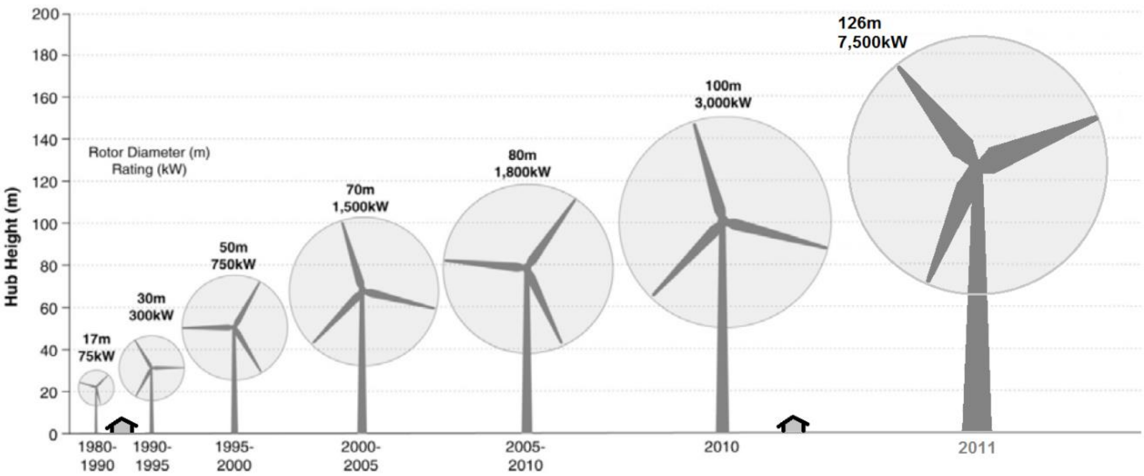

Figure 1: Development of wind turbines size and nominal capacity from 1980-2005. (Wikipedia, 2016)

With the increased size of wind-turbines the forces and stresses will increase substantially as well. When the wind-turbine are subjected to wind forces, large aerodynamic loadings will occur and have potential to cause complex dynamic vibrations which may lead to resonance. A consequence of this is that the foundations of the wind-turbines are subjected to large cyclic loading and may therefore suffer from problems related to fatigue.

Design of the foundations varies a lot depending on geotechnical conditions and design requirements. However, a commonly used foundation design is a circular spread footing as shown in Figure 2 . This thesis will try to give further insight to the capacity under the loaded area for these foundations subjected to fatigue loading. For further understanding of the foundation's behavior, it is proposed the following simplification: Since the foundation is circular with the load subjected over a thin circular area, one can simplify this by isolating a small piece of the foundation and simulate its behavior. It is assessed that the boundary conditions are fixed in the loading direction, preventing axial deformation. The boundary condition in the radial direction, aka perpendicular to the loading direction, will be assumed free.

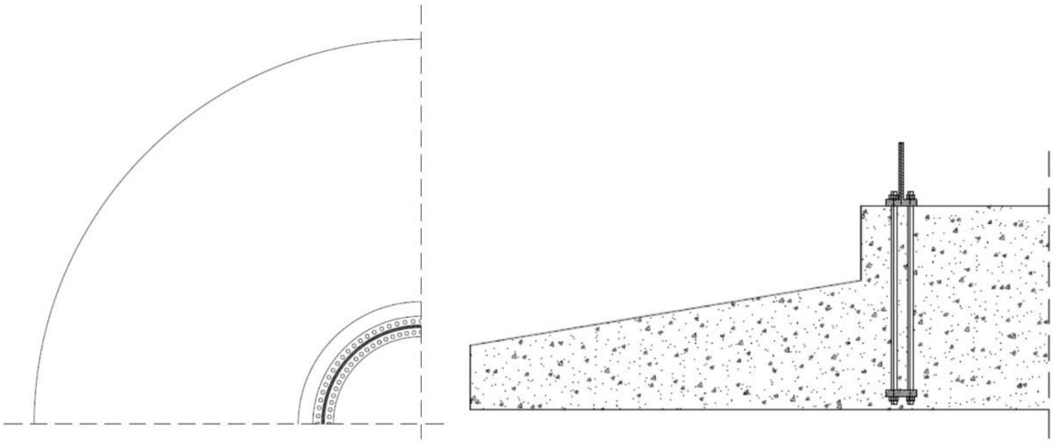

Figure 2: Circular spread footing foundation for a wind turbine.

The main scope of this thesis is to analyze the effect of steel fiber in the proposed simplification compared to a minimum reinforcement and no reinforcement. A total of 18 tests has been conducted, where the test specimens were created in accordance with the simplification of an isolated piece form the foundation and the deformation in loading direction is prevented by threaded bars cast into the specimens as seen in Figure 3. The size of the specimens used in this thesis is 210x210x525mm (LxWxH). In the investigation there are three groups of specimens with six specimens for each group. In each group half of the specimens are tested with static and half with dynamic loading.

Figure 3: Test specimen as a result of the proposed simplifications and boundary conditions.

1.2 Limitations of the investigation

The first limitation in this project is related to number of tests. There are in total 18 specimens which are divided in 3 groups where each group should be tested for both static and dynamic loading. This gives a total of 3 specimens for each variable tested. Usually experimental results will vary a lot, and such a low number of tests will therefore not give a reliable and accurate result. Ideally a larger number of tests should be done to get more reliable results, but because of limited time the number of tests had to be reduced.

Another limiting factor for this thesis is the use of normal concrete. High strength concrete is normally used in foundations of wind-turbines. Unfortunately, using high strength concrete for this project is not possible. The hydraulic jack where the tests are to be performed have a limited capacity which means that the compressive cube strength of the concrete has to be kept below 50 MPa.

Due to the simplifications made regarding a small isolated specimen with the given boundary conditions there are also some limitations of the results. These limitations are related to the uncertainty of the results being applicative to reality with regard to simplifications and scale factor.

1.3 Previous work

This thesis could be considered an extension of two earlier projects from 2011 and 2014. In 2011 Furnes and Hauge did a similar thesis, also in collaboration with the Norwegian University of Science and Technology (NTNU) and DNV GL. In their thesis "*Fatigue capacity of partially loaded areas in concrete structures"* they looked at the validity of factors used to increase the concrete strength under partially loaded areas when a structure is subjected to fatigue loading. Their main focus was the factors used in Bulletin 43 from fib regarding splitting reinforcement in concrete (Furnes & Hauge, 2011). Furnes and Hauge tested 6 specimens subjected to static load where half included splitting reinforcement and 6 specimens subjected to dynamic loading where all included splitting reinforcement. Their main conclusion was that the indicated factors in Bulletin 43 and NS3473 are adequate for design of partially loaded areas subjected to fatigue.

In 2014 Bognøy, Mo and Vee also did a similar thesis in collaboration with NTNU and DNV GL named "*Fatigue Capacity of partially loaded Areas in Concrete Structures submerged in Water"*. In their thesis they looked at how submerging the specimens in water would affect the validity of factors used to increase the concrete strength under partially loaded areas for dynamically loaded concrete. Their main focus was the factors for partially loaded areas from NS-EN 1992-1-1 and the influence of fatigue life according to DNV-OS-C502 (Bognøy, et al., 2014). In their thesis they tested a total of 18 specimens all submerged in water where half of the specimens include splitting reinforcement. Of the 18 specimens 6 were subjected to static loading and 12 subjected to dynamic loading. Their main conclusions are that "The proposed partial amplification factor for fatigue of 1,3, is of appropriate scale". Their findings also show that for fatigue life according to DNV-OS-C502 the C_1 factor is appropriate for unreinforced concrete subjected to partially loaded areas and concrete with sufficient splitting reinforcement will give an increase in fatigue life.

2 Literature review

2.1 Fatigue

2.1.1 Fatigue in general

Fatigue is a process of material weakening over time caused by cyclic loading (Per.Kr.Larsen, 2010). This material weakening is due to the fact that every material contains microscopic cracks or defects which over repeated cyclic loading will slowly weaken the material. In general, the whole process of fatigue failure can be divided into three stages; crack initiation, crack propagation and final rupture.

Crack initiation:

This is the stage where microcracks occur and slowly expands and coalesce into macro cracks. No materials are without defects. Concrete for instance have lots of defects from creep and shrinkage, while macroscopic crystalline materials such as steel are more homogeneous and have fewer defects (Almar-Næss, 2009). The exact nature of microcrack propagation and coalescence varies for different materials and is not always understood to the full extent.

Crack propagation:

With the formation of macrocracks these cracks will gradually change direction and grow perpendicular to the tensile stresses. This stage is often the most readily identifiable of the fatigue process. As shown in Figure 4, these cracks will lead to local stress concentrations around the crack tip. The stress concentrations may exceed the yield stress even if the global stresses are way below yielding. If the material over time is subjected to cyclic loads, the cracks will propagate, reducing the cross-sectional area and weakening the structure.

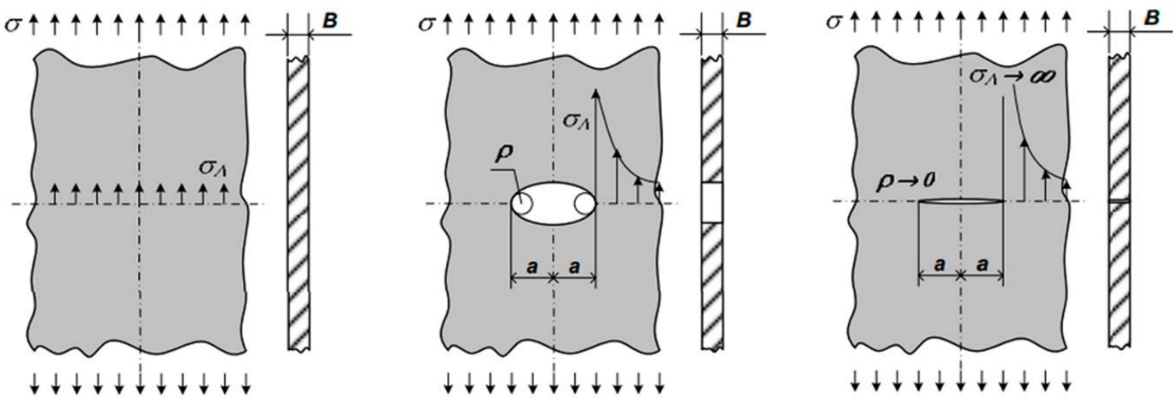

Figure 4: Stress-concentrations in thin plates with no disturbance (left), elliptical hole(middle) and crack(right) (Bratfos, u.d.).

Final rupture:

When the remaining cross-section is too small, the global stresses will exceed the yield stress, and fracture occurs in the material. This stage of fatigue fracture is called the Final rupture and dictates the collapse of the structural element.

2.1.2 Fatigue in concrete

Because concrete is a non-isotropic material its behavior during fatigue loading is significantly different from isotropic materials like steel and aluminum. In his study "*Fatigue of concrete by constant and variable amplitude loading"* Jan Ove Holmen observed that the strain development in concrete throughout the fatigue lifetime could be described by a nonlinear phase at the start and end with a linear phase in-between (Holmen, 1979).

The inhomogeneous nature of concrete makes it harder to precisely predict the main causes to the development of crack initiation and crack propagation in fatigue. Murdock and Kesler proposed a hypothesis where they stated that progressive deterioration of the bond between the binding matrix and the aggregate, as seen in Figure 5, may be the main attribution to crack initiation in concrete (Murdock & Kesler, 1960). These bond cracks are a result of different stress-strain behavior of the aggregate and cement matrix. During loading, thermal expansion, creep and shrinkage, the two materials deform differently causing excessive shear and tension forces between the aggregates and cement matrix.

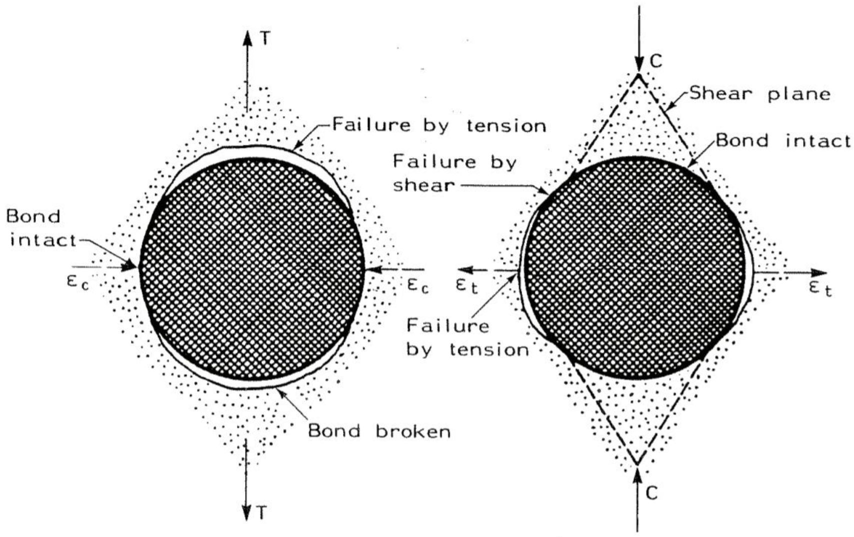

Figure 5: Local stresses around aggregate particle under tensile and compressive loading (Petkovic, 1991)

Holmen released a study in 1979 where he found that in addition to what was stated by Murdock and Kesler, there was also development of microcracs in the cement matrix itself (Holmen, 1979). Under fatigue loading these microcracs will grow until the formation of microcracs coaless in a localized narow zone, creating a dominant macrocrack that will propagate until fatigue failure.

There are many factors that influence the crack initiation and propagation rate changing the fatigue life of the structure. Some of these factors has been studied extensively and are well understood while others are not fully understood yet. Important factors that needs to be taken into account when accessing fatigue life are as follows:

<u>Water/cement ratio:</u> Different cement types and water/cement ratios in the concrete lead to different compressive strengths. Higher compressive strength will also give higher fatigue life for a given load. However, as shown by Comite Euro-International du Beton (CEB) in their publish *Fatigue of concrete structures,* the increase in fatigue strength in relation to the compressive strength is negligible (CEB, 1988).

<u>Moisture content:</u> There have been conducted many experiments regarding the effect of moisture content in concrete under fatigue loading. Van Leeuwen and Siemes amongst many others support the fact that high moisture content in concrete leads to a significant reduction in fatigue life (Van_Leeuwen & Siemes, 1979). In their study *Effects of moisture changes on flexural and fatigue strength of concrete,* Galloway *et al.* came to the conclusion that the gradient of humidity is more important than the percentage of humidity, i.e. if the concrete is in a drying phase or saturation phase (Galloway, et al., 1979).

<u>Extreme cold:</u> The mechanical properties of concrete are affected by the change in temperature. Though there is little to no change in fatigue strength for concrete when subjected to high temperatures, a study done by Ohlsson et al. shows that cold temperatures however have an effect on fatigue strength (Ohlsson, et al., 1990). In their study they find that the fracture energy significantly increases when the temperature is lowered from 20^{o}C to -35^{o}C, giving a higher fatigue strength. It is theorized that this is due to ice crystals in microcracks and pores contributing with a redistribution of stresses in the crack tip.

<u>Different load forms:</u> Most of the naturally occurring cyclic loads, such as wind and wave loads, resemble a sinusoidal load. Because of this, experimental testing in fatigue is therefore most commonly done with sinusoidal loading. However, Tepfers *et al.* have shown that the shape of the cyclic load may significantly influence the fatigue life (Tepfers, et al., 1973). In their study they looked at the fatigue life of prisms subjected to sinusoidal, sawtooth and rectangular loads as illustrated in Figure 6. The result indicates that fatigue damage for each cycle is larger when the time under high stress is larger.

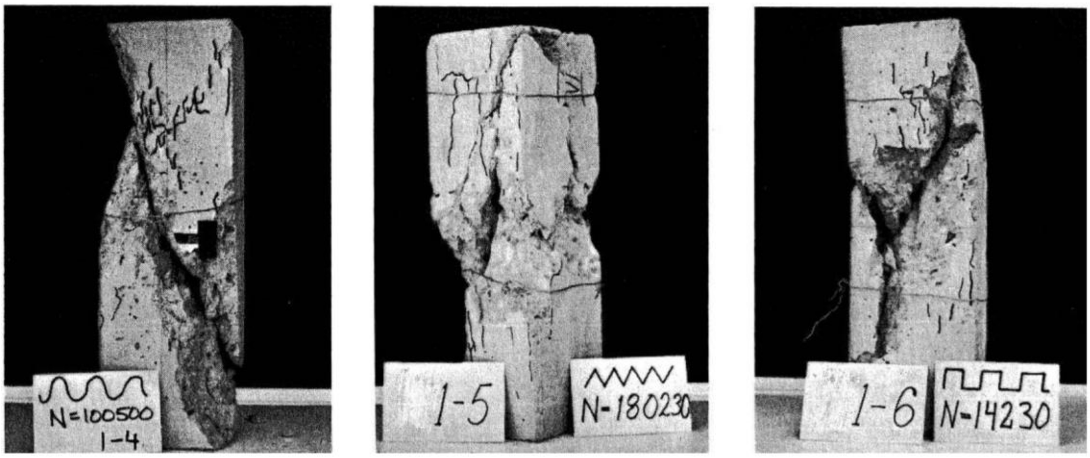

Figure 6: Test prisms subjected to different load types (Tepfers, et al., 1973)

<u>Rest period:</u> According to Hilsdorf & Kesler periods without loading or with low stress level in between the cyclic loading will give an increase in fatigue life (Hilsdorf & Kesler, 1966). In their study they found that rest periods up to 5 min. will prolong the fatigue life, while longer rest periods does not have an additional effect. Petkovic provides the insight that the effect of the rest period is dependent on when in the loading history it occurs and the stress level due to the cyclic load (Petkovic, 1991).

2.1.3 SN-curve and Miners Hypothesis

When talking about fatigue life, it is referring to the number of cycles of a specific stress range the material can resist before failure (Per.Kr.Larsen, 2010). For verification of the structure, this means that the number of load cycles n of a specific stress range subjected to the material must be less or equal to N. It is important to note that even though there are many different types of cyclic loads, for fatigue they are most often described by a sinusoidal waves like the one shown in Figure 7. For cyclic loads it is not just the maximum load stress σ_{max} that is of importance for the design life. Load factors such as the minimum load stress σ_{min}, the stress range $\Delta\sigma$ and the stress amplitude σ_a, which are defined in Figure 7, are also important factors in assessing fatigue life.

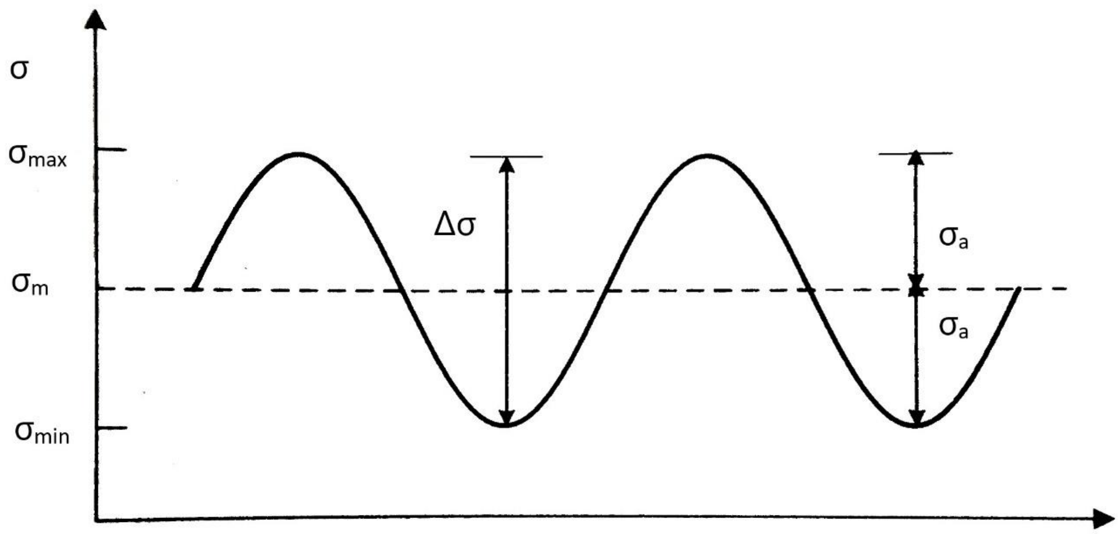

Figure 7: Typical periodical load (Per.Kr.Larsen, 2010).

The first experiments of fatigue as a fracture mechanism were done by August Wöhler around 1860 by studying railroad axels subjecting to repeated loads (Per.Kr.Larsen, 2010). He discovered that the relation between the stress amplitude S (also denoted σ_a) and the number of cycles to failure N could be described with a linear curve when using logarithmic scales as shown in Figure 8. These so-called SN-curves, or Wöhler-curves, have since been the most common way for presenting empirical results of fatigue life, where stress amplitude S is given as:

$$S = \sigma_a = \frac{\sigma_{max} - \sigma_{min}}{2} \tag{1}$$

where:

σ_a is the stress amplitude.
σ_{max} is the maximum stress.
σ_{min} is the minimum stress.

Some materials such as steel have an endurance limit, which is the level of stress where fatigue will not occur even after an infinite number of cycles. This can be seen in Figure 8, where the curve converges as the number of cycles goes towards infinity. In the logarithmic scale the endurance limit is indicated by a constant line, and if the applied stress is below the endurance limit of the given material, the structure is said to have an infinite fatigue life.

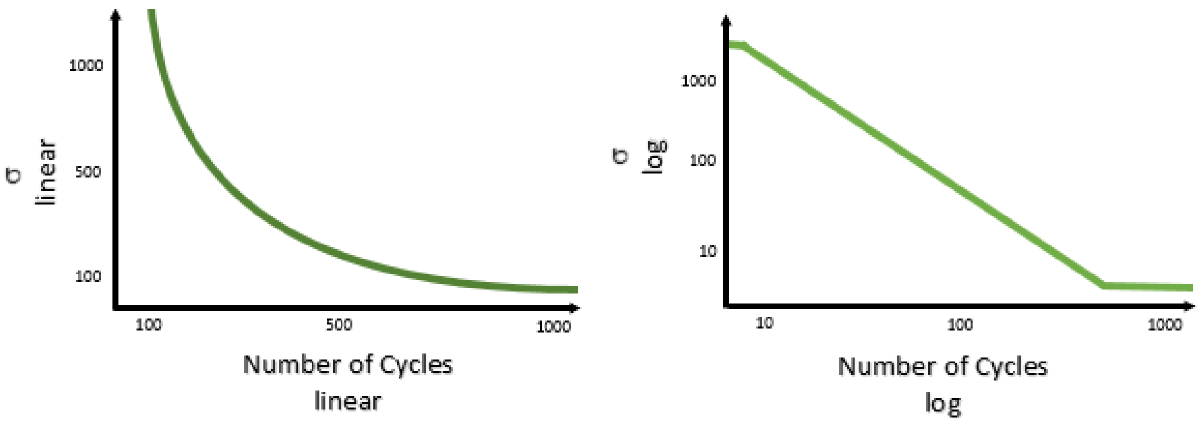

Figure 8: SN-curves plotted with linear (left) and logarithmic scales(right) (Hiatt, 2016)

The occurrence of cyclic loading is often caused by wind, water or earthquake. In such cases the load is seldom a sinusoidal wave with one stress amplitude as depicted in Figure 7. These loads will often be messy wave loads more closely resembling a stochastic process. Such loads can be simplified by decomposing it into several sinusoidal loads with different stress amplitudes and frequencies. With this simplification the material will be subjected to several different loads, and with different load frequencies.

Even though it was popularized by M. A. Miner in 1945, A. Palmgren proposed the hypothesis already in 1924 that for a given load *i* the stress-cycles n_i subjected to the material will give a contribution to the total utilization of the structure. This would implicate that the structure will fail if the following expression is fulfilled:

$$\sum_{i=1}^{k} \frac{n_i}{N_i} = \eta \qquad (2)$$

where:

k	is the number of stress contributions.
n_i	is the numbers of each stress contribution.
N_i	is the number of contributions to failure for n_i.

Here, η is the total utilization of the structure which usually is a constant is assumed to be 1. Experiments on steel elements with stochastic stress spectrums shows large spread and values from 0,3< η < 3,0 (Per.Kr.Larsen, 2010). The precision of the hypothesis depends for instance on the form the stress spectrum and of the sequence of exchange between big and small stress widths. The calculated lifetime also depends much on the choice of material factor.

2.1.4 Calculating fatigue life of concrete

There are several different formulas for estimating the fatigue life of concrete. One widely accepted formula is the Aas-Jakobsen´s formula (Torrenti, et al., 2013). Aas-Jakobsen and Lenshow showed, through a statistical study on a large number of test results, that the fatigue strength of plain concrete is linear to the loading ratio *R*, giving the following formulation for fatigue life:

$$\frac{\sigma_{max}}{f_c} = 1 - \beta(1 - R)LogN \tag{3}$$

where:

f_c is the short-term compressive resistance under static loading.
β is the material constant. Usually set to β = 0.0685.

and the loading ratio *R* is defined as:

$$R = \frac{\sigma_{min}}{\sigma_{max}} \tag{4}$$

Another known equation was proposed by Jan Ove Holmen in his study "*Fatigue of Concrete by constant and variable amplitude*" in 1979. The study consisted of 462 cylindrical specimens tested with static and dynamic loading, leading to the following equation:

$$logN = (1 - S_{max})\,(12 + 16\,S_{min} + 8\,{S_{min}}^2) \tag{5}$$

where:

$$S_{max} = \frac{\sigma_{max}}{f_{ck}} \quad \text{and} \quad S_{min} = \frac{\sigma_{min}}{f_{ck}}$$

When conducting a verification of fatigue life, it is common to use established standards. This thesis will take a further look at the three well known standards Eurocode 2, Model code 2010 and DNV-OS-C502 in regards of calculating fatigue life for concrete.

2.1.4.1 Eurocode 2

Eurocodes are developed by the European Committee for Standardization and specify how structural design should be performed within the European Union. Eurocode 2 part 1-1, noted EN-1992-1-1, gives the general calculation rules for concrete structures. Fatigue verification is assessed in EN-1992-1-1 section 6.8, where it is noted that verification shall be performed separately for concrete and steel. In ultimate limit state (ULS) the Eurocode gives two methods for verification of concrete for fatigue life. These calculations are based on a verification that the construction can withstand a high cycle fatigue load of 10^6 cycles rather than calculating the fatigue life for the given strains. Because of this validity check Eurocode 2 can't be used for calculating exact fatigue life for given stresses and will therefore not be used for fatigue calculations in this thesis.

2.1.4.2 Fib Model Code 2010

Model Code 2010 was created by the International Federation for Structural Concrete (Fib) with the objective to serve as a basis for the development of future codes and standards. It is claimed by Fib that Model Code 2010 is one of the most comprehensive codes on concrete structures (fib, 2013). The Model Code 2010 does however not cover low cycle fatigue with cycles under 10^4, and it does not take the structure's climate into account. However, in the standard DNVGL-ST-0126 section 5.6.3.8 they compensate for structures in water by raising the number of cycles N_i to the power of 0.8 (i.e. $N_i^{0.8}$).

Verification of fatigue design is done according to four different levels of simplifications, starting at level I which is the most simplified, up to level IV which is the least simplified method. Level IV utilizes the Palmgren–Miner summation (see Equation (2)) on top of the calculations in level III. This thesis will therefore be using the verification method associated with level III. This procedure uses a partial safety factor γ_{Ed} at the loading side as an alternative to a partial safety factor γ_{Rd} at the resistance side. The partial safety factor should be assumed $\gamma_{Ed} = 1.1$, however it can be set to $\gamma_{Ed} = 1.0$ if the stress analysis is sufficiently conservative or accurate. As in Eurocode 2, Model Code 2010 section 7.4.1 also preforms verification for concrete and steel separately.

Concrete

Fatigue life of concrete varies with the subjected loading. Model code takes this into account by differentiating between compression, compression – tension, tension-compression and tension:

Compression: In pure compression the number of cycles to failure N can be determined as:

$$N = N_1 \ if \ logN_1 \leq 8 \tag{6}$$

$$N = N_2 \ if \ logN_1 > 8 \tag{7}$$

where N_1 and N_2 can be calculated from Equation (8) and (9) respectively:

$$logN_1 = \frac{8}{Y-1}\left(S_{cd,max} - 1\right) \tag{8}$$

$$logN_2 = 8 + \frac{8\ln(10)}{Y-1}\left(Y - S_{cd,min}\right)\log\left(\frac{S_{cd,max} - S_{cd,min}}{Y - S_{cd,min}}\right) \tag{9}$$

with:

$$Y = \frac{0.45 + 1.8\, S_{cd.min}}{1 + 1.8\, S_{cd.min} - 0.3\, S_{cd.min}^2} \tag{10}$$

and the minimum and maximum compressive stress levels $S_{cd.min}$ and $S_{cd.max}$ defined as:

$$S_{cd.min} = \frac{\gamma_{Ed}\, \sigma_{c.min}\, \eta_c}{f_{cd.fat}} \tag{11}$$

$$S_{cd.max} = \frac{\gamma_{Ed}\, \sigma_{c.max}\, \eta_c}{f_{cd.fat}} \tag{12}$$

where:

γ_{Ed} is a partial safety factor at the loading side, often assumed = 1.1.
$\sigma_{c.min}$ is the minimum compressive stress.
$\sigma_{c.max}$ is the maximum compressive stress.
$f_{cd.fat}$ is the design fatigue reference strength for concrete in compression given by Equation (14).
η_c is the averaging factor of concrete stress.

For a cracked cross-section with varying stresses as seen in Figure 9, it is possible to take into account the stress gradient. This is done by utilizing the averaging factor η_c for stress in the compression zone as calculated in Equation (13). σ_{c1} and σ_{c2} are respectively the minimum and maximum absolute value of the compressive stress within a distance of 300 mm from the surface.

$$\eta_c = \frac{1}{1.5 - 0.5\, \frac{|\sigma_{c1}|}{|\sigma_{c2}|}} \tag{13}$$

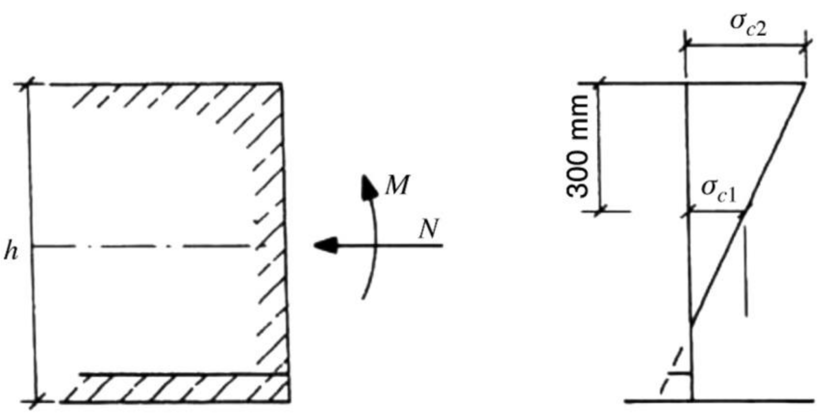

Figure 9: Definition of stress σ_{c1} and σ_{c2} in the compression zone of a cracked section.

The design fatigue reference strength for concrete in compression $f_{cd.fat}$ is defined as:

$$f_{cd.fat} = \frac{f_{ck.fat}}{\gamma_c} \tag{14}$$

With the partial safety factor for concrete being γ_c = 1.5, and the characteristic fatigue reference strength $f_{ck.fat}$ may be estimated as:

$$f_{ck.fat} = \beta_{cc}(t)\,\beta_{c.sus}(t,t_0)\,f_{ck}\left(1 - \frac{f_{ck}}{400}\right) \tag{15}$$

$\beta_{c.sus}(t,t_0)$ is a coefficient which takes into account the effect of high mean stresses during loading. For fatigue loading Model Code 2010 suggests its value as 0.85. In most practical cases the actual frequencies of loading are significantly lower than those applied in experiments, which is the reason $\beta_{c.sus}(t,t_0)$ = 0.85 has been chosen. $\beta_{cc}(t)$ is a coefficient taking into account the age of the concrete at the beginning of loading, and is given as:

$$\beta_{cc}(t) = exp\left\{s\left[1 - \left(\frac{28}{t}\right)^{0.5}\right]\right\} \tag{16}$$

where

t is the concrete age in days.

s is a factor depending on the strength class of the cement and is given in Table 1.

f_{cm} [MPa]	Strength class of cement	s
≤ 60	32.5 N	0.38
	32.5 R, 42.5 N	0.25
	42.5 R, 52.5 N, 52.5 R	0.20
> 60	all classes	0.20

Table 1: Coefficients for different types of cement

<u>Compression – tension:</u> Compression – tension is described by Model Code 2010 as a stress state where the maximum tension stress $\sigma_{ct.max} \leq 0.026 \cdot |\sigma_{c.max}|$ where $|\sigma_{c.max}|$ is the absolute value of the compressive strength. In compression – tension the number of cycles to failure N is given as:

$$logN = 9(1 - S_{cd.max}) \tag{17}$$

<u>Tension and tension – compression:</u> Tension-compression is the stress state where $\sigma_{ct.max} > 0.026|\sigma_{c.max}|$. The number of cycles until failure N for pure tension and tension-compression is calculated as:

$$logN = 12(1 - S_{td.max}) \tag{18}$$

where the maximum tensile stress level $S_{td.max}$ is given as:

$$S_{td.max} = \frac{\gamma_{Ed}\,\sigma_{ct.max}}{f_{ctd.fat}} \tag{19}$$

Here $f_{ctd.fat}$ is the design fatigue reference tensile strength of the concrete given by:

$$f_{ctd.fat} = \frac{f_{ctk,0.05}}{\gamma_{c.fat}} \tag{20}$$

where

$\gamma_{c.fat}$ is the partial safety factor for concrete under fatigue loading given $\gamma_{c.fat}$=1.5.
$f_{ctk,0.05}$ is the 5th percentile of the tensile strength of concrete.

Steel

When calculating the fatigue life of reinforcement steel Model Code 2010 gives the characteristic fatigue strength function $(\Delta\sigma_{Rsk})^m \cdot N = const$ in the form of the generalized S-N curve shown in Figure 10. The generalized S-N curve shows a piecewise function dependent on the parameters k_i and the stress range $\Delta\sigma_{Rsk}$ at N^* number of cycles, which can be found in Table 2.

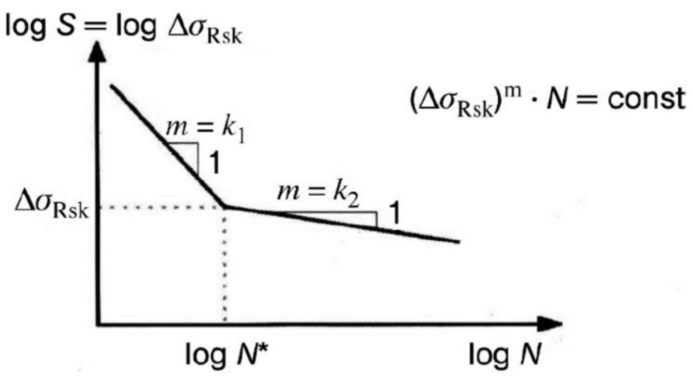

Figure 10: Shape of the characteristic fatigue strength curves (S–N curves) for steel.

The values given in Table 2 for φ > 16 mm represent the S–N curve of a 40mm bar. For diameters between 16 and 40 mm it is recommended to interpolate between the values for < 16 mm and for the 40 mm bar. For the values of bent bars with D < 25 φ one should use the values for straight bars multiplied by a reduction factor x depending on the ratio of the diameter of mandrel D and bar diameter ϕ, where $x = 0.35 + \frac{0.026D}{\phi}$.

	N*	Stress exponent		Δσ_Rsk (MPa)	
		k_1	k_2	at N* cycles	at 10^8 cycles
Straight and bent bars D ≥ 25 ϕ					
ϕ ≤ 16 mm	10^6	5	9	210	125
ϕ > 16 mm	10^6	5	9	160	95
Bent bars D < 25 ϕ	10^6	5	9	–	–
Welded bars including tack	10^7	3	5	50	30
Marine environment	10^7	3	5	65	40

Table 2: Parameters of S–N curves for reinforcing steel (embedded in concrete)

Using the generalized S-N curve with the correct parameters the fatigue requirement will be met if the calculated maximum acting stress range $\Delta\sigma_{Es}$, satisfies the condition:

$$\gamma_{Ed}\ \Delta\sigma_{Es} \leq \frac{\Delta\sigma_{Rsk.n}}{\gamma_{s.fat}} \tag{21}$$

where

$\Delta\sigma_{Rsk.n}$ is the stress range relevant to *n* cycles.
$\gamma_{s.fat}$ is the partial safety factor for steel given $\gamma_{s.fat}$ =1.15.

By using the requirement of Equation (21) combined with the S-N curve given from Figure 10 it is possible to derive a function for the number of cycles until failure *N* for the steel reinforcement given in the following equations where *N** is found in Table 2:

$$N = N_1 \ \ if \ \ \Delta\sigma_{Es} > \Delta\sigma_{Rsk,N^*} \tag{22}$$

$$N = N_2 \ \ \text{if} \ \ \Delta\sigma_{Es} < \Delta\sigma_{Rsk,N^*} \tag{23}$$

where

$$logN_1 = logN^* - k\ log\left(\frac{\sigma_{Es}\ \gamma_{Ed}\ \gamma_{s.fat}}{\sigma_{Rsk,N^*}}\right) \tag{24}$$

$$logN_2 = k\ log\left(\frac{\sigma_{Rsk,N^*}}{\sigma_{Es}\ \gamma_{Ed}\ \gamma_{s.fat}}\right) - logN^* \tag{25}$$

2.1.4.3 DNV-OS-C502

DNV GL is one of the world's largest accredited certification bodies and classification societies, providing classification and technical assurance to the maritime, power, renewable and oil & gas industries among other things. Their standard for offshore concrete structures DNV-OS-C502 provides a simple verification compared to Model Code, but also taking climate into account.

Verification of fatigue design is done according to section M. As in Model Code 2010, DNV-OS-C502 also utilizes the Palmgren-Miner summation. However, instead of the cumulative damage ratio η = 1, DNV-OS-C502 uses η = 0.33 for structural parts with no access for inspection and repair, η = 0.5 for below or in the splash zone and η = 1 for structural parts above the splash zone.

As in Eurocode 2 and Model Code 2010, DNV-OS-C502 also preforms verification for concrete and steel separately.

Concrete

For verification of concrete the number of cycles to failure *N* can be determined as:

$$logN = C_1 \frac{\left(1 - \frac{\sigma_{c.max}}{f_{rd}}\right)}{\left(1 - \frac{\sigma_{c.min}}{f_{rd}}\right)} \tag{26}$$

where the factor C_1 shall be taken as:

- 12.0 for structures in air.
- 10.0 for structures in water having stress variation in the compression-compression range.
- 8.0 for structures in water having stress variation in the compression-tension range.

$\sigma_{c.max}$ is the numerically largest compressive stress.
$\sigma_{c.min}$ is the numerically smallest compressive stress. If $\sigma_{c.min}$ is in tension $\sigma_{c.min}$ = 0.
f_{rd} is the reference compressive strength for the type of failure in question.

For concrete subjected to compression, f_{rd} should be equal f_{cd}. For a cracked cross-section with varying stresses, it is possible to calculate stresses with a linear stress distribution in the compression zone as seen in Figure 9. As in Model Code 2010, one should take into account the stress gradient by utilizing an averaging factor α giving a reference compressive strength $f_{rd} = \alpha \cdot f_{cd}$, where:

$$\alpha = 1.3 - 0.3 \frac{|\sigma_{c1}|}{|\sigma_{c2}|} \tag{27}$$

The design life may be increased further by multiplying the value of log *N* by the factor C_2 from Equation (29) if the calculated design life log *N* is larger than *X* given by:

$$X = \frac{C_1}{(1 - \left(\frac{\sigma_{c.min}}{f_{rd}}\right) + 0.1\, C_1)} \tag{28}$$

$$C_2 = 1 + 0.2\,(logN - X) > 1.0 \tag{29}$$

<u>Steel</u>

For reinforcement steel the maximum stress $\sigma_{s.max}$ in the reinforcement subjected to fatigue loading should always be less than the characteristic strength of reinforcement f_{sk} divided by the material coefficient for reinforcement γ_s. For verification of reinforcement steel under fatigue loading the number of cycles to failure can be calculated as:

$$logN = C_3 - C_4 \log(\Delta\sigma_s) \tag{30}$$

where $\Delta\sigma_s$ is the stress range of the reinforcement given by:

$$\Delta\sigma_s = \sigma_{s.max} - \sigma_{s.min} \tag{31}$$

And the factors dependent on reinforcement type bending radius and corrosive environment, C_3 and C_4 can be found in Table 3.

For reinforcement bars used in a structure which is exposed to moderate (NA) and mildly (LA) aggressive environment		
	C_3	C_4
Straight reinforcement bars	19.6	6.0
Bent around a mantel of diameter less than $3 \cdot \varphi$	15.9	4.8
For intermediate bending diameters between 3·φ and straight bars, interpolated values may be used.		
For straight reinforcement bars in a concrete structure, which is exposed to specially (SA) or severely (MA) aggressive environment		
	C_3	C_4
400 > Δσ > 235	15.70	4.50
235 > Δσ > 65	13.35	3.50
65 > Δσ > 40	16.97	5.50

Table 3: Values for factors C_3 and C_4.

2.2 Fiber reinforced concrete

2.2.1 General

Concrete is a material with low tension capacity which will cause problems when the concrete is subjected to axial tension-forces and moments. To solve this problem reinforcement must be added in the tension zone to take care of the tensile stresses. An alternative to this is to combine ordinary reinforcement with fibers. This will give many advantages, for instance increasing the ductility of the concrete (Home, 2019).

Figure 11: Ordinary steel-fibers.

There are many different materials to be used where steel (see Figure 11), glass or plastic are the most common ones. For the fibers to work well it`s important with good anchoring between the fibers and the concrete. To achieve this, many different geometric forms as shown in Figure 12 can be used.

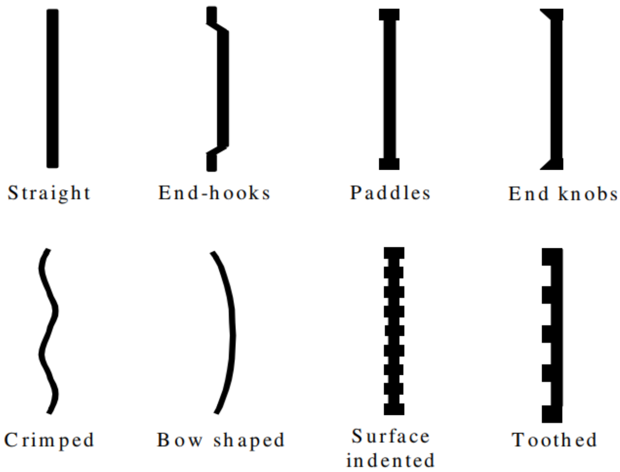

Figure 12: Different types of steel fibers (Hanjari, 2006).

There are many factors influencing the fibers ability to improve the properties of the concrete mix. One important factor is the amount of fibers mixed into the concrete. This is often called “volume fraction” and means the volume of the fibers related to the total volume of fiber and concrete. This value often lies between 0.1-3%. Another important factor is what is called “the aspect ratio”. This gives the ratio between the length of the fibers and their diameter. Usually the aspect ratio ranges from 30-150.

2.2.2 Compression

The stress-strain relation for concrete under compression is almost linear up to about 30% of the compressive strength (Löfgren, 2005). After this point a gradual softening happens to the concrete compressive strength, where the stress-strain relation exhibits a strain softening until failure. The main explanation of the concrete macroscopic behavior under compression failure is proposed by Neville (1997). This explanation states that there is an interface between aggregate and the hardened cement paste, and that in these interfaces micro cracks develop even at smaller load levels. These cracks will develop through the weakest part of the concrete, and eventually results in crushing.

When fibers are added into the concrete it becomes more ductile (see Figure 13). How the fibers affect the concrete is highly dependent of the fiber type, size and properties, the amount of fibers added to the concrete and the properties of the matrix. Generally, it can be concluded that conventional steel fibers at moderate dosages (<1%) do not affect the pre-peak properties, whereas the strain at crack location and the failure strain increase. However, with microfibers and fiber volume (>1%) it is possible to increase the compressive strength.

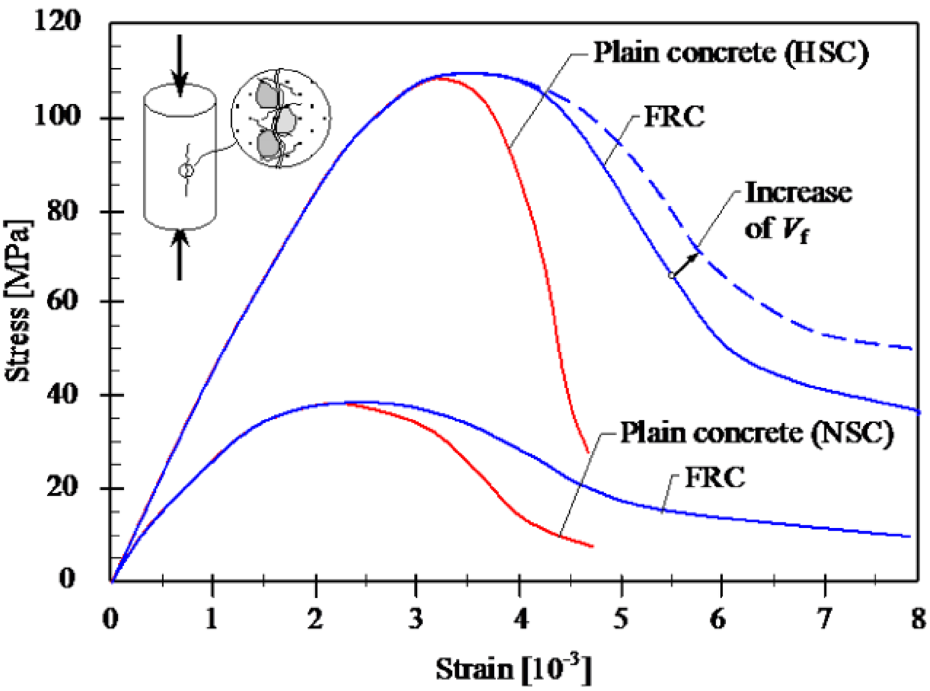

Figure 13:Compression behavior of fiber reinforced concrete (FRC) and plain concrete (Löfgren, 2005).

2.2.3 Tension

The important effect fibers have on tensile strength of concrete is the tensile fracture behavior. In plain concrete the tensile load carrying capacity will decrease a lot after crack widths of about 0,3 mm (Löfgren, 2005). By adding fibers, the concrete will be able to carry considerable loading after cracking. After the crack initiation, the fibers crossing the cracks will often be able to carry more load than other weak zones in the matrix. Therefore, new cracks will continue to form in the brittle matrix. When many cracks have formed the fibers will have plastic deformations by being pulled out of the concrete matrix. The ultimate failure in the concrete will occur when the fibers are completely pulled out of the concrete. This process will give the fiber reinforced concrete (FRC) much more ductile behavior than plain concrete, and some residual capacity after the peak of the stress-strain diagram.

2.2.4 Calculation of tensile capacity of FRC

Various test methods can be used to determine the tension capacity of FRC. Usually a three-point bending test as shown in Figure 14 is used to experimentally determine the residual flexural tension stress of the concrete $f_{ftk,res}$. This test is described in NS-EN 14651. The residual tensile stress is defined as the remaining tension capacity of the FRC after cracking.

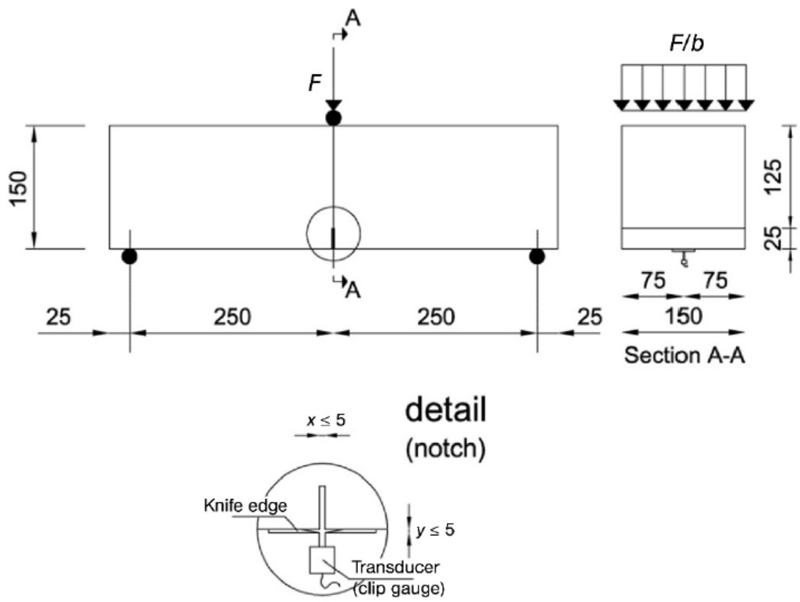

Figure 14: Test-setup required by NS-EN 14651 (dimensions in (mm)).

When doing this bending-test, a beam is subjected to a point-load at midspan, and a force-deformation diagram is plotted, as shown in Figure 15. Usually, the deformation is expressed in terms of crack mouth opening displacement (CMOD), which is the width of the crack at the bottom of the beam shown in the detail in Figure 14. This value is then measured by four predefined crack mouth openings ($CMOD_1$- $CMOD_4$) as shown in Figure 15.

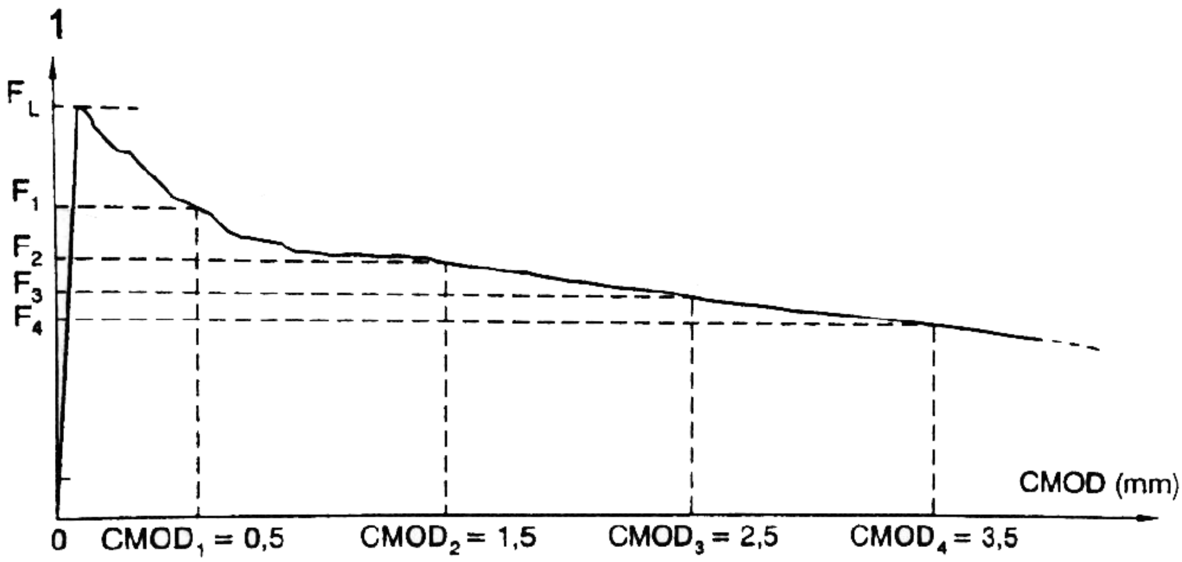

Figure 15: Typical F-CMOD curve for plain concrete and FRC (Kanstad, et al., 2011) .

To determine the relation between vertical displacement, δ and the CMOD, NS-EN 14651 gives the following empirical relation:

$$\delta = 0{,}85\ CMOD + 0{,}04 \tag{32}$$

where:

δ is the deflection of the test beam.

By use of basic mechanics, linear stress-distribution over the cross-section and moment of resistance for an uncracked cross-section, the residual flexural tensile stress on the beam $f_{R,j}$ can be calculated by the following expression:

$$f_{R,j} = \frac{3\ F_j\ l}{2\ b\ h_{sp}^2} \tag{33}$$

where:

F_j is the load corresponding to CMOD = $CMOD_j$.
l is the span length.
b is the specimen width.
h_{sp} is the distance between the notch tip and the top of the specimen.

From the test-results a characteristic value of the residual flexural bending stress (the 0,05-quantile) can now be determined as follows:

$$f_{Rk,j} = f_{R,j} - k\ s \tag{34}$$

The s is the standard-deviation in the test-series, and k = 1,7. The following expression can now be used to find the residual tensile strength, $f_{ftk,res,2,5}$ (Kanstad, et al., 2011):

$$f_{ftk,res,2,5} = 0{,}37\ f_{Rk,3} \tag{35}$$

where:

$f_{Rk,3}$ is the residual flexural tensile strength with CMOD = 2,5mm.

The formula given in Equation (35) can easily be shown by use of some basic mechanics and utilizing the stress distribution of a fiber reinforced cross-section.

Further an expression for the tension capacity F_{Rk} can be found by adding the contribution from the concrete and the reinforcement as follows:

$$F_{Rk} = f_{ftk,res,2,5} bh + A_S\, f_{yk} \tag{36}$$

where:

A_s is the total cross-section of the vertical reinforcement in the specimen.
f_{yk} is the characteristic yield stress of the reinforcement.
b is the width cross-section.
h is the height of the cross-section.

<u>Fiber orientation factor:</u>

When the fibers are mixed into the concrete their orientation will be difficult to determine. This will cause problems with respect to the utilization of the fibers. Optimally the fibers should be perpendicular to the cracks, as shown in Figure 16(a), to transfer maximum of stresses. Since the orientation of the fibers is difficult to control, a good solution will be to assume a fully random orientation of the fibers, as illustrated in Figure 16 (d). Then some of the fibers also can be used to transfer share forces.

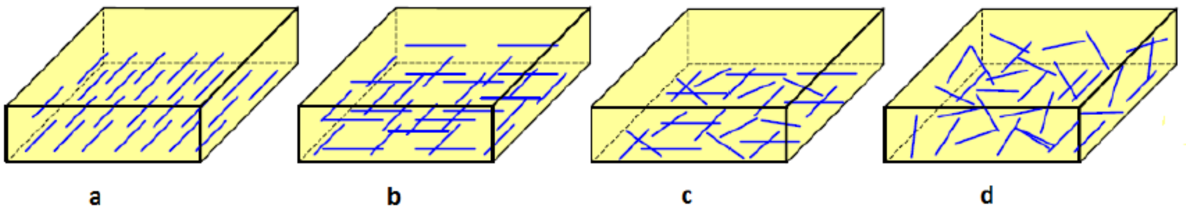

Figure 16: Different fiber orientations (Löfgren, 2005).

To handle this problem, SINTEF has made a recommendation giving a normalized residual tensile strength, $f_{ftk,res,2,5,norm}$ as follows (Kanstad, et al., 2011):

$$f_{ftk,res,2,5,norm} = \frac{f_{ftk,res,2,5} \, v_{f,norm}}{v_f \, (4\alpha - 1)} \tag{37}$$

where:

$f_{ftk,res,2,5}$	is the characteristic residual tensile strength desired by testing.
α	is the fiber orientation factor calculated by measuring number of fibers and volume-ratio, α is 0,5 means isotropic fiber orientation.
v_f	is the measured volume ratio of the fibers.
$v_{f,norm}$	is the nominal volume ratio of the fibers in the prescription of the concrete.

If the fiber orientation factor α has another value than 0,5. The following formula should be used:

$$f_{ftk,res,2,5,struct} = \frac{f_{ftk,res,2,5} (4 \, \alpha_{struct} - 1) \, v_{f,struct}}{v_{f,norm}} \tag{38}$$

where:

$v_{f,struct}$	is the volume ratio of fibers in the actual part of the construction.
α_{struct}	is the fiber orientation factor documented for the construction.

<u>Theoretical residual tensile strength</u>

The residual tensile strength $f_{ftk,res,2,5}$ for FRC can also be determined theoretically. SINTEF also gives an empirical expression for a theoretical residual flexural tensile strength given by the following expression:

$$f_{ftk,res,2,5} = \eta_0 \, v_f \, \sigma_{fk,mid} \tag{39}$$

where:

v_f	is volume ratio of fibers.
η_0	is capacity factor, the ratio between normal force resultant of the fibers with actual directional distribution, and the force resultant in the unidirectional fibers with the same stress.
$\sigma_{fk,mid}$	is the main stress in all fibers that crosses the crack with random distributed anchor lengths and directions. This parameter is strongly dependent of both the type of fiber and the quality of the concrete and has to be determined from relevant tests.

The capacity-factor η_0 can be set to 1/3 for fibers with random orientation. If the fiber orientation is documented by testing the following relations capacity factor and fiber orientation factor can be used:

$$\eta_0 = \frac{4}{3}\alpha - \frac{1}{3} \quad \text{for} \quad 0{,}5 < \alpha < 0{,}8 \tag{40}$$

$$\eta_0 = \frac{2}{3}\alpha \quad \text{for} \quad 0{,}3 < \alpha < 0{,}5 \tag{41}$$

Where the fiber orientation factor α and the fiber area ratio ρ is given by the following expressions:

$$\alpha = \frac{\rho}{v_f} \tag{42}$$

$$\rho = n\frac{A_f}{A_c} \tag{43}$$

where:

n	is the number of fibers.
A_f	is the cross-section area of one fiber.
A_c	is the cross-section area of the actual part of the cross-section.

2.2.5 Fatigue in fiber reinforced concrete

Adding fibers into the concrete can potentially improve its mechanical properties, also when it comes to fatigue. The main benefit of adding steel fibers to the concrete is that the fibers increases the ability to absorb energy. This is because of what is called crack-bridging, which is illustrated in Figure 17 (HANJARI, 2006). Crack-bridging means that the forces will use more energy to gradually pull out the fibers which will be absorbed in the structure.

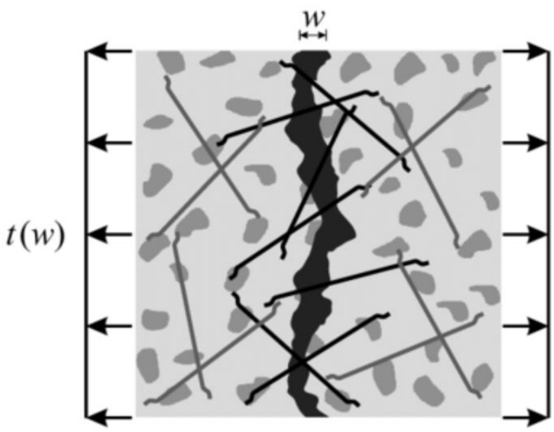

Figure 17: Crack-bridging (Zhan, 2016).

Although steel fibers contribute to the energy absorption, the addition of fibers has also been found to have a dual effect on the structural behavior under cyclic loading. Increasing the fiber content and the aspect ratio increases the amount of energy used in crack growth of FRC under fatigue loading. Based on research conducted by M. Grzybowski, there seems to be a reduction in the fatigue life of FRC compared to plain concrete for volume percentage above 0,25% (Grzybowski & Meyer, 1993). On the other hand, T. Paskova reported in 1994 that fibers substantially improve fatigue life of concrete for all volume percentages of fibers. From the conflicting evidence available, M.K. Lee (2004) concluded that there was an optimal fiber content. For example, J. Zhang reported in 1998 that there was an optimal fiber volume concentration of 1% (Zhang, 1998).

2.3 Partially loaded areas

2.3.1 General

Partially loaded areas are the cases when the loaded area is smaller than the total cross-section of the concrete, as shown in Figure 18 (a). When this type of loading is applied, the stresses will spread outwards further down in the cross-section. The length of the zone where this happens is denoted d_2 in the same figure.

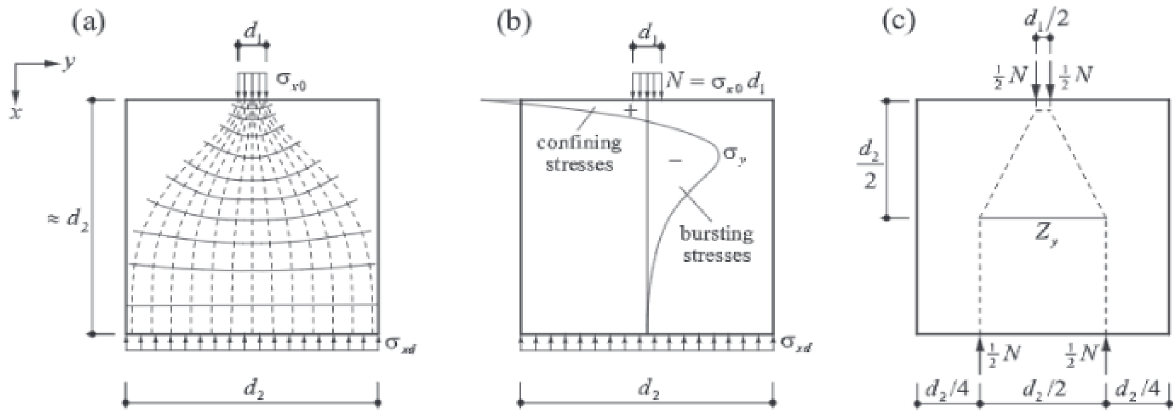

Figure 18: a) Normal-stress distribution, b) Transverse stress distribution, c) Truss model (Tomislav, et al., 2018).

This will lead to a further change in direction of the main stress trajectories (the direction of the main stresses) as illustrated with curved dotted lines in Figure 18 (a) (Betongelementforeningen, 2010). This load-spread will then cause forces in the horizontal directions.

Through experiments, it is shown that there is a zone with transverse compression right below the force, which transforms to transverse tension further below as shown in Figure 18(b). The reason for the transverse compression is that the vertical compressive stresses under the applied force will bow outwards, which demands a radial lateral compression in the core. This means that an outer tension-ring is needed to establish the lateral compression which occurs in the core when the load spreads. This is illustrated in Figure 19.

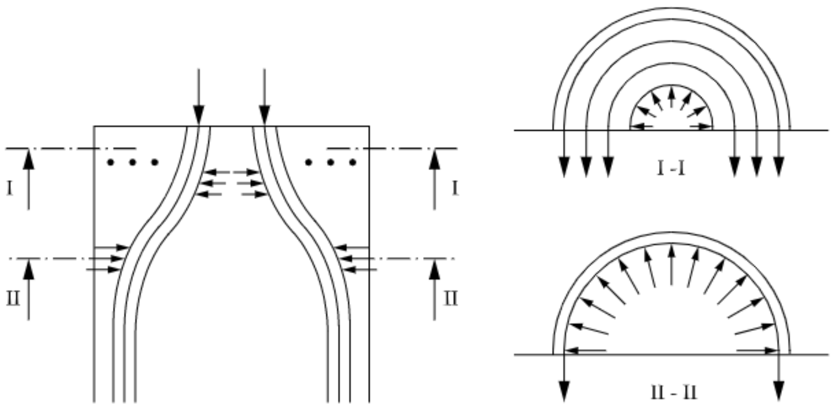

Figure 19: Principle of splitting under centric load.

2.3.2 Eurocode 2 & Fib Model Code 2010

In Eurocode 2, partially loaded areas are described in section 6.7. For partially loaded areas both compression at the top and the transverse tension forces must be considered. In Model Code 2010, partially loaded areas are covered in part 7.2.3.1.7. They give the exact same formulas for compression as Eurocode 2.

First, the Eurocode describes how to take care of the compressive stresses at the top of the specimen. The following figure is given in the Eurocode to describe the problem:

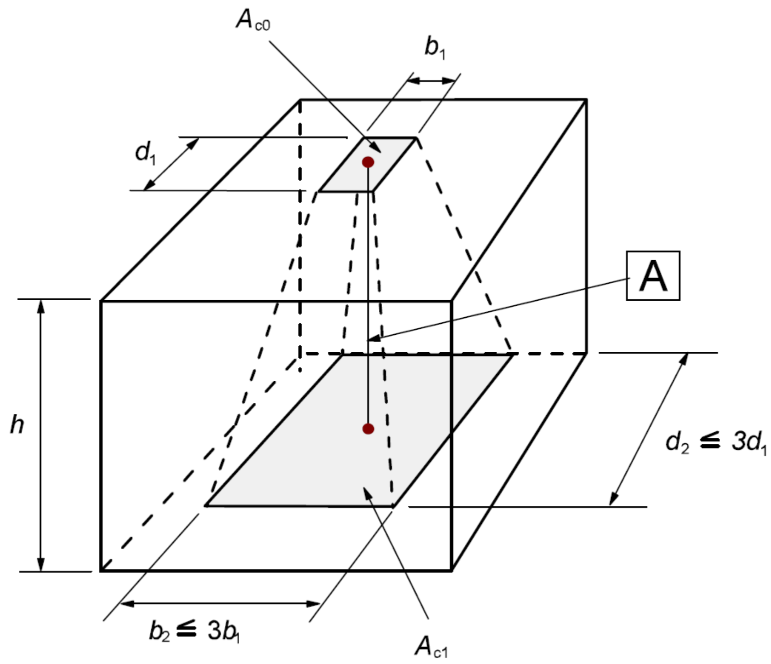

Figure 20: Computationally load distribution area given in Eurocode 2.

The following formula is given for the compression capacity for a partially loaded area:

$$F_{Rdu} = A_{c0}\, f_{cd} \sqrt{\frac{A_{c1}}{A_{c0}}} \leq 3{,}0\, f_{cd}\, A_{c0} \tag{44}$$

where:

F_{Rdu}	is the dimensioning capacity in compression.
A_{c0}	is the loaded area at the top of the specimen.
A_{c1}	is the maximum design distribution area with a similar shape to A_{c0}.
f_{cd}	is the dimensioning compressive strength of the concrete.

The computationally distribution area A_{c1} needed to transfer the force, F_{Rdu} presupposes that the following requirements are fulfilled:

- The height for the load distribution in the load direction should correspond to the conditions given in Figure 20.
- The center of the computationally distribution area A_{c1} lies on the attacking line through the center of the loaded area A_{c0}.
- If there is more than one compressive force acting on the concrete cross-section, the designed distribution areas should not overlap.

If the load is not evenly distributed over the area A_{c0} or if large shear forces are working, the dimensioning compression capacity F_{Rdu} should be reduced.

For the tensile stresses in the more remote region of the stress field the codes substitute the stress field by two force trajectories T and F. The tensile splitting force T should then be resisted by specially provided reinforcement. Calculating the needed splitting reinforcement is described in part 6.5.3. The value of the occurring tension force T depends on whether the specimen is partly of fully discontinuous (if the load propagation is fully or limited by the renders of the specimen).

For partial discontinuity regions ($b \leq \frac{h}{2}$ (see Figure 21 (left))) the following formula should be used:

$$T = \frac{1}{4}\frac{b-a}{b}F \tag{45}$$

For full discontinuity regions ($b \geq \frac{h}{2}$ (see Figure 21 (right))) the following formula should be used:

$$T = \frac{1}{4}\left(1 - 0{,}7\frac{a}{h}\right)F \tag{46}$$

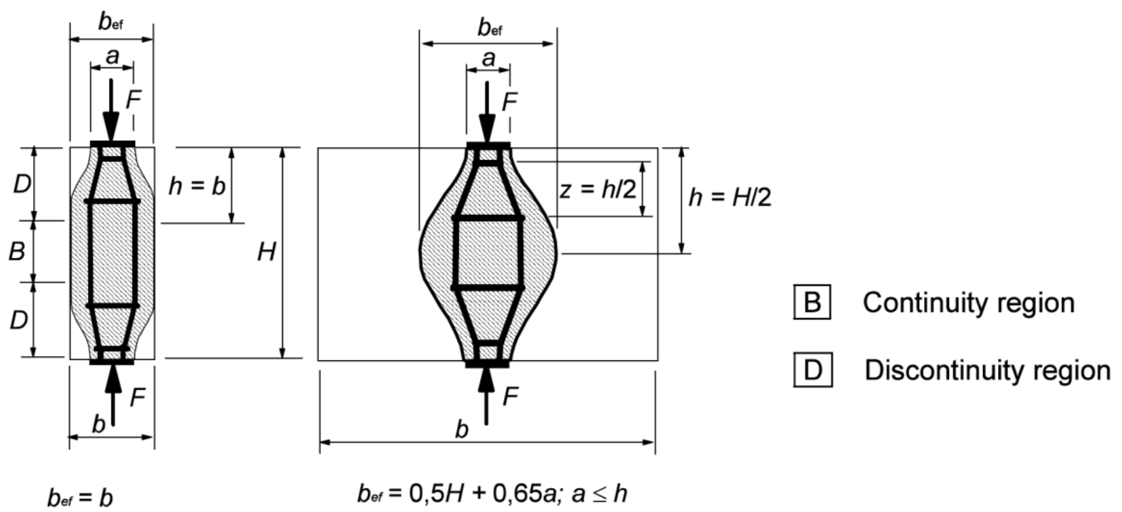

Figure 21: Partial discontinuous specimen(left), Fully discontinuous specimen(right).

2.3.3 DNV-OS-C502

For partially loaded areas DNV-OS-C502 and Eurocode 2 use many of the same formulas. Where the Eurocode only has one expression for the capacity, DNV-OS-C502 has two expressions together with more complementary text. The code use one expression for normal situations and one expression if the ratio between the largest and the smallest dimension (the ratio between a_1 and a_2 in Figure 22) is smaller than two, and the distributed area A_2 is assumed to have the same geometric form as A_1 (the loaded area).

DNV-OS-C502 gives the following two expressions:

<u>Normal situation:</u>

$$F_{Rdu} = A_1\, f_{cd} \sqrt[3]{\frac{A_2}{A_1}} \tag{47}$$

<u>Ratio less than 2:</u>

$$F_{Rdu} = A_1\, f_{cd} \sqrt{\frac{A_2}{A_1}} \leq 3{,}0\, f_{cd}\, A_1 \tag{48}$$

where:

A_1	is the loaded area at the top of the specimen.
A_2	is the maximum design distribution area with a similar shape to A_1.

The code also has some requirements for reinforcement transfer the tension forces. In the two principal directions the reinforcement A_{sa} and A_{sb} is given as follows:

$$A_{sa} = 0{,}25\, F_f \left(1 - \frac{a_1}{a_2}\right) \tag{49}$$

$$A_{sb} = 0{,}25\, F_f \left(1 - \frac{b_1}{b_2}\right) \tag{50}$$

where:

a_1 and b_1	is the dimensions of the loaded area.
a_2 and b_2	is the dimensions of the maximum design distribution area.
F_f	is the applied force at the top of the specimen.

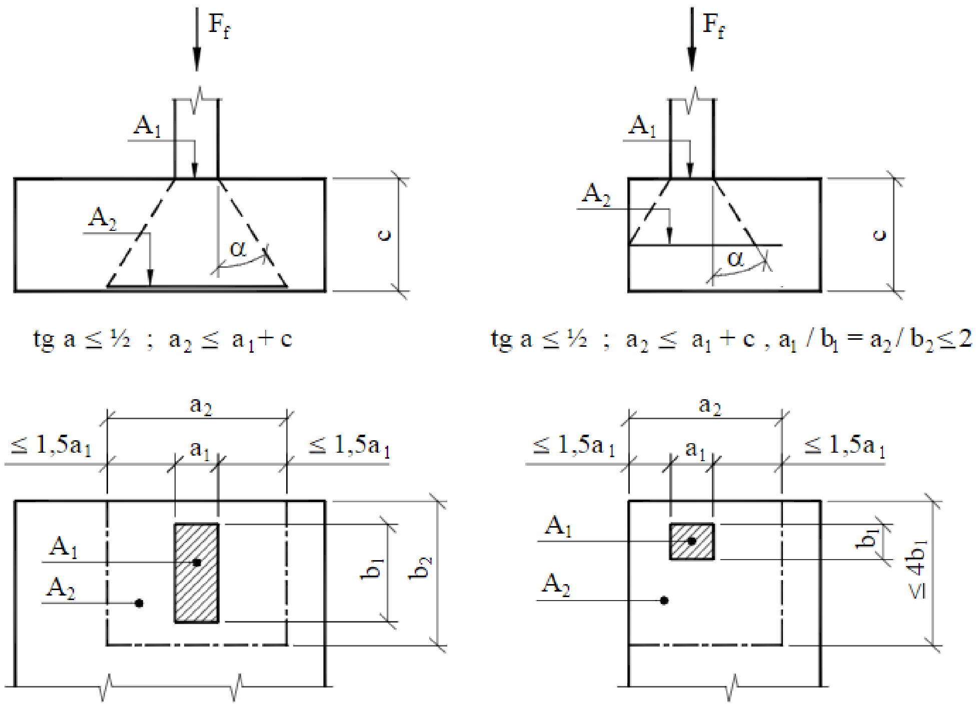

Figure 22: Geometry for partially loaded areas given in DNV-OS-C502.

It is also given that the cross-sectional dimensions of the distribution area shall not be assumed larger than the sum of the dimensions of the loaded surface measured in the same main directions and the concrete thickness measured parallel to the direction of the force. The code also gives a formula for lightweight concrete. The dimensions of the distribution area A_2 shall neither be assumed greater than 4 times the dimensions of the loaded area A_1 measured in the same main directions

The code also states that the reinforcement shall be placed such that its center of gravity is placed at a distance from the loaded area equal to half the length of the side of the distribution area in the same direction, but not greater than the distance to the distributed area. The reinforcement bars should also be distributed over a width equal to the length of the distributed area side normal to the bars, and over a height that equals half the side of the distributed area parallel to the bars.

The code also states that when calculating the requires tension reinforcement, expansion of soft supports, fluid pressure and similar must be taken into account.

2.3.4 Insufficient splitting reinforcement

There is little literature or guidance for capacity of partially loaded areas when there is insufficient or no splitting reinforcement in the tie. EC2, Model Code 2010 and DNV-OS-C502 gives no guidance for these cases, however Model Code 1990 section 3.3.2 states that the splitting force T can be resisted by the tensile strength of concrete in the tension zone with a cross-sectional height according to Figure 23. Here the tensile splitting force T is calculated according to the conservative method of substituting the stress field by two force trajectories given in Equation (45).

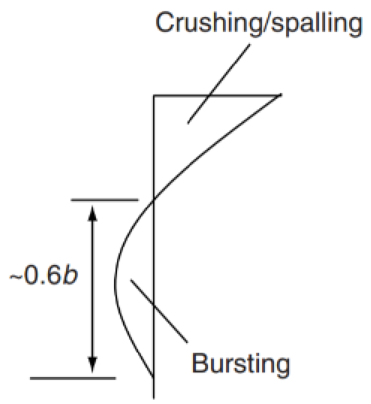

Figure 23: Transverse tresses in cross-section for partially loaded areas.

2.3.5 Partially loaded areas for fiber reinforced concrete

"SFRC Consortiums guidance in the design guideline for structural applications of SFRC" is a guideline for handling FRC in partially loaded areas. Section 6.7 say that the tensile splitting force can be resisted by the fibers only where the residual tensile capacity is distributed over a cross sectional height equal to 0,8 times the heigh as seen in Figure 24. This value is based on a cracked cross section and is a bit higher than the value used for uncracked cross section which is 0,6 times the height.

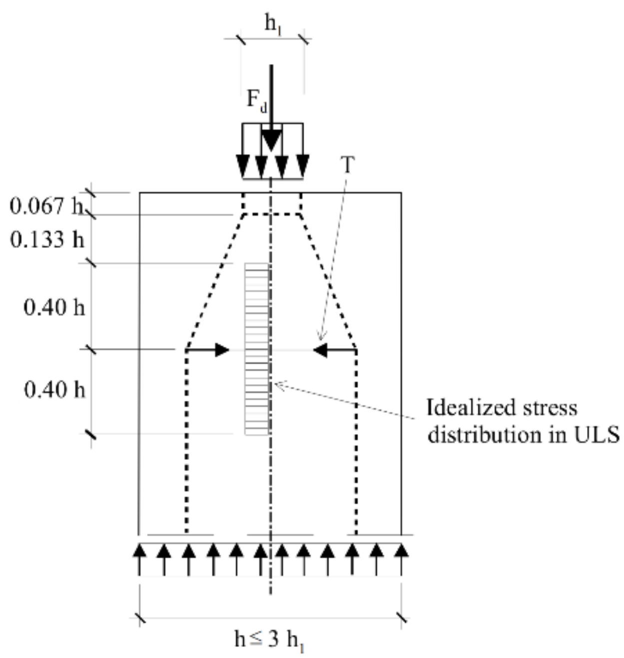

Figure 24: Cross sectional height of residual tensile capacity for design of partially loaded areas using FRC (Kasper, et al., 2014).

2.4 Confined boundaries

When talking about confining the lateral displacement of a specimen subjected to longitudinal compression, one is simply preventing the specimen to move or deform in the lateral direction when compression forces are applied. It is important to distinguish between active confinement and passive confinement. Active confinement occurs where the confining boundary condition is an external force to counteract displacement (Shin & Andrawes, 2010). Such a case causes a constant stress in the confined direction of the specimen, which leads to an initial displacement in the opposite direction of the direction meant to be confined. This displacement is meant to counteract the displacement caused by the initial load situation leading to a final displacement in the confined direction equal to zero. In passive confinement, in the other hand, the confining pressure is occurs only as a direct result of the lateral dilation of concrete when the loading is applied. This way no external force is applied to counteract the displacement beforehand.

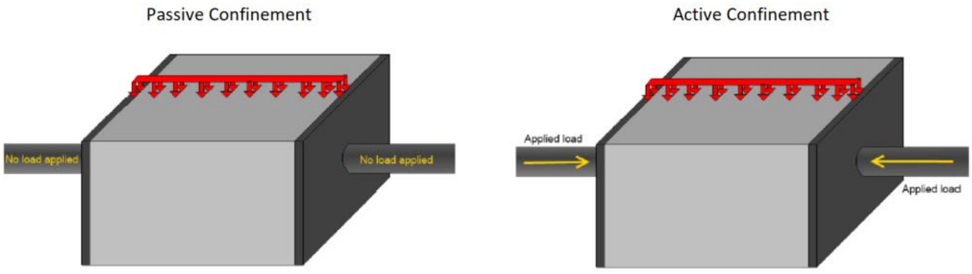

Figure 25: Passive and active confinement of concrete.

The effect of constrains on concrete has been extensively studied throughout the years, with confinement resulting in a change in the stress-strain relationship, achieving higher strength. Eurocode 2 section 3.1.9 provides an opportunity to increase the characteristic strength for concrete when confined. However, this formulation is based on a confinement where the confining stresses in both lateral directions are the same. This means that if the specimen is confined in only one lateral direction Eurocode 2 section 3.1.9 can't be used even though the confinement would still lead to an increased strength.

Most of the work based on concrete behavior and confinement is under static loading, and until recent years relatively few studies on the effect of confinement and fatigue loading were conducted. In 2000 Tan T. Hooi conducted a study on the effects of passive confinement on fatigue in concrete. The study was based on cylindrical test specimens with spiral reinforcement as confinement (Hooi, 2000). His research shows that the susceptibility to high cycle fatigue damage is increased due to the passive confinement but lateral confinement in general increases the strength, which leads to a lower stress level $S_{cd.max}$. Hooi concluded that the increase in strength due to confinement outweighs the increase in susceptibility to fatigue damage, giving an overall increase to fatigue life. Based on the research Hooi suggested a formula to calculate fatigue strength for concrete with passive constrain, but just like Eurocode 2, Hooi's formulas are based on equal constraining strains in every lateral direction.

Few studies have been conducted on uniaxial confinement in fatigue loading. One study conducted by H. L. Wang and Y. P. Song in 2011 did look at uniaxial confinement with tension, tension-compression and compression fatigue loading, though the confinement was active (wang & Song, 2010).

3 Test specimens

Because this thesis is a continuation of the work done by Furnes & Hauge in 2011 and Bognøy et al. in 2014, it is imperative to keep important variables in the test specimens the same as earlier. This way it is possible to directly compare results, which will give a greater understanding of the implications of fiber reinforcement for dynamic loading. Therefore, the dimensions of the test specimens are set to 210x210x525mm. Due to some unforeseen difficulties regarding delivery, there are some differences between earlier test specimens, however these changes will not affect the comparability.

For this thesis 3 different types of test specimens have been created: minimum reinforced (A), unreinforced (B) and steel fiber reinforced (C) (see Table 4). Each group had 6 specimens, which in total gives 18 specimens. To control the concrete strength before testing of each specimen 33 standardized test-cubes at 100x100x100 mm were created and these test cubes are categorized in Table 5. In addition, 3 standardized beam specimens 150x150x525mm were cast with FRC to determine the residual tensile stress at 2.5mm

Specimen type	Reinforcement type	Nr. of strain gauges	Test type	
A	Minimum reinforcement	3	A1 – A3	Static
			A4 – A6	Dynamic
B	No reinforcement	2	B1 – B3	Static
			B4 – B6	Dynamic
C	Fiber reinforcement	2	C1 – C3	Static
			C4 – C6	Dynamic

Table 4: Specimen types with their reinforcement layout.

	Fiber reinforced concrete (Denoted C1 – C15)	Non-fiber reinforced concrete (Denoted 1 - 18)
28-day strength	3	3
For static testing	3	3
For dynamic testing	9	12
Sum	15	18

Table 5: Number of test-cubes in each specimen group.

The hydraulic jack available has limitations at 1000kN static pressure and 700kN dynamic pressure. It is due to these limitations that the compressive strength of the concrete is chosen as c25/30 (B25). Concrete will continue gaining strength after 28 days. Because of the longevity of dynamic testing some specimens will be tested after 28 days, and it would be optimal if the concrete strength does not vary significantly between the different tests. The mix used can be seen in Table 6.

Receipt without fiber		Receipt with fiber	
Durability class	M90	Durability class	M90
Strength class	B25	Strength class	B25
V/(c+ks)-ratio	0.63	V/(c+ks)-ratio	0.63
Consistency [mm]	200	Consistency [mm]	220
Air content [%]	2.0	Air content [%]	2.0
Projected density	2348.14	Projected density	2342.60
Measured consistency [mm]	***235***	***Measured consistency [mm]***	***225***
Measured air content [%]	***1.9***	***Measured air content [%]***	***1.3***
Measured density [kg/m³]	***238124***	***Measured density [kg/m³]***	***2372.26***

Table 6: Concrete mixtures.

The different types of test specimens were differentiated by their reinforcement layout only. In compliance with previous work the specimens were to be cast with four stirrups of ϕ6 with a vertical distance of 80mm between each stirrup at the lower part of all the specimens. Due to problems with delivery the reinforcement was changed to ϕ8, as this will have little to no impact on the specimens capacity or behavior. There was also one ϕ10 in each corner of the stirrups. Specimen type A had a minimum reinforcement at the top with a nominal cover of 40mm. This minimum reinforcement consisted of 2 bars of ϕ8 in each of the horizontal directions, as can be seen in Figure 26. For specimen type C there was added reinforcement fibers to the concrete mix. The steel fibers used for this project were of the type DE50/1.0N from Mapei with tensile strength of 1100MPa. 25 kg/m^3 of fibers was added to the concrete.

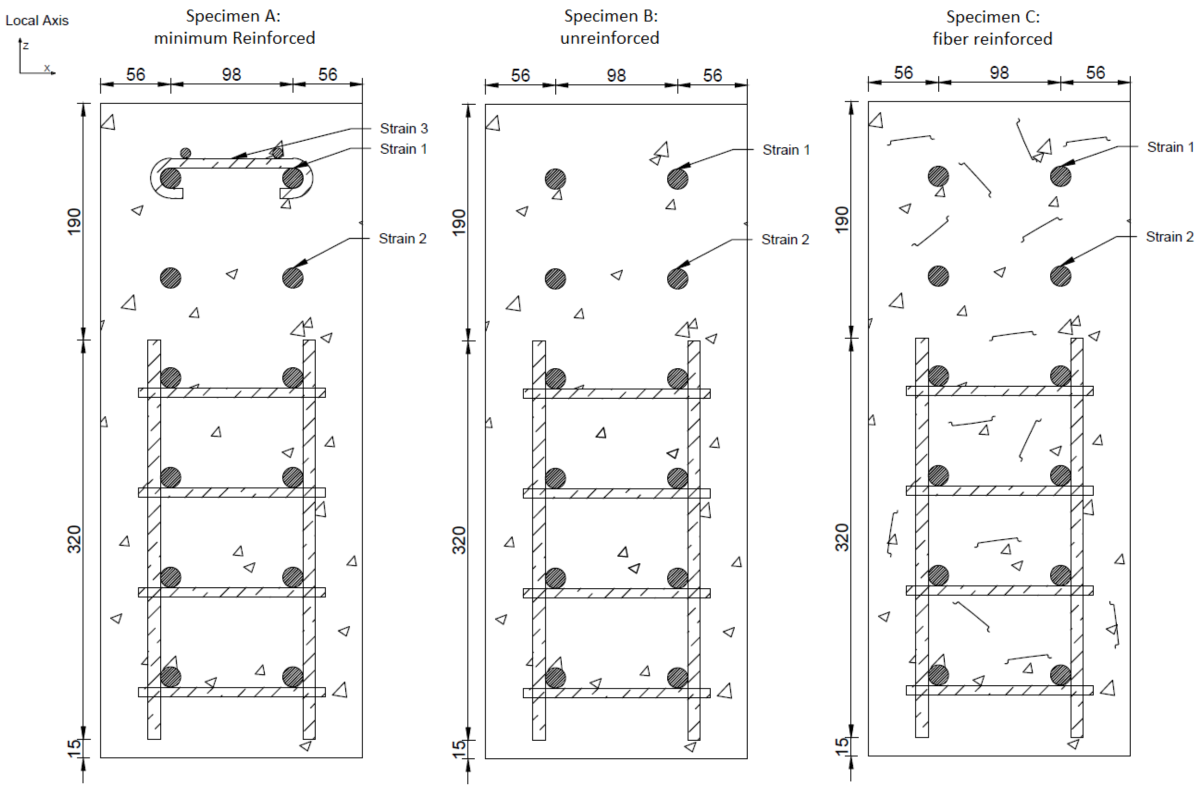

Figure 26: Reinforcement layout for specimen type A (Minimum reinforcement, B (No reinforcement) & C (Fiber reinforcement).

It is important to assess the implications due to the simplification of extracting a small piece of the foundation. By doing this one has to account for the fact that the foundation will not deform in the direction parallel to the line load. To prevent this deformation in the test specimen six layers of threaded bars was used, with two bars in each layer. The bars had a diameter of 16mm and spacing of 80mm in the vertical direction. Specifications of the bars can be seen in Table 7.

Diameter [mm]	Length [mm]	Property class	Yield strength [MPa]	Ultimate limit strength [MPa]	Minimum tensile strength [kN]
16	330	8.8	640	800	125

Table 7: Properties of threaded bars.

The test specimens were outfitted with strain-gauges. The strain gauges were of type FLA-3-11 from TML and had a gauge factor of 2.12 +/- 1% and a gauge resistance of 119.6 +/- 0,5 ohm. This way the internal strains in the specimens could be monitored during testing. For all three specimen types strain gauges were mounted on the two top threaded bars to the right for monitoring the local Y-direction (see Figure 26). These were fastened on the threaded bars as shown in Figure 27. Unfortunately, due to lack of reinforcement to fasten the strain-gauges on only specimens of type A had a third strain gauge in the local y-direction.

Figure 27: Strain gauges fastened on threaded bars.

The casting forms were built of plywood and consisted of 3 batteries with 6 specimens in each battery. The specimens were cast on the 14th of February and deformed the day after. Test cubes and beams were stored for curing in a water bath at 20 ^{0}C at NTNU. To ensure high humidity for the test specimens and preserve the water content within the specimens, they were wrapped in soaked cloth and sprayed with water before sealing them in a plastic vapor barrier as shown in Figure 28. This guaranteed that the humidity of the specimens was close to constant during the entire curing and shipping process.

Figure 28: Test specimens stored for curing.

4 Test procedure

4.1 Introduction

The test specimens for this thesis were tested at DNV GLs laboratory at Høvik in Oslo in the period from the 18th of March to the 6th of April. To establish a reference for the concrete strength, three standardized test-cubes of the same concrete were tested the same day as a specimen test was conducted. The standardized test-cubes were tested at NTNU in Trondheim due to the lack of equipment for this test at DNV GLs laboratory.

4.2 Testing equipment and rig setup.

The hydraulic jack used for testing of the specimens was an MTS Instron 8500 with a digital instrumentation controller. This machine has a static capacity of 1000kN, and a dynamic capacity of 800kN. Just as in Bognøy *et.al.* the test specimens were tested fully submerged in a water container. The container consists of an acrylic glass tube with a diameter of 400mm fastened to a steel base plate. An O-ring was used between the tube and the plate to ensure a watertight seal. When the concrete cracks, there is a possibility that large pieces may break off and hit the wall of the water containment. To prevent this from occurring two acrylic glass plates were loosely fitted to the side of the specimen in such a way that they do not act ass confinements, but only serve to prevent total collapse of the specimens as shown in Figure 29.

Figure 29: Rig setup showing specimen submerged in water container with load transferring plates and hinge. Acrylic glass plates shown preventing total collapse of specimen.

To ensure correct load condition a 70x210x25 mm steel bar was placed centered on the specimen and a 210x210x50mm steel bar in top of that for proper load distribution. To prevent uneven loading a hinge with diameter of 180mm and height of 50mm was mounted on top of the load distribution plate. Due to a hole in the top piston for mounting equipment another distribution plate was used between the hinge and top piston with dimensions 200x200x80mm. This setup can be seen in Figure 29 and Figure 32.

Figure 30: Slanted loading of specimen B4 during dynamic test.

During the first dynamic test (specimen B4) the loading plate started to slant towards one side, with an increasing angle for every cycle. This resulted in local crushing on one side of the loaded area as shown in Figure 30. Through a close inspection it was reviled that with a change in angle, the hinge would create an eccentricity of the load leading to an unfavorable load situation. This eccentricity would increase for an increasing angle and thus worsening the situation. To minimize this effect the hinge was turned upside down, leading to a significantly reduced eccentricity with a change in angle, as can be shown in Figure 31. All the following dynamic tests were therefore conducted with the hinge oriented in the other direction.

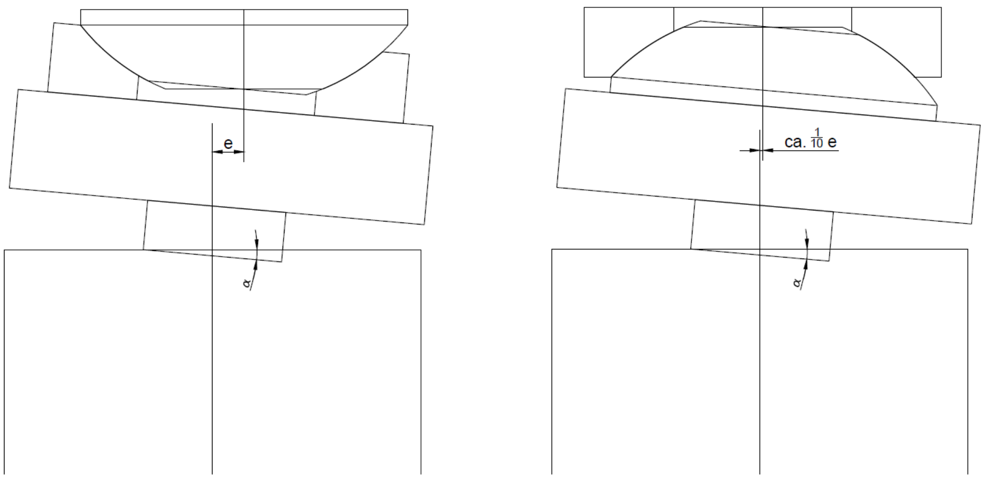

Figure 31: Orientation of hinge and equivalent change in eccentricity at angle α.

To measure the vertical displacement of the specimens, LVDT`s were mounted on the steel base plate of the water container, measuring on the underside of brackets mounted to the distribution plate as shown in Figure 32. These LVDTs were mounted in the direction of the corners of the specimens outside the water container as seen in Figure 32. For all static tests and the dynamic test of specimens B4-B6 only LVDT 1 and LVDT 2 were used. Because of the slanting of loading plate for specimen B4 and the development of LVDT 1 and LVDT 2 for specimen B6 as discussed in section 7.3 it was decided to include 3 LVDTs. Because there are three LVDTs it is possible to get an indication of the behavior of the load plane by looking at the change in displacement for the three LVDTs.

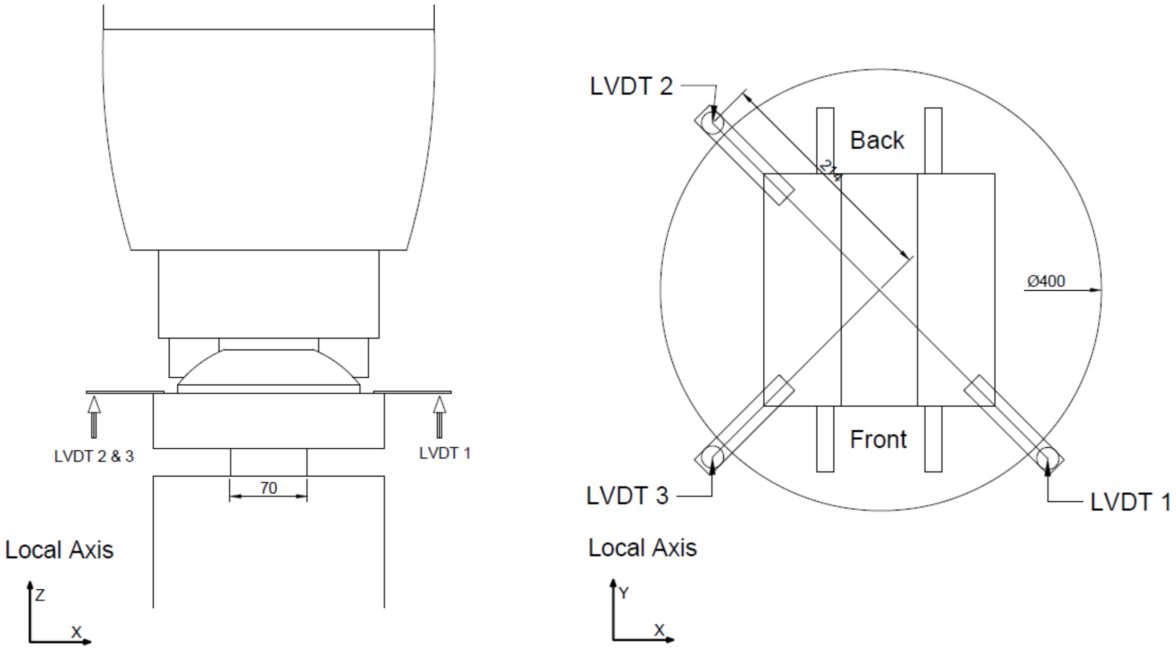

Figure 32: Placement of the LVDT`s.

4.3 Static test procedure

Test specimens A1-A3, B1-B3 and C1-C3 were tested statically. Static tests were done as a displacement-controlled test which means that the displacement is changing in a constant pace throughout the test, while the applied load varies. The rate of displacement was set to 0,4mm/min, and no specified stop criteria were set. Failure of the specimen was considered defined when the load started to decrease while the deformation was increasing. All specimens were tested beyond failure, though how far beyond failure was considered subjectively based on crack opening, residual capacity and shape of the force-displacement curve.

Data sampling for static testing was done with a sample rate of 5 Hz, and Table 8 shows the data that was sampled for each specimen.

A1-A3		**B1-B3**		**C1-C3**	
Channel	**Measurement**	**Channel**	**Measurement**	**Channel**	**Measurement**
1	Time [s]	1	Time [s]	1	Time [s]
2	Load [kN]	2	Load [kN]	2	Load [kN]
3	Stroke [mm]	3	Stroke [mm]	3	Stroke [mm]
4	Strain 1 [μm/m]	4	Strain 1 [μm/m]	4	Strain 1 [μm/m]
5	Strain 2 [μm/m]	5	Strain 2 [μm/m]	5	Strain 2 [μm/m]
6	Strain 3 [μm/m]	6	LVDT 1 [mm]	6	LVDT 1 [mm]
7	LVDT 1 [mm]	7	LVDT 2 [mm]	7	LVDT 2 [mm]
8	LVDT 2 [mm]				

Table 8: Sampled data for each specimen during static testing.

4.4 Dynamic test procedure

The test specimens A4-A6, B4-B6 and C4-C6 were tested dynamically. Dynamic testing was done as a force-controlled test which means that the force is changing in a constant/predicted pace throughout the test, while the applied displacement varies. Dynamic loading was applied in a sinusoidal wave with a frequency of 1Hz. The minimum load (lower peak of sinusoidal load) was set to 10% of mean fracture load F_{max} (static test) for the given specimen type, and maximum load (upper peak of sinusoidal load) was set to 70% of mean fracture load F_{max}. To ensure correct stress level S_{cd} the mean fracture load F_{max} was adjusted for the change in concrete strength, which was tested before the dynamic test was started. Due to the low number of dynamic tests for each specimen type it was concluded that all specimens were to be loaded with the same stress level (0.7/0.1). This way one could directly compare the results to one another with a higher reliability. The stroke limit was set to 5mm and a maximum and minimum load limit of 25kN above maximum load and 25kN below minimum load respectively was used.

Data sampling for dynamic testing was done with a sample rate of 20 Hz, and Table 9 shows the data that was sampled for each specimen.

A4-A6		**B4-B6**		**C4-C6**	
Channel	**Measurement**	**Channel**	**Measurement**	**Channel**	**Measurement**
1	Time [s]	1	Time [s]	1	Time [s]
2	Load [kN]	2	Load [kN]	2	Load [kN]
3	Stroke [mm]	3	Stroke [mm]	3	Stroke [mm]
4	Strain 1 [μm/m] *	4	Strain 1 [μm/m]	4	Strain 1 [μm/m]
5	Strain 2 [μm/m] *	5	Strain 2 [μm/m]	5	Strain 2 [μm/m]
6	Strain 3 [μm/m]	6	LVDT 1 [mm]	6	LVDT 1 [mm]
7	LVDT 1 [mm]	7	LVDT 2 [mm]	7	LVDT 2 [mm]
8	LVDT 2 [mm]			8	LVDT 3 [mm]
9	LVDT 3 [mm]				
* For specimen A6 strain 1 and strain 2 was not functioning and therefore not logged					

Table 9: Sampled data for each specimen during dynamic testing.

5 Calculated capacity for specimens

5.1 General

Expected strength and capacity for the test specimens were found through hand calculations based on the information gathered in the literature review for this thesis. The expected static capacity was based on concrete strength at 28 days, while the expected number of cycles during dynamic loading will be dependent of stress level $S_{cd.max}$=0.7. In the effort of obtaining the most exact fracture load, all calculations were based on mean concrete strength, and safety factors were neglected. That being said, the original subscripts were being used in a large extent to prevent confusion between formulas listed in chapter 2: Literature review.

5.2 Capacity of statically loaded specimens

5.2.1 Specimen type A and B

Specimen type A has two ϕ8 mm reinforcement bars situated 48 mm from the top. This amount of reinforcement is not sufficient splitting reinforcement according to Eurocode 2 and FIB Model Code 2010. Eurocode 2 and FIB Model Code 2010 gives no guidance when there is insufficient reinforcement in the tie. Furthermore, the placement of this reinforcement will under partially loaded area described by Eurocode 2 and FIB Model Code 2010 be in the crushing zone of the cross section as shown in Figure 33 . It is therefore concluded that the minimum reinforcement in specimen type A will be neglected during the calculations. The expected capacity of specimen type A will therefore be calculated in the same manner as for specimen B.

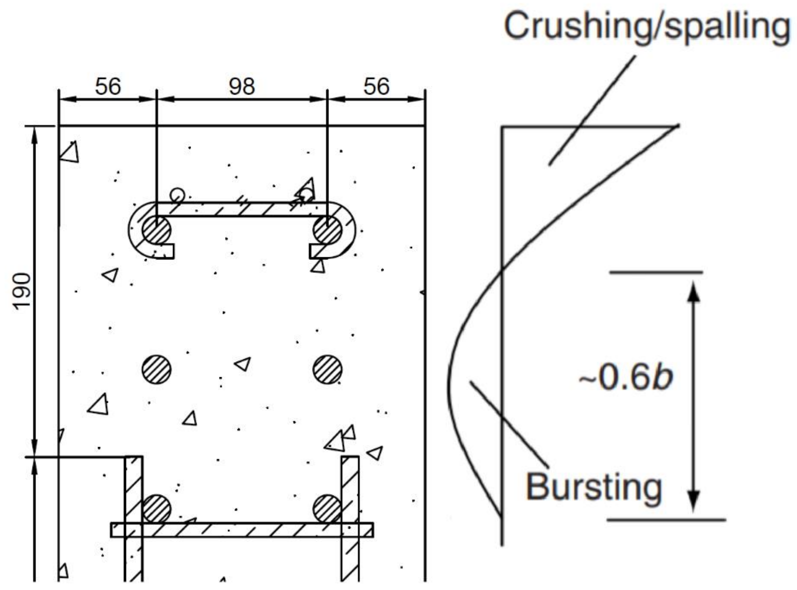

Figure 33: Crushing and bursting zone of test specimen under partially loaded area.

Static capacity due to partially loaded areas is the lowest of the compressive capacity and the tensile capacity. The bearing capacity concrete under local compression according to Equation (44) is F_{Rdu}=936.97kN. For the mean tensile capacity of concrete f_{tm} linear interpolation of values found in table 3.1 from Eurocode 2 is used and calculations from Model Code 1990 will therefore give a tensile capacity F_{ctd}=444.53 kN leading to a capacity lower than the capacity of loaded area F_{Ac0}=540.96 kN.

According to the studies conducted by Furnes & Hauge and Bognøy et.al. the capacity of their unreinforced specimens subjected to partially loaded areas show a slightly higher capacity compared to the capacity of loaded area F_{Ac0}. Taking into consideration that their unreinforced specimens are directly comparable to the specimens in this study it is reasonable to conclude that the static capacity of specimen type A and B should also be slightly higher than the capacity of loaded area F_{Ac0}=540.96 kN. The fact that the calculation method used is conservative and the mean tensile capacity of concrete f_{tm} is found by linear interpolation and not through testing further supports this conclusion and the lowest capacity of the test specimens will therefore be set to the concrete strength multiplied by the loaded area.

Specimen type	A_{c0} [mm²]	$f_{ck.28}$ [MPa]	$F_{max.28}$ [kN]	$f_{ck.test}$ [MPa]	$F_{max.test}$ [kN]
A	14700	36.80	540.96	38.96	572.71
B	14700	36.80	540.96	38.96	572.71

Table 10: Expected capacity F_{max} at 28 days and expected capacity for specimen type A and B.

5.2.2 Specimen type C

In addition to the calculations for the tensile capacity according to Model Code 1990, the capacity of specimens with steel fiber reinforced concrete can be estimated according to *"SFRC Consortiums guidance in the design guideline for structural applications of SFRC"*. This calculation only considers a cracked cross section, even though fiber reinforcement will give an increased capacity of an uncracked cross section. Because there is no reliant way of calculating the increased effect on an uncracked cross section the calculated tensile capacity will be the highest of either cracked or uncracked capacity. The expected tensile capacity of the FRC-specimen will therefore be higher than the calculated capacity.

The compressive capacity of the specimen according to Equation (44) is F_{Rdu}=879,20kN, and the tensile capacity according to Model Code 1990 gives $F_{ctd.concrete}$=428,65kN. The tensile capacity was also calculated according to *SFRC Consotrium* to be $F_{ctd.2.5}$=317,5kN, which is for the cracked cross section. Thus, the maximum capacity from partially loaded areas is 428,65kN which is lower than the capacity of the loaded area A_{c0}. As mentioned in Section 5.2.1 because the calculations used in the codes is conservative and studies conducted by Furnes & Hauge and Bognøy et.al. show a higher capacity than for loaded area F_{Ac0}, the capacity of specimen type C will not be set lower than the capacity of the loaded area F_{Ac0}.

Specimen type	A_{c0} [mm²]	$f_{ck.28}$ [MPa]	$F_{max.28}$ [kN]	$f_{ck.test}$ [MPa]	$F_{max.test}$ [kN]
C	14700	34.53	507.59	35.94	528.32

Table 11: Expected capacity F_{max} at 28 days and expected capacity for specimen C.

5.3 Capacity of dynamically loaded specimens

As seen in Chapter 2.1.4, the calculation of fatigue life relies on the concrete strength f_{ck} and the concrete stresses $\sigma_{c.}$ and σ_{ct} to determine the stress level of the concrete S_{cd}. The hand calculations in this chapter have been simplified from a stress level to a capacity level basis. Because of the way Model Code 2010 calculates its characteristic fatigue reference strength $f_{ck.fat}$ the calculations will still be conducted in the stress field. The concrete strength f_{ck} will be expressed as maximum capacity F_{max} divided by load area A_{c0}, while the compressive stresses $\sigma_{c.min}$ and $\sigma_{c.max}$ are expressed as the applied force F_{load} divided by load area A_{c0}.

5.3.1 Different formulas for calculating fatigue life

The uncertainty in calculating fatigue life of concrete structures is emphasized by the large number of formulas for calculating the fatigue life. From Figure 34 one can see this vast difference in fatigue life due to the different formulas. A stress level S_{cd} of 0.7 gives an approximate range from 2 000 to 100 000 cycles depending on the formulas used. It is important to note that the reason that Model Code is not plotted for all number of cycles is because the formulas in Model Code does not account for short cycle fatigue with N < 10 000 cycles.

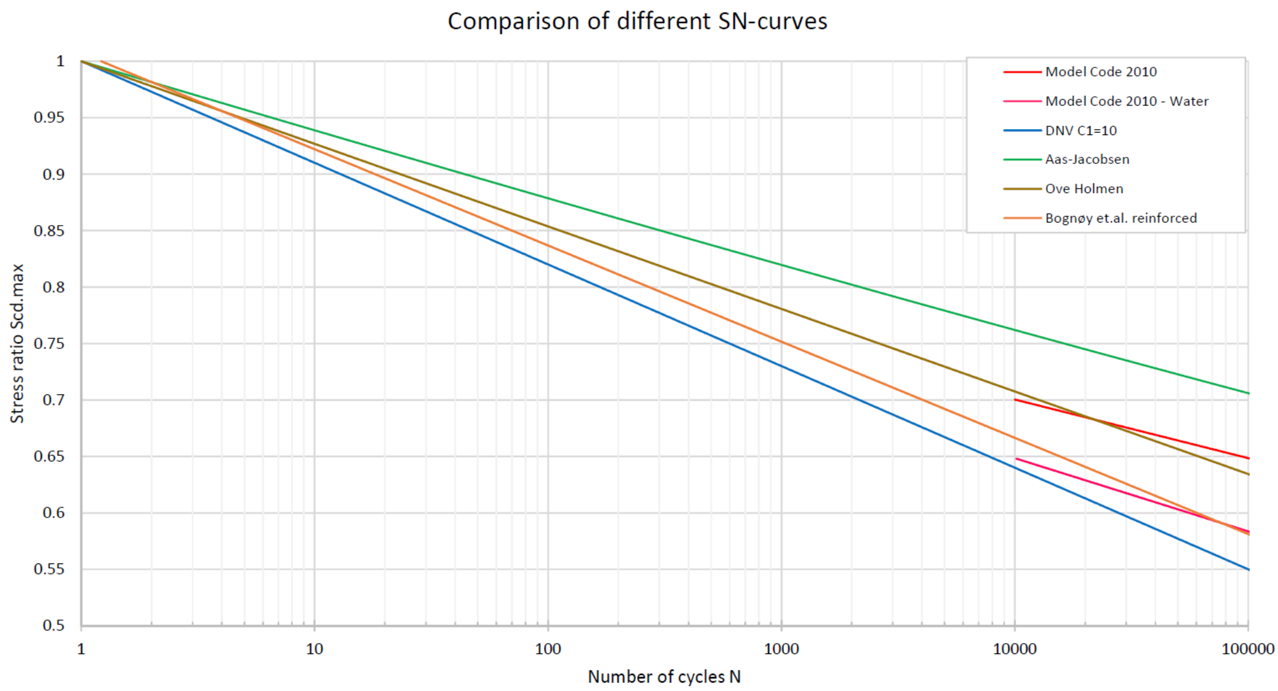

Figure 34: SN-curve for concrete structures by different calculations

As Bognøy et.al. concluded in their thesis, the environmental effect of a structure submerged in water has significant impact on its fatigue life. Though there are many formulas for calculating fatigue life, few consider the effect that the structure is submerged in water. The formulations from DNV-OS-C502 takes this into account by setting the value of C_1=10 and with a suggestion form DNVGL-ST-0126, Model Code can account for this by raising the number of cycles N_i to the power of 0.8 (i.e. $N_i^{0.8}$). However, Model Code does not account for short cycle fatigue with N < 10 000 cycles. From Figure 34 one can see that Model Code with respect to water is far from the range of S_{cd} = 0.7, and Model Code can thus not be used for estimating fatigue life of the test specimens. From their thesis Bognøy *et. al.* found that calculation from DNV-OS-C502 with respect to unreinforced structures submerged in water conform fairly well with their test results. It is therefore conceivable that DNVs formulations are good estimates for life cycles of the test specimens in this thesis. Based on the findings from Bognøy et.al. and the large spread between different formulas this thesis will mainly focus on DNV-OS-C502 and results from Bognøy et.al. for estimates and comparison.

5.3.2 Expected fatiuge life

With the use of DNVs formulation for structures submerged in water (C1 = 10) and a load level $S_{cd.max}$=0.7 the expected fatigue life is calculated for specimens A, B and C similarly giving 2154 expected cycles to failure. The standard deviation F_{SD} of the specimen capacity F_{max} gives a possible deviation of load level, leading to an expected fatigue life with a varying range. As seen from Table 12 the upper and lower end of the range varies for the different specimen types but are in the approximate range from 1000 to 4000 cycles.

Specimen type	Capacity, F_{max} [kN]	Standard deviation [kN]	Load level, $S_{cd.max}$		Number of cycles, N	
A	638.335	22.86	Upper	0.726	Upper	4002
			Mean	0.7	Mean	2154
			Lower	0.676	Lower	1108
B	621.57	22.16	upper	0.726	Upper	3991
			mean	0.7	mean	2154
			lower	0.676	lower	1111
C	634.75	27.55	upper	0.732	Upper	4538
			mean	0.7	mean	2154
			lower	0.671	lower	956

Table 12: Expected fatigue life of specimen A, B and C with an upper and lower range.

6 Static test results

6.1 Concrete strength and residual tensile strength

Test results from the 33 test cubes are plotted in Figure 35, where the 15 cubes of fiber reinforced concrete are plotted as blue dots and the 18 of standard concrete as orange dots. A regression line is calculated for the two concrete mixes to get an approximation of their strength development. It is known from concrete technology that neither the compressive nor the tensile strength of concrete will develop linearly. The strength development of concrete will depend on many factors, but in general the strength will develop quickly in the beginning slowing down with increasing time. For that reason, the regression lines representing the development in the concrete strength are calculated using cubic polynomials as shown in Figure 35.

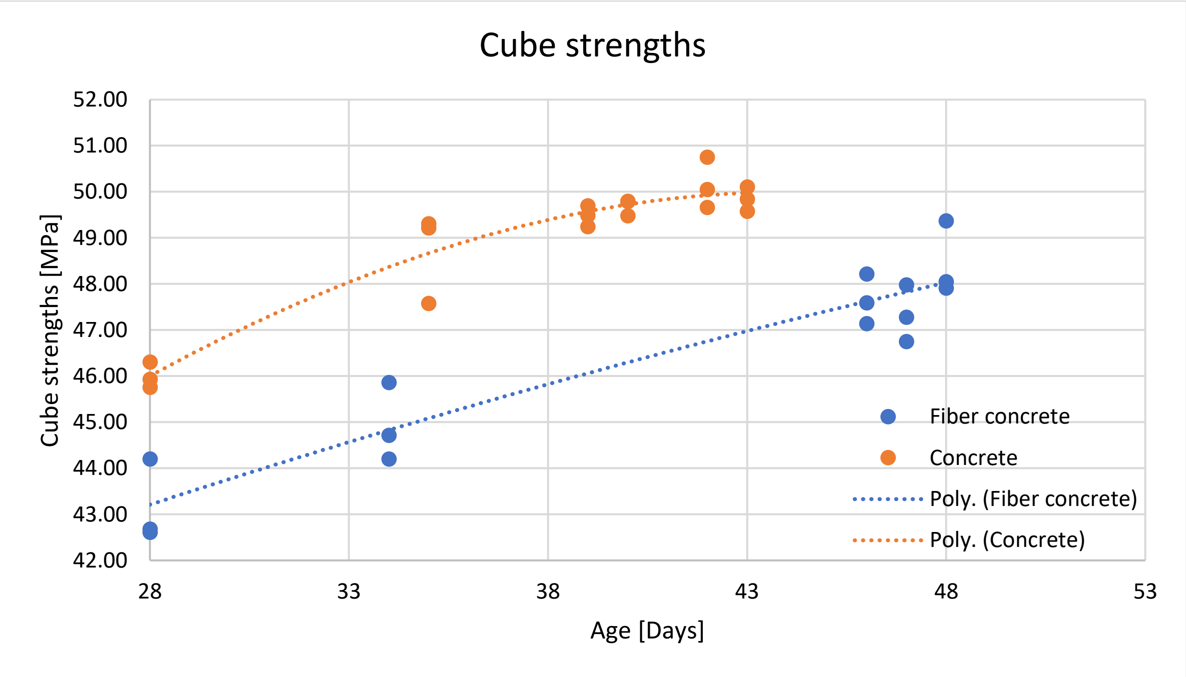

Figure 35: Cube strength of each test-cube.

For every testing day conducted the average cube strength of the 3 test cubes can be seen in Table 13, giving the reference concrete strength of each test specimen tested at the same date. In the calculations for the test specimens the cylinder strength is used rather than the cube strength. The cylinder strengths are calculated as 0.8 times the cubic strength.

28 days testing:	Date	Cube strength [MPa]	Calculated cylinder strength [MPa]
Normal concrete	14-Mar	46.00	36.80
Fiber concrete	14-Mar	43.16	34.53
Static testing:			
A1-A3 & B1-B3	21-Mar	48.70	38.96
C1-C3	20-Mar	44.93	35.94
Dynamic testing:			
A4	28-Mar	50.15	40.12
A5 & A6	29-Mar	49.84	39.87
B4	25-Mar	49.48	39.58
B5 & B6	26-Mar	49.69	39.75
C4	1-Apr	47.65	38.12
C5	2-Apr	47.34	37.87
C6	3-Apr	48.44	38.75

Table 13: Average concrete strength of test-specimens.

In addition to the test-cubes some test-beams were also tested to get the residual tensile strength of the FRC. The test-beams were tested according to the standardized testing procedure given in NS-EN 14651. A total of 3 test-beams were tested and then the mean value of these were further used in the calculations. When testing the beams, the CMOD-value was measured and the test was stopped at CMOD= 2,5mm. Further the relation between CMOD and displacement given in Equation(32) was used to find the applied force. The table given below shows the calculated applied force at CMOD=2,5mm as well as the residual flexural tensile stresses and the residual tensile stresses of the 3 beams.

Test beams	Force at CMOD= 2,5mm [kN]	Residual flexural tensile strength [MPa]	Residual tensile strength [MPa]
Test-beam 1	8,6	2,93	1,09
Test-beam 2	14,2	4,85	1,79
Test-beam 3	8,7	2,92	1,08
Mean value		3,57	1,32
Standard deviation		0,90	0,33

Table 14: Residual flexural tensile stress and residual tensile stress of test-beams.

6.2 Static capacities

6.2.1 General

In this part the results from the static tests of specimen type A, B and C are presented. The following parts shows the static capacity of each specimen type as well as the calculated mean value and standard deviation of the three specimens within each group to see the spread in the results. the respective load ratios are calculated as maximum load capacity of the specimen divided by the expected/calculated capacity. As earlier mentioned, the concrete strength continued to increase after 28 days. Since the expected static capacities of the specimens are all based on a strength calculation using cylinder strength at 28 days the expected maximum load is multiplied with the percentage increase of cylinder strength at the time of testing.

6.2.2 Specimen type A: Minimum reinforcement

In the table below the static results for specimen type A are given.

Specimen	Cylinder strength at test-date [MPa]	Cylinder strength increase	Expected maximum load [kN]	Maximum load [kN]	Load ratio	Test date
A1	38,96	1,06	573,42	657,54	1,15	21.03.19
A2	38,96	1,06	573,42	651,30	1.14	21.03.19
A3	38,96	1,06	573,42	606,20	1.06	21.03.19
Mean value [kN]				638,35	1,11	
Standard deviation [kN]				22,87	0,04	

Table 15: Static rest results for specimen type A.

As seen in Table 15 specimens A1-A3 had an average static capacity of 638,35kN, which means a strength increase of 11% compared to the precalculated static capacity of 573,42kN (see Appendix A1). From the results of Furnes & Hauge and Bognøy et.al. this slight increase in capacity is expected for unreinforced specimens, and the results confirm that theory of partially loaded areas and equations from Model Code 1990 are conservative. Even though the reinforcement was located in the theoretical compression zone it is possible that the reinforcement did contribute to the capacity increase.

Capacities from specimens A1-A3 had a standard deviation of 22.87kN which is equivalent of 4% of the capacity. This is a relatively low standard deviation considering that only three specimens were tested statically. Optimally a higher number of specimens should be tested to get a better statistical basis and one could therefore question the validity of the standard deviation on the basis of too few test specimens. When only three specimens are tested one can therefore argue that the highest and lowest value in the test series would be a better choice to indicate the spread than a standard deviation. Based on these few specimens the fact that two of the capacities are within 6kN to each other while the third differs with approximately 50kN might also give a small indication that the actual capacity lies closer to 650kN.

6.2.3 Specimen type B: No reinforcement

In the table below the static results for specimen type B are given.

Specimen	Cylinder strength at test-date [MPa]	Cylinder strength increase	Expected maximum load[kN]	Maximum load[kN]	Load ratio	Test date
B1	38,96	1,06	573,42	628,74	1,10	21.03.19
B2	38,96	1,06	573,42	591,57	1,03	21.03.19
B3	38,96	1,06	573,42	644,40	1,13	21.03.19
Mean value [kN]				621,57	1,09	
Standard deviation [kN]				22,16	0,04	

Table 16: Static test-results for specimen type B.

As seen in Table 16, specimens B1-B3 had an average static capacity of 621,57kN, which means an average strength increase of 9% compared to the precalculated static capacity of 573,42kN (see Appendix A1). As mentioned in section 6.2.2 this is expected as the results of Furnes & Hauge and Bognøy et.al. also show this trend for unreinforced specimens.

Capacities from specimens B1-B3 had a standard deviation of 22.16kN which is equivalent of 4% of the total capacity. This is a relatively low standard deviation considering the low number of specimens tested. Looking at the spread in capacities one can see similar trend as for specimen type A where the difference between B1 and B2 being twice the difference between B1 and B3, however the spread is much more even than for specimen A.

Also here it could be discussed whether the standard deviation gives a good representation of the spread for such few measurements, however Furnes & Hauge and Bognøy et.al. tested unreinforced specimens similar to specimen type B. Results from Furnes & Hauge show an increase of 22% with a standard deviation of 6%, however they did not conduct static testing in water, and the results are unfortunately not directly comparable. Bognøy *et. al.* did test their specimens under similar conditions as specimen type B, and their results of the unreinforced specimens are directly comparable to results of specimen B. Table 17 show the static capacity of specimen 1-3 tested by Bognøy *et. al*. with the respectable cylinder strength and calculated load ratio.

Static capacity (Bognøy et.all)			
Specimen	**Maximum load[kN]**	**Cylinder strength [MPa]**	**Load ratio**
Specimen 1	552,72	33,11	1,14
Specimen 2	460,64	33,73	0,93
Specimen 3	504,04	33,73	1,02
Mean value [kN]	505,80		1,03
Standard deviation [kN]	37,60		0,09

Table 17: Static test results of unreinforced specimens tested by Bognøy et. al. (Bognøy, et al., 2014)

As given in Table 17, Bognøy et.all got much lower static capacities than specimen B1-B3 because the concrete strength is different. To directly compare the results between the two test-series it is better to use the load ratio because it is independent of the concrete strength. Results from Bognøy *et. al.* show a mean value resulting in a capacity increase of 3% witch is slightly lower than the 9% from B1-B3. Their highest value at a capacity increase of 14% is close to the highest value B3 at 13%. Specimen 1-3 from Bognøy *et. al.* have a standard deviation of 9% with an even spread where the difference between specimen 2 and 3 is approximately the same as the difference between specimen 1 and 3. Compared with the results from specimen type B the results from Bognøy *et. al.* are very reasonable, and it is therefore possible to add all the measurements into one series. By utilizing all 6 test results in one series the new mean load ratio would be 1,06 resulting in a capacity increase of 6% with a standard deviation equal to 7% of the capacity. This new mean value and standard deviation would be more reliable for specimens of type B than the beforementioned mean value from B1-B3 due to the higher number of tests.

6.2.4 Specimen type C: Fiber reinforced

In table below the results from the static testing of specimen type C are given.

Specimen	Cylinder strength at test-date [MPa]	Cylinder strength increase	Expected maximum load [kN]	Maximum load [kN]	Load ratio	Test date
C1	35,94	1,04	527,90	619,71	1,17	20.03.19
C2	35,94	1,04	527,90	673,39	1,27	20.03.19
C3	35,94	1,04	527,90	611,15	1,16	20.03.19
Mean value [kN]				634,75	1,20	
Standard deviation [kN]				27,55	0,05	

Table 18: Static test-results for specimen type C.

As seen in Table 18 specimens C1-C3 had an average static capacity of 634,75kN, which means a strength increase of 20% compared to the precalculated static capacity of 527,90kN. An increase in static capacity is expected because fiber reinforcement will give an increased capacity of an uncracked cross section. This increase is not accounted for in the calculations because there is no reliant way of calculating the increased tensile capacity due to fibers, and the calculations therefore only considers a cracked cross section.

Capacities from specimens C1-C3 had a standard deviation of 27.55kN which is equivalent of 5% of the capacity. This is a relatively low standard deviation considering that only three specimens were tested statically. Due to the uncertainties related to fiber orientation factor and fiber distribution it would not be surprising if specimens C1-C3 had a relatively high standard deviation, however there are no indications of this being an issue for such small specimens based on the standard deviation. The spread in results show C1 and C3 with approximately 9kN difference while C1 and C2 have a difference of approximately 54kN which might give a small indication that C2 may be the specimen with the most favorable fiber orientation and the mean capacity for specimen type C lies closer to 620kN.

6.2.5 Comparison of specimen type A, B and C

In table below the results from the mean values and the standard deviation of the load ratios for specimen type A, B and C is given.

Specimen type	Mean value	Standard deviation
A1-A3	1,11	0,04
B1-B3	1,09	0,04
B + Bognøy et.al.	1,06	0,07
C1-C3	1,20	0,05

Table 19: Mean value of load ratio and standard deviation for specimen type A, B and C.

As shown in Table 19, partially loaded area of unreinforced specimens (type B) show an increase of 9% in capacity compared to capacity of the loaded area, however when including results from Bognøy et.al. the increase is reduced to 6%. Specimen type A was shown to have a capacity 11% higher than loaded area. If capacity increase due to partially loaded area is 6% then it would be reasonable to assume that the remaining 5% is due to the minimum reinforcement. However, due to few test specimens, and the standard deviation from unreinforced specimens overlapping the load ratio from minimum reinforcement the effect of the minimum reinforcement is very uncertain.

From these results, partially loaded areas of fiber reinforced specimen (type C) is shown to have the highest load ratio of 1,2. If capacity increase due to partially loaded area is 6% then it would be reasonable to assume that the remaining 14% is due to the fiber reinforcement. This represents an increase of 8% compared to minimum reinforced specimens and 13% compared to unreinforced specimens. Even though specimen type C had the highest load ratio, specimen type C is also in the category with the highest uncertainty which will affect the results. This is especially true for full scale castin.

6.3 Force-displacement relation

6.3.1 General

To get an indication of the ductility of the specimens, a force-displacement diagram of each of the specimens' types are plotted. In the plots of the force-displacement relations, the applied force is plotted against the average displacement measured by the LVDTs. An alternative would be to use the stroke displacement measured in the machine, however this displacement also includes the deformation of the machine and rig setup. Because of this, the displacement measured in the machine would not indicate the strain in the concrete.

6.3.2 Specimen type A: Minimum reinforcement

In Figure 36 the force-displacement diagram of specimens A1-A3 is shown.

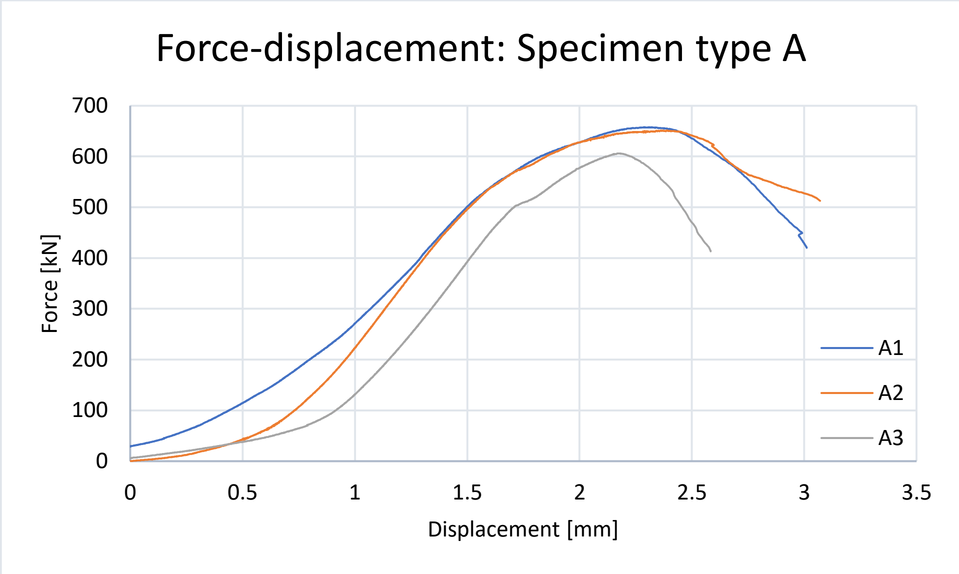

Figure 36:Force-displacement curves for specimen type A

The three curves had some different slopes in the beginning of the loading. As one can see A3 and A2 have a smaller slope than A1 in the beginning of the load process (around 0-0,5mm of displacement). Since the slope of the curves represents the stiffness of each specimen, this indicates that A2 and A3 use more time to achieve full contact between the load and its top surface, which may be caused by imperfections on the top surface. Theoretically the force-displacement curves should be perfectly linear, but since the top-surfaces of the specimen had some imperfections and the specimen didn't manage to transfer the load perfectly into the specimen, it shows that the curves have a lower slope in the beginning until full contact is established.

When full contact between the load and the top surface was achieved, A2 and A3 seemed to have approximately the same slope (around 1,5mm displacement). Since the slope of the curves indicates the e-modulus or the stiffness of the specimens, this result was expected. This is because the stiffness is expected to be the same for all the three specimens since the same concrete mixture was used for all of them. Even though the axial stiffness of concrete also depends on the cross-sectional area and the height of the specimen, these parameters are also the same for all the 3 specimens.

It seemed like the curve of specimen A3 decreased a bit more quickly than A1 and A2 after reaching the top point of the curve where the capacity of each specimen was reached. This might indicate that A3 had the lowest ductility of the 3 specimens. The concrete is a very brittle material and the concrete in the tensile zone has very low tensile capacity. Therefore, reasonable to think that this ductility comes from the reinforcement in the top, which was placed in the top of each specimen. If the ductility only comes from the reinforcement one could argue that all the 3 curves should have the same slope in the end. This might then indicate that the concrete itself also had some contribution to the ductility.

6.3.3 Specimen type B: No reinforcement

In Figure 37Figure 36 the force-displacement diagram of specimens B1-B3 is shown.

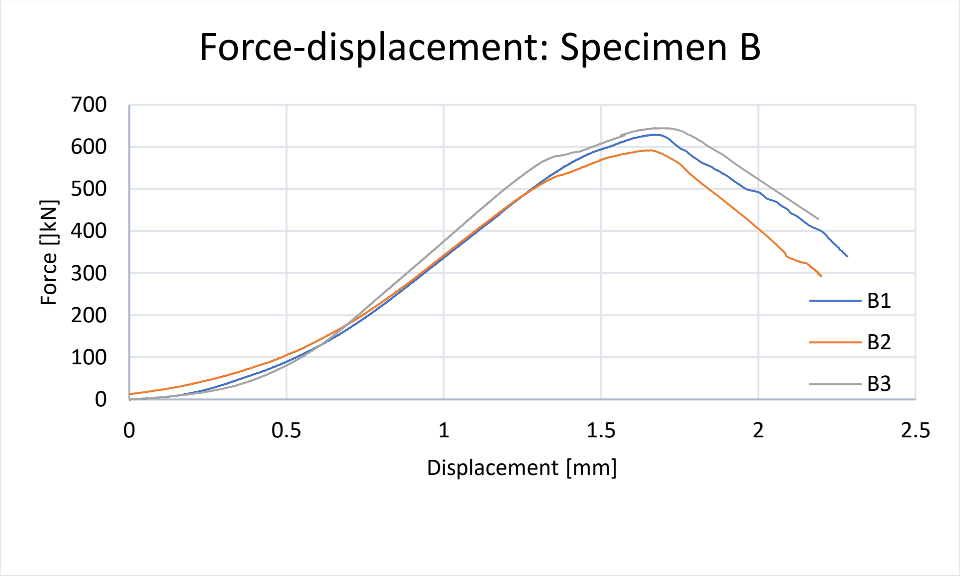

Figure 37:Force-displacement curves for specimen type B.

As shown in Figure 37, the three specimens were almost identical until fracture. This was expected since the same concrete mixture was used for all the 3 specimens. As also seen, they had almost the same stiffness development in the beginning. Further the three specimens have nearly the same slope all the way to the top point of the curve. This indicated that the three specimens have approximately same e-modulus and axial stiffness. This was also expected since the three specimens are equal with respect to both material and geometry. The specimens also had almost the same behavior after reaching the maximum force indicated by the top point of the curve. This indicates that these three specimens had almost the same ductility.

6.3.4 Specimen type C: Fiber reinforcement

In Figure 38 the force-displacement diagram of specimens C1-C3 is shown.

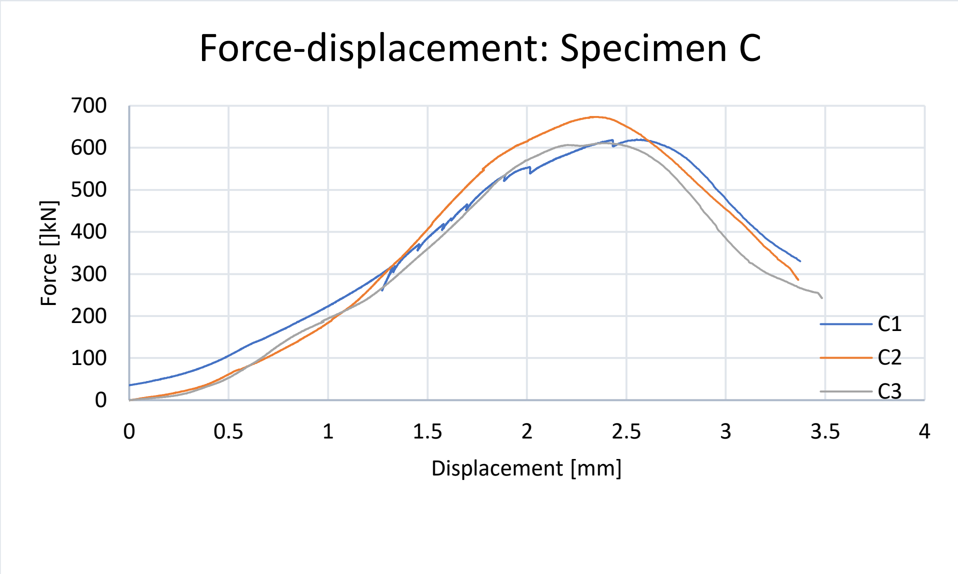

Figure 38:Force-displacement curves for specimen type C.

As seen in Figure 38 the fiber reinforced specimens had curves with small slopes. This indicates that the fibers make the concrete more ductile and that the fiber will decrease the e-modulus of the concrete. The curves follow each other quite well under loading. That indicates that the possible difference in fiber orientation is quite small. The curve of C1 is also a bit uneven towards the top point. This might indicate that the fibers are gradually being pulled out resulting in a sudden stress distribution in the concrete.

6.3.5 Comparison of specimen type A, B and C

In Figure 39 the force-displacement diagram of specimens C1-C3 is shown.

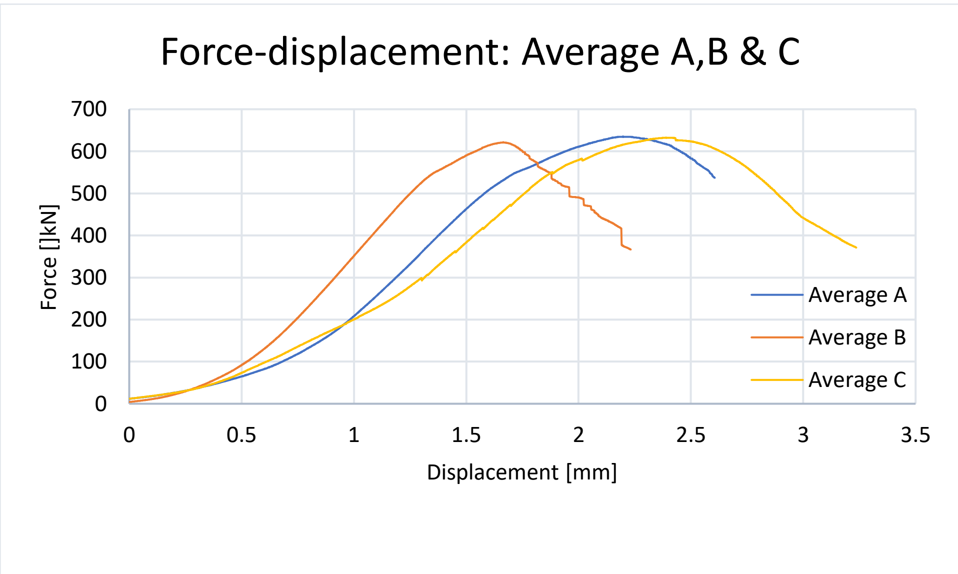

Figure 39: Average curves for force-displacement of specimen type A, B and C.

In Figure 39 shows the average curves of force-displacement of specimen type A, B and C. The result shows that it seems that specimen type C was the most ductile one, specimen type A and then B. The curves for specimen type C were also plotted longer to show the ductility. The fact that C is the most ductile one is fairly as expected since the steel fibers in will contribute to the crack bridging in the concrete. The reinforcement in A might also give some contribution to the ductility. The added minimum reinforcement in A will give some contribution to the ductility, but not as much as the fibers. The final specimen type, B, was shown to have a much more brittle fracture than A and C. Specimen type B starts to increase a little bit faster than A and C. The brittle behavior of specimen type B was also as expected since these specimens didn't have any reinforcement in the top.

6.4 Strain development in threaded bars and reinforcement

In this part the strain development for each specimen type is presented. The strain diagrams are categorized for each strain gage, SG1, SG2 and SG3, where each strain gage is further plotted for specimen 4-6 in each diagram. The strain diagrams of each specimen type show how the strains in SG1, SG 2 and SG 3 in each specimen. The plots show the strain in each strain gage related to the applied force to the specimen.

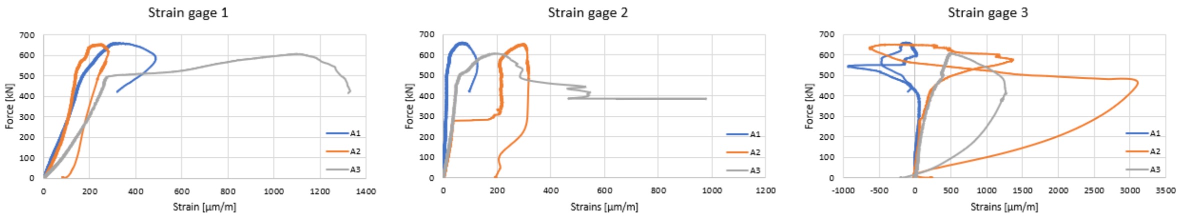

Figure 40: Strain development for specimen type A.

First, the strain development of specimen type A is presented. As shown, the strains in SG1 and SG2 were almost constant until a load of around 500kN, which is 78% of the mean static capacity. After around 500kN the reinforcement was activated and carried the increase until the load until yielding capacity of the steel was reached.

SG3 seemed to start the yielding a bit earlier than SG1 and SG2. SG3 seemed to reach yielding around 440kN, which is around 88% of the strain gages mounted on the threaded bars. The strains in the threaded bars were also expected to be lower since the load spread was in the direction perpendicular to the bars.

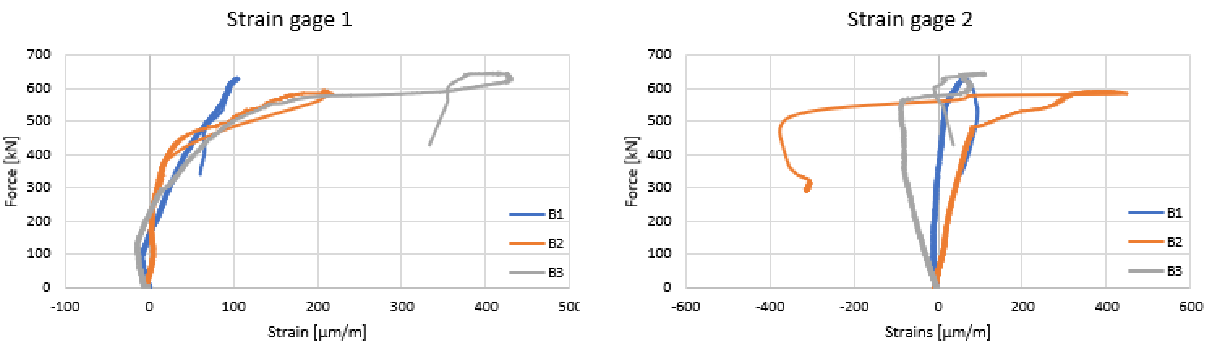

Figure 41: Strain development for specimen type B.

Further, the strain development of specimen type B is presented. As earlier mentioned, specimen type B didn't have any minimum reinforcement in the top. Therefore, only two strain gages were mounted, in the same place as for specimen type A. Also, here SG1 and SG2 are shown to

As shown, the strains in SG1 and SG2 were almost constant until a load of around 500kN, which is 78% of the mean static capacity. After around 500kN the reinforcement was activated and carried the increase until the load until yielding capacity of the steel was reached.

SG3 seems to start the yielding a bit earlier SG1 and SG2. As shown in Figure 41 SG3 seems to that yielding around 440kN, which is around 88% of the strain gages mounted on the threaded bars. The strains in the threaded bars were also expected to be lower since the load spread was in the direction perpendicular to the bars.

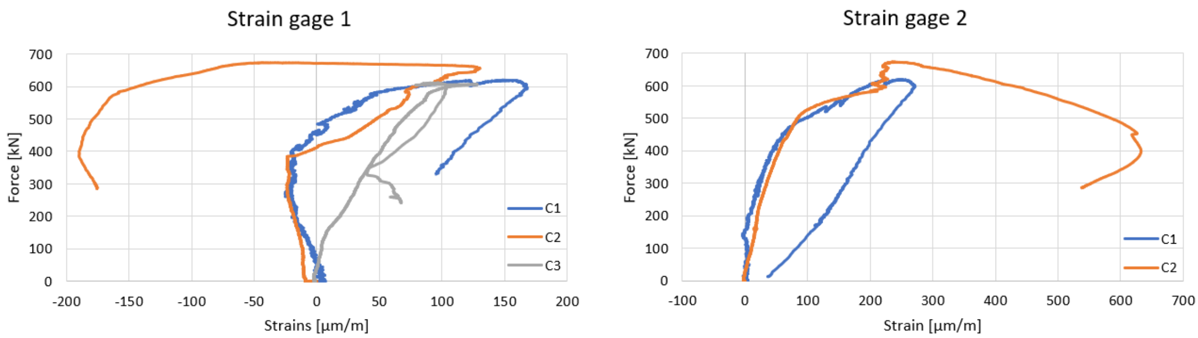

Figure 42: Strain development for specimen type C.

Finally, the strain development in specimen type C is presented. As shown, the strains in SG1 and SG2 were almost constant until a load of around 500kN, which is 78% of the mean static capacity. After around 500kN the reinforcement was activated and carried the increase until the load until yielding capacity of the steel was reached.

SG3 seems to start the yielding a bit earlier SG1 and SG2. As shown in Figure 42 SG3 seems to that yielding around 440kN, which is around 88% of the strain gages mounted on the threaded bars. As seen in the figures, the curves contain some irregularities, especially for C1. As for the force-displacement curve and the LVDT-displacement curve this might indicate the activation of the fibers.

6.5 Crack patterns and local crushing

The formation of cracks and crushing of concrete for specimens subjected to static loading is a fairly quick proses. For the 9 specimens that were tested statically all the specimens had roughly the same cracks patterns (see Appendix D). It starts with crushing of the uneven loading surface until full contact is reached. During this early phase spalling of cover concrete directly under the loaded area often occurred as shown in Figure 43.

Figure 43: Spalling of concrete and local crushing under loaded area of specimen A1. Also showing vertical cracking in compression zone.

For increasing load, local crushing directly under the loading plate was observed with large cracks forming mostly vertical in the compression zone illustrated in Figure 43. Simultaneously a main crack pattern formed to one side often forming a line from center of loaded area downward at an angle to the underside of the second threaded bar and then to the top of the third threaded bar continuing towards the bottom corner or lower edge of the specimen, as drawn in a red line in Figure 44.

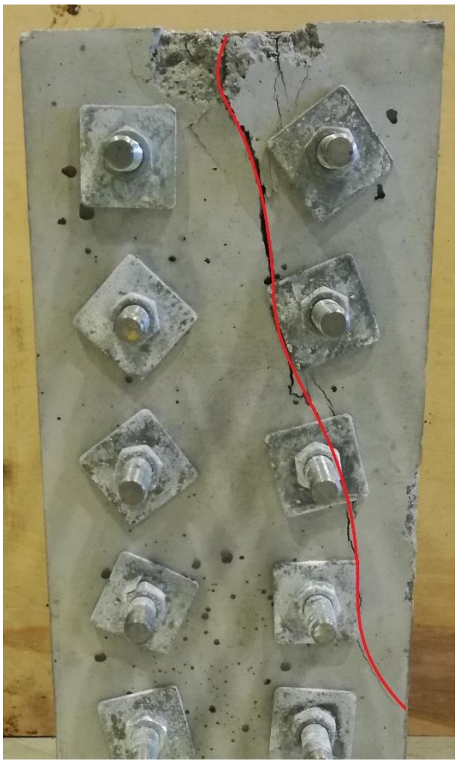

Figure 44: Main crack direction for specimen B1 shown as red line.

7 Dynamic test results

7.1 Fatigue capacity

7.1.1 Specimen A: Minimum reinforcement

Specimen A4 to A6 was tested with dynamic loading from the 28th to the 29th of march. The loading applied during the test is shown in Table 20, where the adjusted static capacity was calculated using the mean static capacity of specimen type A multiplied by the percentage increase in cylinder strength.

Test specimen	Test date	Cylinder strength at test-date [MPa]	Cylinder strength increase	Adjusted static capacity [kN]	Dynamic max load [kN]	Dynamic min load [kN]	Dynamic stress level
A4	28.03	40,12	1,030	657,35	457,00	65,00	0,70
A5	29.03	39,87	1,023	653,26	457,00	65,00	0,70
A6	29.03	39,87	1,023	653,26	457,00	65,00	0,70

Table 20: Loading applied to test specimens A4 – A6.

The results form Dynamic testing of specimen type A is presented in Table 21, with an average number of cycles to failure at 7148 cycles and a standard deviation of 3659 cycles. The average number of cycles to failure is more than 3 times higher than the expected number at approximately 2100 cycles. The average number of cycles to failure is also above the expected upper boundary of the range at approximately 4000 cycles, though results from A5 is within this range.

Test specimen	Dynamic stress level	Cycles to failure	Average cycles to failure	Standard deviation
A4	0,70	5576	7148	3659
A5	0,70	3664		
A6	0,70	12204		

Table 21: Number of cycles to failure of specimen A4 – A6 with stress level 0.7.

In Figure 45 the results are plotted in a logarithmic scale alongside DNVs formulation. Here the formulation from DNV (see Equation (26)) with respect to water, a C_1 value of 10, is plotted in blue, and the expected value and range for the number of cycles to failure is illustrated with the black solid and dotted lines.

$$logN = C_1 \frac{\left(1 - \frac{\sigma_{c.max}}{f_{rd}}\right)}{\left(1 - \frac{\sigma_{c.min}}{f_{rd}}\right)} \tag{26}$$

On the logarithmic scale the spread in results shown as green dots in Figure 45 is about the same as the expected range, though the values are somewhat higher. By calculating a non-linear regression line for specimen type A with the same formulation as DNV and C_1 as a varying factor the results from A4 to A6 will give $C_1 = 11.40$ (± 0.65). Even though the test sample is extremely small the standard deviation is relatively low, and the results gives an indication of higher fatigue life than DNVs suggestion of $C_1 = 10$ as evident in Figure 45.

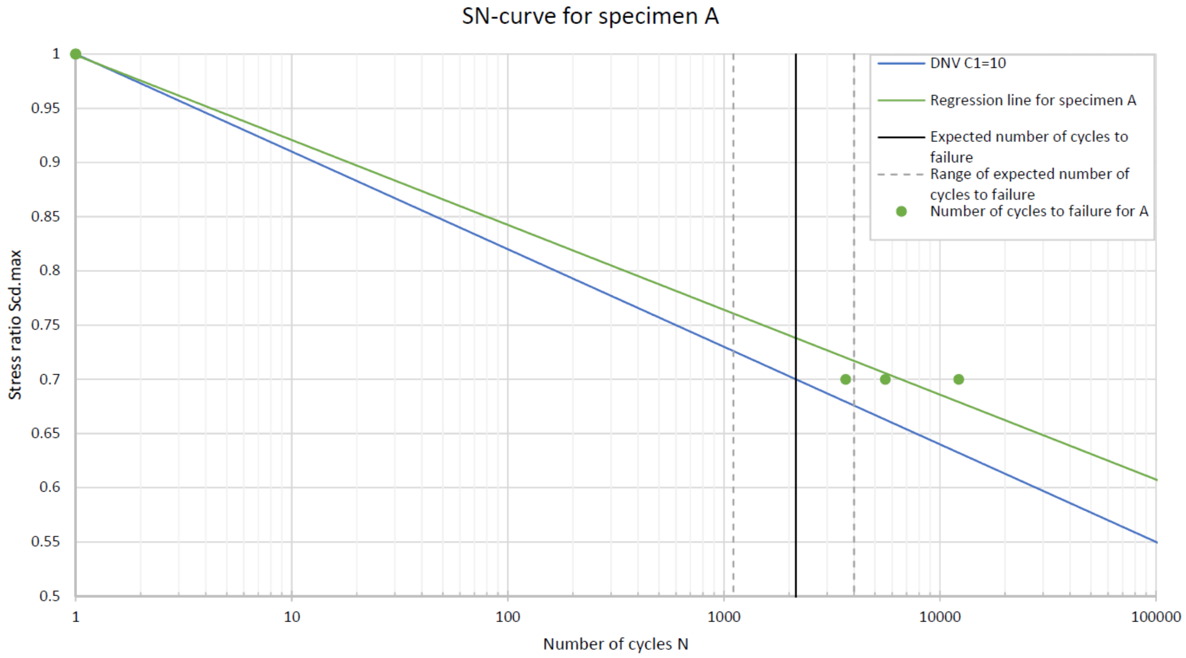

Figure 45: SN-curve for specimen type A compared to DNV.

Bognøy et.al concluded in their thesis that the effect of partially loaded area in fatigue loading is not present when there is no splitting reinforcement. One can therefore assume that the higher fatigue life of specimen type A is due to the minimum reinforcement. Bognøy et.al. conducted their thesis with sufficient splitting reinforcement, and a regression line from their result is plotted in Figure 46 alongside the regression line for specimen type A and DNV. From Figure 46 it is evident that specimen type A has a slightly higher fatigue life than the reinforced specimen form Bognøy et.al. It is important to note that the reinforced specimens from Bognøy et.al has a higher static capacity than specimen A, with a load ratio of 1.48 compared to 1.11. Thus, at the same load $F_{load.max}$ the reinforced specimens from Bognøy et.al will have a higher fatigue life, but at the same stress level $S_{cd.max}$ specimen type A will have a higher fatigue life as depicted in Figure 46. This may be caused by the extra reinforcement increasing the number of crack initiation points leading to more crack propagation, however with such few test samples it is important to stress the uncertainty of the results, and this perceived increase in fatigue life may diminish with sufficient sample data.

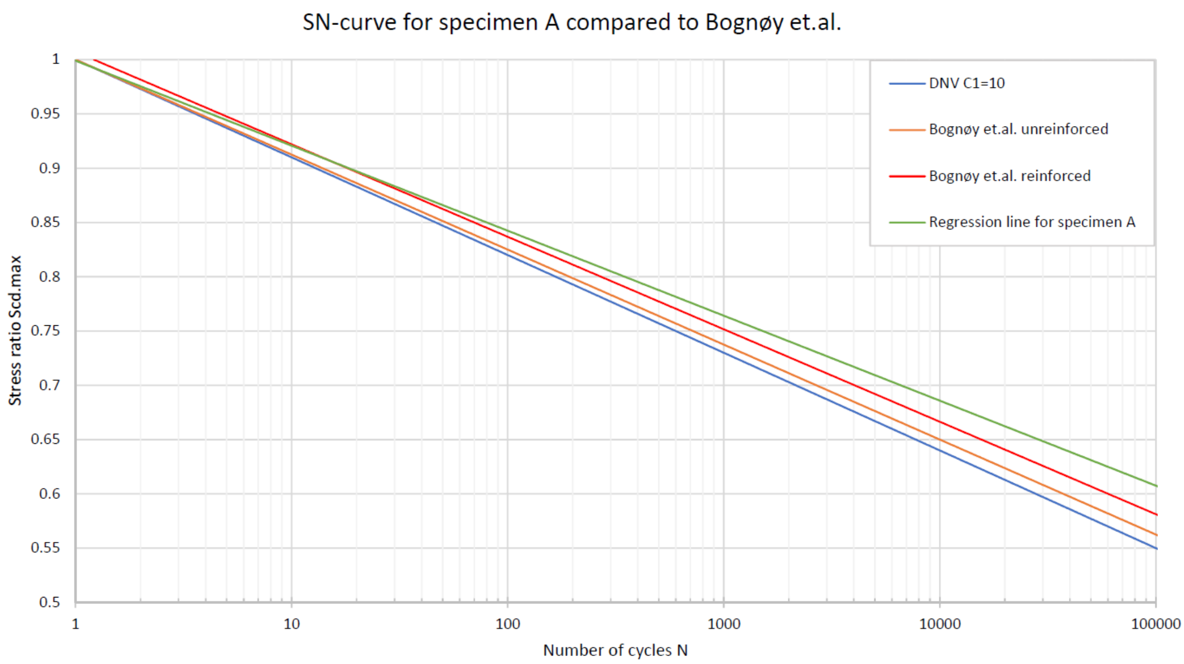

Figure 46: SN-curve for specimen type A compared to Bognøy et.al.

7.1.2 Specimen B: No reinforcement

Specimen B4 to B6 was tested with dynamic loading from the 25th to the 26th of march. The loading applied during the test is shown in Table 22, where the adjusted static capacity was calculated using the mean static capacity of specimen type B multiplied by the percentage increase in cylinder strength.

Test specimen	Test date	Cylinder strength at test-date [MPa]	Cylinder strength increase	Adjusted static capacity [kN]	Dynamic max load [kN]	Dynamic min load [kN]	Dynamic stress level
B4	25.03	39,58	1,016	631,46	442,00	63,00	0,70
B5	26.03	39,75	1,020	634,17	445,00	6,300	0,70
B6	26.03	39,75	1,020	634,17	445,00	63,00	0,70

Table 22: Loading applied to test specimens B4 – B6.

The results form Dynamic testing of specimen type B is presented in Table 23, with an average number of cycles to failure at 852 cycles and a standard deviation of 455 cycles. The average number of cycles to failure is approximately half of the expected number at 2154 cycles. The average number of cycles to failure is also below the expected lower boundary of the range at 1111 cycles, though results from B5 is within this range.

Test specimen	Dynamic stress level	Cycles to failure	Average cycles to failure	Standard deviation
B4	0,70	733	852	455
B5	0,70	1459		
B6	0,70	364		

Table 23: Number of cycles to failure of specimen B4 – B6.

The results are plotted in a logarithmic scale alongside DNVs formulation in Figure 47. Here the formulation from DNV (see Equation (26)) with respect to water, a C_1 value of 10, is plotted in blue, and the expected value and range for the number of cycles to failure is illustrated with the black solid and dotted lines.

$$logN = C_1 \frac{\left(1 - \frac{\sigma_{c.max}}{f_{rd}}\right)}{\left(1 - \frac{\sigma_{c.min}}{f_{rd}}\right)} \tag{26}$$

Even though the results shown as purple dots in Figure 47 are lower than the expected values on the logarithmic scale the spread is only slightly larger than the expected range. By calculating a non-linear regression line for specimen type B with the same formulation as DNV and C_1 as a varying factor the results from B4 to B6 will give C_1 = 8.59 (± 0.74). Even though the test sample is extremely small the standard deviation is relatively low, and the results gives an indication of lower fatigue life than DNVs suggestion of C_1 = 10 as evident in Figure 47.

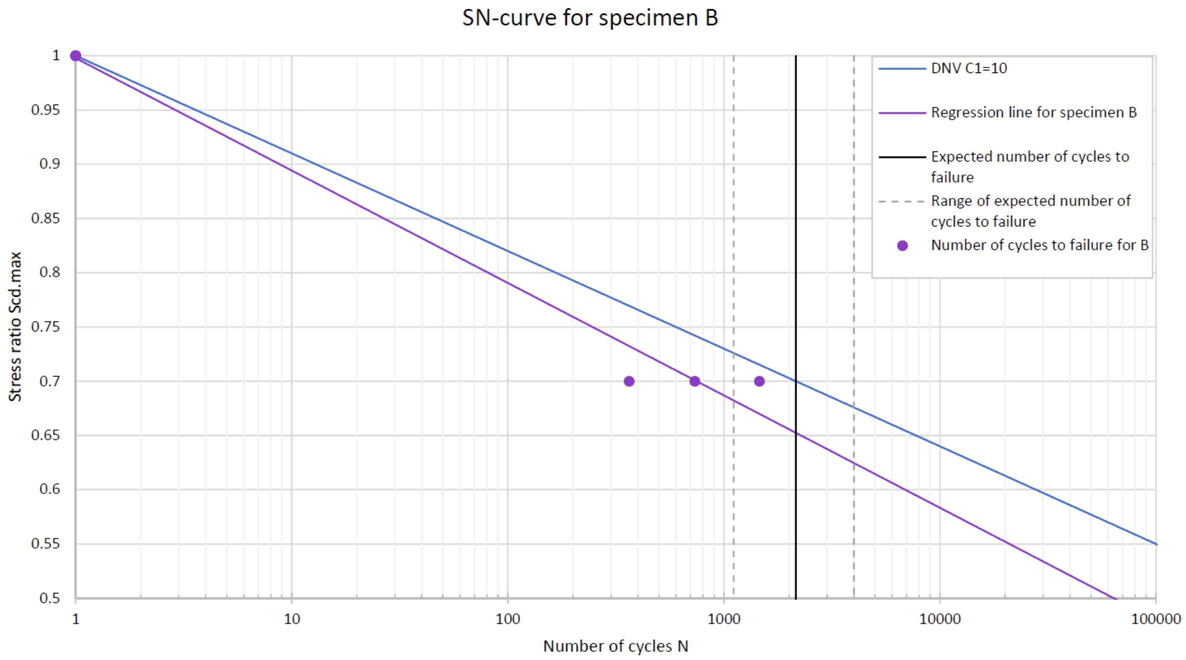

Figure 47: SN-curve for specimen type B compared to DNV.

In their thesis Bognøy et.al. conducted 6 dynamic tests of specimens directly comparable to the specimens of type B, and the results from their tests are shown in orange in Figure 48. The results from Bognøy et.al. show no indication that the effect of partially loaded area in fatigue loading leads to reduced fatigue life when there is no splitting reinforcement, as the results from B4 to B6 indicates. There is in fact a rather large discrepancy between the results from specimen type B and from Bognøy et.al. as seen in Figure 48. As discussed in section 6.2.3, due to the small number of test specimens the indicated results may not be reliable, and it is reasonable to increase the test data by including the results from Bognøy et.al. By utilizing the results for all 9 specimens the calculated regression line will have C_1 = 10,04 (± 0.98). Even though the standard deviation cannot be regarded as low, the C_1 factor gives a clear indication that partially loaded area of unreinforced concrete gives no increase in fatigue life.

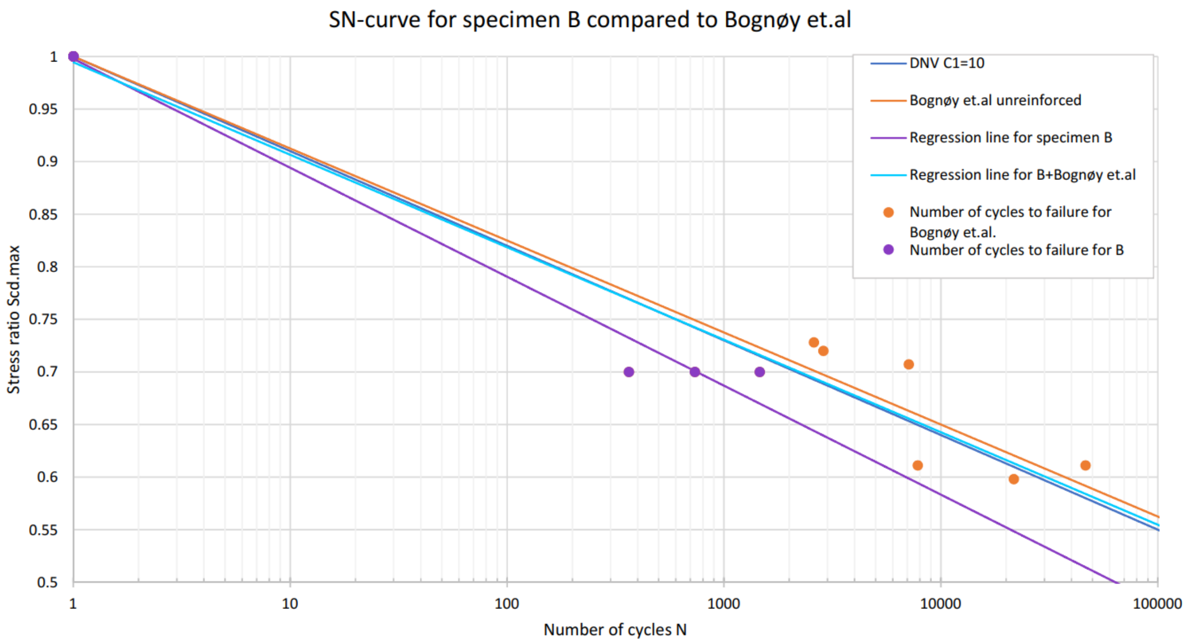

Figure 48: SN-curve for specimen type B compared to Bognøy et.al.

7.1.3 Specimen C: Fiber reinforced

Specimen C4 to C6 was tested with dynamic loading from the 1st to the 3rd of april. The loading applied during the test is shown in Table 24, where the adjusted static capacity was calculated using the mean static capacity of specimen type C multiplied by the percentage increase in cylinder strength.

Test specimen	Test date	Cylinder strength at test-date [MPa]	Cylinder strength increase	Adjusted static capacity [kN]	Dynamic max load [kN]	Dynamic min load [kN]	Dynamic stress level
C4	1.04	38,12	1,061	673,25	471,30	67,30	0,70
C5	2.04	37,87	1,054	668,84	471,30	67,30	0,70
C6	3.04	38,75	1,078	684,38	471,30	67,30	0,69

Table 24: Loading applied to test specimens C4 – C6.

The results form Dynamic testing of specimen type C is presented in Table 25 , with an average number of cycles to failure at 7324 cycles and a standard deviation of 5206 cycles. The average number of cycles to failure is more than 3 times higher than the expected number at approximately 2100 cycles. The average number of cycles to failure is also above the expected upper boundary of the range at approximately 4500 cycles, though results from C5 is within this range, and C6 is relatively close to the upper boundary.

Test specimen	Dynamic stress level	Cycles to failure	Average cycles to failure	Standard deviation
C4	0,70	14441	7324	5206
C5	0,70	2132		
C6	0,69	5400		

Table 25: Number of cycles to failure of specimen C4 – C6.

In Figure 49 the results are plotted in a logarithmic scale alongside DNVs formulation. Here the formulation from DNV (see Equation (26)) with respect to water, a C_1 value of 10, is plotted in blue, and the expected value and range for the number of cycles to failure is illustrated with the black solid and dotted lines.

$$logN = C_1 \frac{\left(1 - \frac{\sigma_{c.max}}{f_{rd}}\right)}{\left(1 - \frac{\sigma_{c.min}}{f_{rd}}\right)} \tag{26}$$

On the logarithmic scale the results shown as yellow dots in Figure 49 are not only higher than expected, but their spread is also larger than the expected range. By calculating a non-linear regression line for specimen type C the results from C4 to C6 will give C_1 = 11.22 (± 1.02). These results gives an indication of higher fatigue life than DNVs suggestion of C_1 = 10 as evident in Figure 49, though the standard deviation is a little on the high side considering the indicated increase in fatigue life.

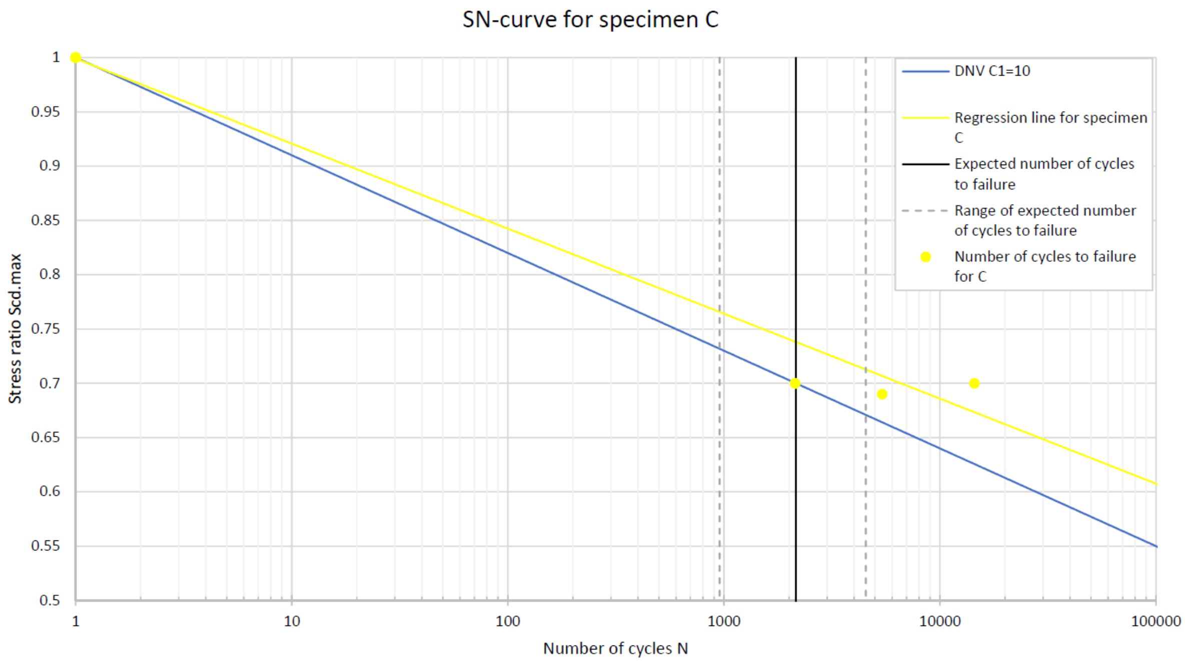

Figure 49: SN-curve for specimen type C compared to DNV.

Bognøy et.al. concluded in their thesis that the effect of partially loaded area in fatigue loading is not present when there is no splitting reinforcement. This is also observed and discussed in Section 7.1.2. One can therefore assume that the higher fatigue life of specimen type C is due to the SFRC. Bognøy et.al. conducted their thesis with sufficient splitting reinforcement, and a regression line from their result is plotted in Figure 50 alongside the regression line for specimen type C and DNV. From Figure 50 it is evident that specimen type C has a slightly higher fatigue life than the reinforced specimen form Bognøy et.al. It is important to note that the reinforced specimens from Bognøy et.al has a higher static capacity than specimen C, with a load ratio of 1.48 compared to 1.20. Thus, at the same load $F_{load.max}$ the reinforced specimens from Bognøy et.al will have a higher fatigue life, but at the same stress level $S_{cd.max}$ specimen type C will have a higher fatigue life as depicted in Figure 50. This may be caused by the SFRC being favorable in fatigue loading, however with such few test samples it is important to stress the uncertainty of the results, and this perceived increase in fatigue life may diminish with sufficient sample data.

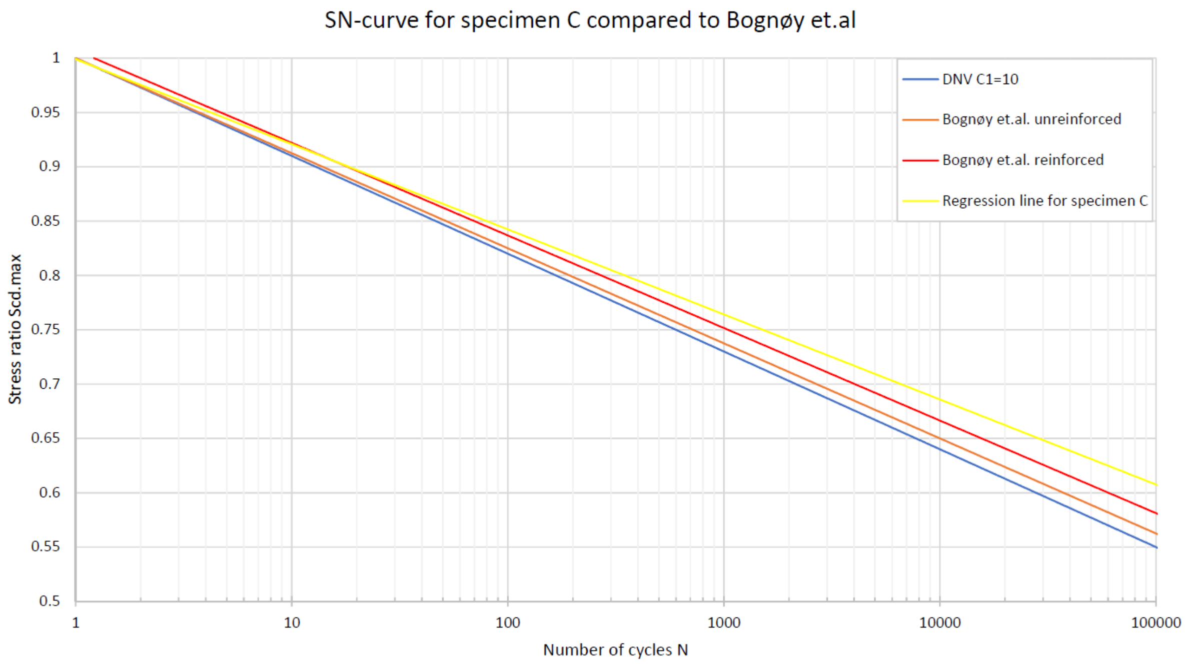

Figure 50: SN-curve for specimen type C compared to Bognøy et.al.

7.1.4 Comparing the specimen type A, B and C

For a direct comparison between the unreinforced, minimum reinforced and fiber reinforced specimens their respective SN-curves have been plotted in Figure 51 alongside DNV. As discussed in Section 7.1.2 the regression line for specimen type B and Bognøy et.al. gives a more precise SN-curve than the results from specimen type B alone. The regression line for specimen type B and Bognøy et.al. is therefore plotted in Figure 51 instead of the regression line for B. From Figure 51 one can see that results from specimen type A and specimen type C are quite close, which will imply that concrete with a minimum reinforcement and fiber reinforced concrete with a residual tensile stress of 1.32MPa gives roughly the same increase in fatigue life.

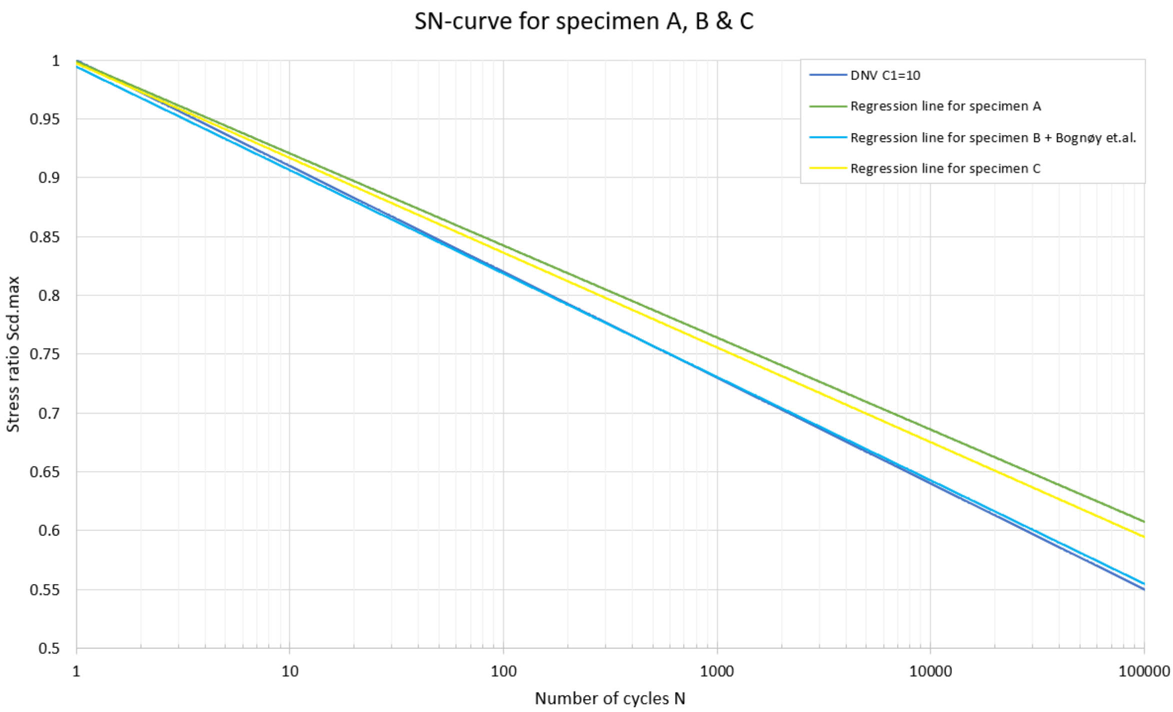

Figure 51: SN curve of Specimen type A, B and C compared to DNV

7.2 Displacement development from stroke during lifecycle

The initial displacement registered during loading to mean load before the dynamic loading is applied is displayed in Table 26. There is a rather large discrepancy in the initial displacement between A4 and the two other specimens of type A. Though the discrepancy is much smaller, the same can be said about C4 compared to C5 and C6. It is believed that this is due to the uneven surface of the loaded area of the test specimens. The initial displacement is measured from a load of 1 kN to mean load. It is therefore reasonable to think that at 1 kN the loading plate is yet not in full contact with the specimen due to the uneven surface. A4 was also the most uneven of the three specimens of type A. Apart from A4, the initial displacement for all the specimens are relatively close and there is no strong indication of a difference between the specimen types.

Specimen	Mean load [kN]	Initial displacement [mm]
A4	261	1.90
A5	261	1.42
A6	261	1.37
B4	252,5	1.46
B5	254	1.59
B6	254	1.38
C4	269,3	1.52
C5	269,3	1.27
C6	269,3	1.33

Table 26: Mean load and initial displacement for specimens subjected to dynamic loading.

During the lifetime of specimens subjected to dynamic loading the three phases of deformation described by Holmen is clearly evident as seen in Figure 52. In Figure 52 the displacement is plotted over the fatigue lifetime of the specimens. In the figure the initial displacement is not accounted for, and the deformation is therefore from the start of dynamic loading, and not the total displacement of the specimen. From Figure 52 one can see the non-linear deformation phase during the first 3% to 5% of the lifetime followed by a linear phase. The non-linear phase at the end is more prominent than the phase in the beginning and amounts to roughly 5% to 8% of the total lifetime.

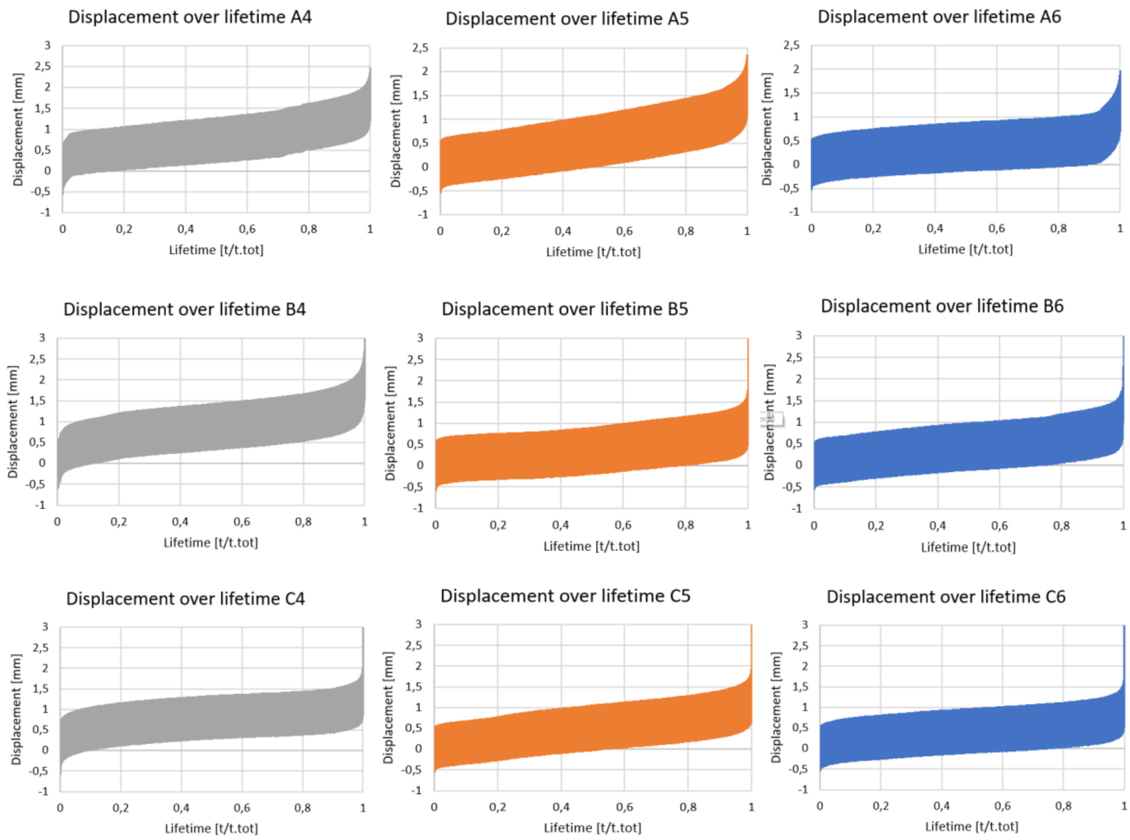

Figure 52: Three phases of deformation during fatigue loading for specimens.

As shown in Figure 52 the linear deformation phase described by Holmen is not always perfectly linear. For instance, specimen A4 has two sudden deformation increases between 70% and 80% of its lifetime, and B5 seems to change to a higher linear deformation rate at around 30% of its lifetime. These uneven developments might give an indication on the crack development in the specimens. For instance, the two sudden deformation increases in specimen A4 might be because that some cracks coalesced into one large crack, though not large enough to cause a final rapture.

For a comparison of the displacement over time it is easier to look at the change in displacement at mean load, which is plotted in Figure 53. The slopes of the second phase of the specimens are fairly similar, and there is no significant difference between the mean slope for all specimen types or the mean deformation during the linear phase. Compared to the other specimens, specimen A4, B4 and C4 have a significantly higher deformation in the first stage. Where A4 has an abrupt end to the first stage. Due to the fact that A4 also was the specimen with the highest initial displacement, this abrupt change might be due to local crushing of an uneven load surface until full contact is achieved. In By looking at the change in displacement at the mean load in Figure 53 it is easier to pinpoint changes like the two sudden deformation increases for specimen A4. One can easily see that A6 has one sudden deformation increase similar to those of A4. This sudden deformation increase is at the start of phase 3 and might be a contributor to the early start of the third phase compared to the other specimens.

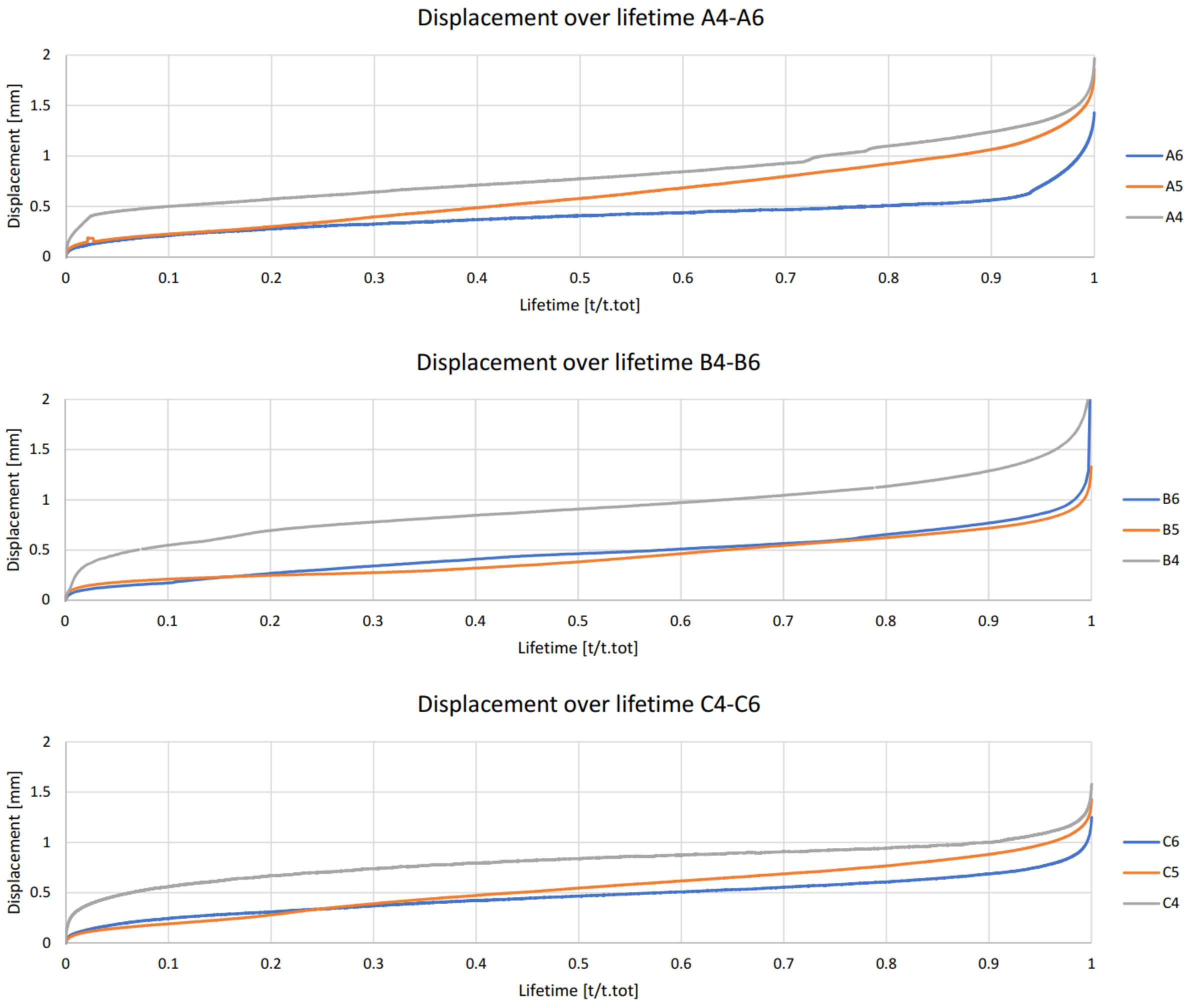

Figure 53: Displacement at mean load over lifetime for specimen A4-A6.

7.3 Displacement development from LVDTs during lifecycle

Due to the specimens being submerged in a water container, the LVDTs had to be placed outside the container, and quite far from the loaded surface. Due to this large eccentricity from the load center the displacements shown in the LVDTs are exaggerated. There is also the problem of placing the LVDTs with precisely the same eccentricity. As mentioned in Section 4.4 local crushing under the loaded area is not always even, and with the cyclic behavior of dynamic loaded specimens this can add up over time. It is therefore concluded that even though the average between the LVDTs shows the same three phase deformation described by Holmen it will be a less accurate for dynamic loading than using the stroke displacement shown in Section 7.2.

As mentioned in Section 4.2 the LVDTs can be used to predict the behavior of the load plane. From Figure 54 one can see that for all the test specimens the change in LVDT 1 is typically in the opposite direction of LVDT 2 and 3. This indicates that the loading plane is tilting in the Y-axes (see Figure 32), and the tilt direction is persistent with the main crack direction of the specimens observed (see Appendix D). This tilt in the Y-axes is also a direct indication of higher local crushing on one side of loading plate, leading to the loading plate slanting towards one side as mentioned in Section 4.2 and further discussed in Section 7.5. Specimens B4 and C4 show an abnormally large spread between LVDT 1 and LVDT 2 compared to the other specimens. However, their development is quite different. B4 has a linear but high divergence from the start, but C4 has a short phase with a large nonlinear divergence at the start followed by a long phase with normal divergence comparative with the other specimens. When taking into account the displacement development of C4 discussed in Section 7.2 the LVDT development in the first phase would be reminiscent of local crushing of an uneven load surface until full contact is achieved. This would also explain the fact that no significant slanting of the loading plate was observed for specimen C4.

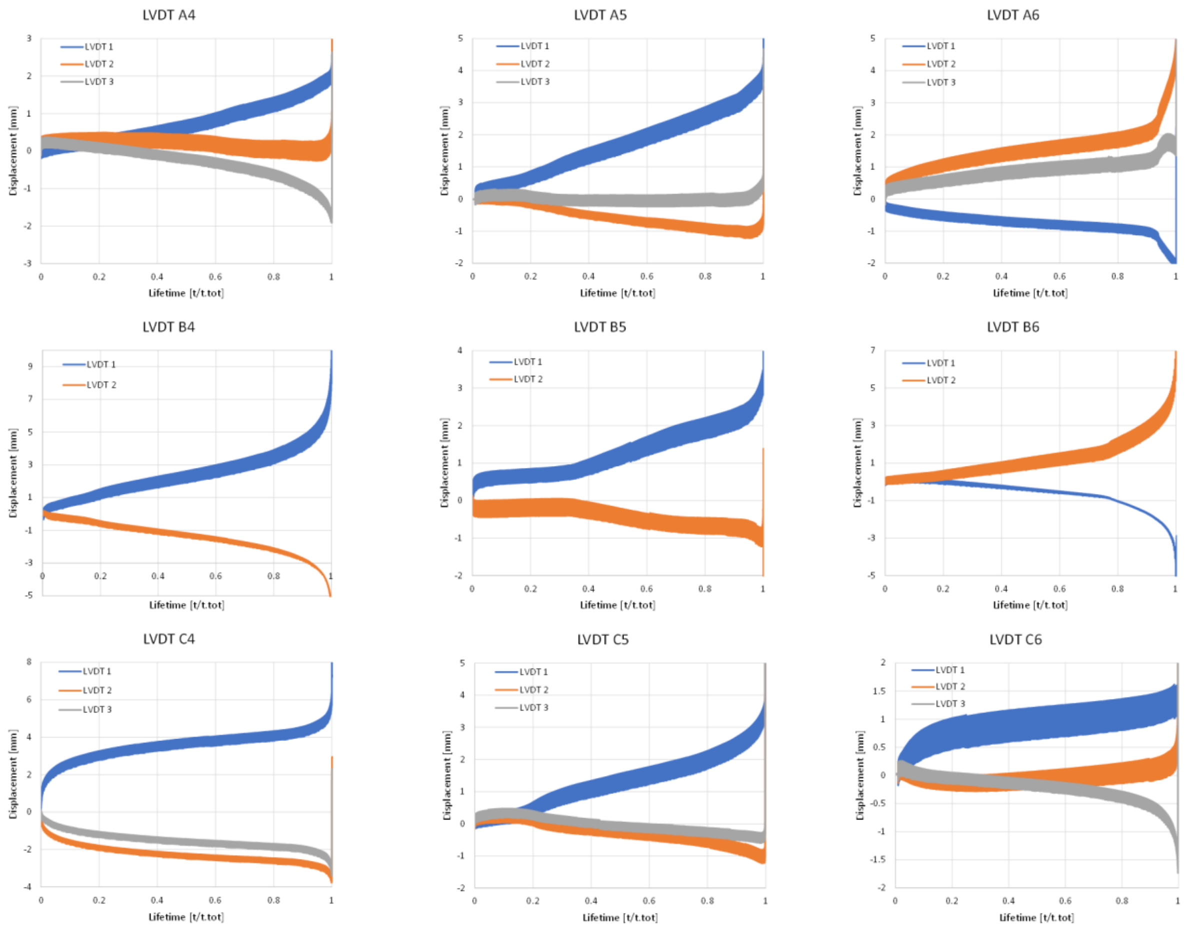

Figure 54: LVDT development for specimen A4-A6, B4-B6 & C4-C6.

The difference between LVDT 2 and LVDT 3 dictates how much the loading plane tilts around the X-axes which is an indication of the crack development at the front relative to the back respectively. It was observed differences between crack width and crack growth on the front and back for all specimens, however, with the exception of C6, the difference was very small. For C6 the main crack was observed on the back of the specimen for a long time, while the front had significantly smaller cracks.

As seen in Figure 54, the difference between thickness of plotted LVDTs vary. This is evident for specimen B6 where plot of LVDT 1 is significantly thinner than for LVDT 2.the thickness of LVDT 1 and LVDT 2 is also varying throughout the lifetime in opposite directions. This difference in thickness can be explained by a rotation of the loading plane, however for specimen type B only 2 LVDTs were plotted, which would not give enough data to determine a precise behavior of the loading plane. It was because of this difference in thickness between LVDTs decided to log the other specimen types with 3 LVDTs.

7.4 Strain development in threaded bars and reinforcement

In this part the strain development for each specimen type is presented. The strain diagrams are categorized for each strain gage SG1, SG2 and SG3 (see Figure 26 and Appendix C for placement), where each strain gage is further plotted for specimen 4-6 in each diagram. The strain diagrams of each specimen type show how the strains in SG1, SG 2 and SG 3 in each specimen varies related to the normalized lifetime.

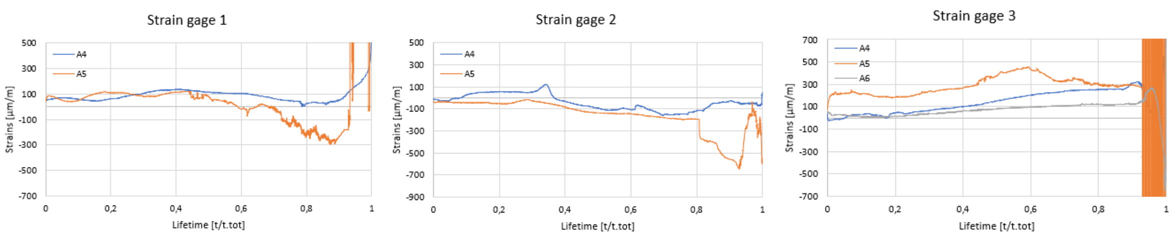

Figure 55: Strain development of specimen type A.

First, the strain in specimen type A is presented. The three figures above describe the development of strains during the lifetime of the dynamic tests. During testing, A6 got SG1 and SG2 broken. Of that reason, A6 isn`t shown in figures for SG1 and SG2. SG1 and SG 2 showed to be quite equal during most of the lifetime. Both in SG1 and SG2, its shown that the strains for A5 were increasing compared to A4. This might indicate that A5 was the weakest one of those specimens. As also shown in the figures for SG1 and SG3, both the minimum reinforcement, and the highest one of the threatened bars seemed to yield around 90% of the lifetime. The yielding of the minimum reinforcement might be reasonable since most of the loading are distributed in this direction. The reason why A6 got such a stable strain development in SG3 is unknown.

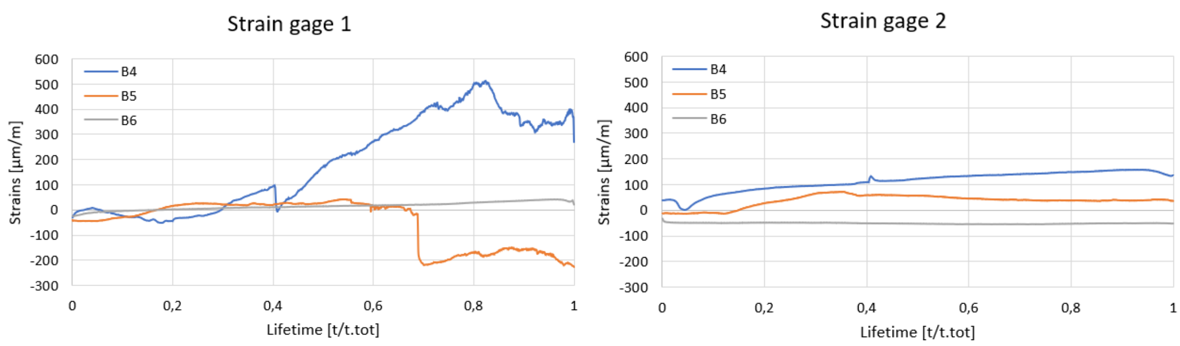

Figure 56: Strain development of specimen type B.

Further, the strain development in specimen type B is presented. The three figures describe the strain development in SG1 and SG2 during the lifetime of the dynamic tests. As shown in Figure 56, SG2 had a quite more stable development than SG1. None of the strain gages seemed to reach yielding within the lifetime for any of the specimens. Even though, SG1 was shown to have a quite more unstable strain development as well was a much higher maximum strain than SG2. The reason for this is unknown. It also seemed quite strange that SG2 had an almost constant strain development under the whole lifetime. This was the case for all three specimens; B1, B2 and B3. Another thing that should be mentioned is the big difference in strain development between SG1 and SG2. For B6 they seem to have quite the same development. For B4 and B5 it`s shown that with increasing time the difference between SG1 and SG2 seems to get larger.

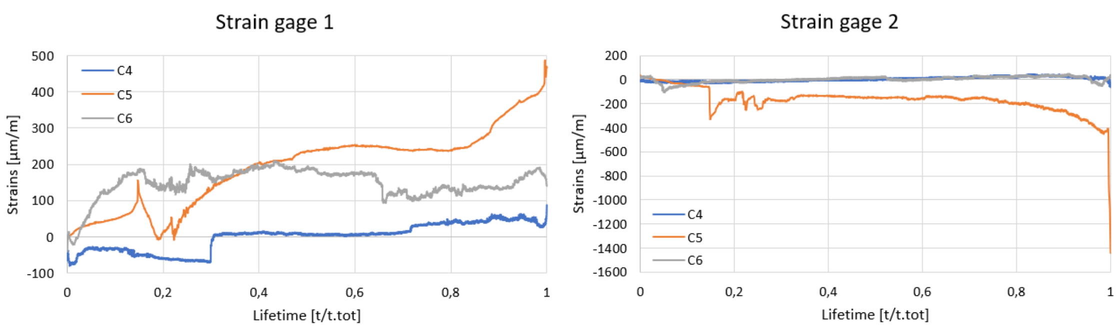

Figure 57: Strain development of specimen type C.

Finally, the strain development in specimen type C is presented. SG2 seem to have the most expected strain development. As seen SG2 was quite stable strain development, until the yielding was reached in the end of the lifetime. This seemed to happen to C5 in both SG1 and SG2. As Figure 57 shows both C4 and C6 seemed to have almost no strains in SG2 during the whole lifetime. SG1 seemed to be quite low for C4 during the whole test. The reason for this is unknown.

7.5 Crack patterns and local crushing

The formation of cracks and crushing of concrete for specimens subjected to dynamic loading is a much slower process than for static. The cracking starts with concrete spalling directly underneath the loading plate followed by small cracks forming in the compression zone. The propagation of cracks and local crushing underneath the loading plate happens slowly throughout the lifetime, but during the last 5% - 10% of its lifetime crack propagation accelerates.

The crack pattern from dynamic loading is very similar to the crack pattern from static loading. Both loading type leads to one main crack direction starting at the center of the specimen under the compression zone leading downwards towards one of the sides. Though there is some cracking on both sides, the difference between the side with the main crack direction and the other side is incomparable as seen in Figure 58. Even though the main pattern is similar between the different loads, there are some significant differences as well. For the dynamically loaded elements local crushing under the loading plate is more severe. In addition, the cracking in the compression zone forms a v-shape, as seen in Figure 58, where the concrete under the loading plate was often observed to be loose, resting in the v-shaped channel. The main crack most often run from the bottom of the v-shape to the underside of the second threaded bar and then to the top of the third threaded bar continuing towards the edge of the specimen, as drawn in a red line in Figure 58.

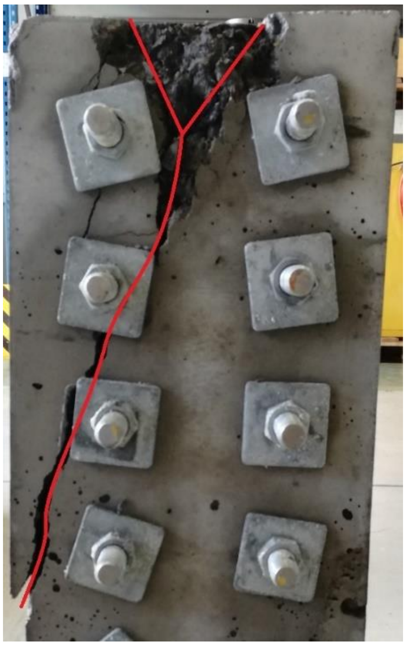

Figure 58: Main crack direction for specimen A5.

As discussed in Section 2.1.1 crack development during dynamic loads will go through the phases of initiation, propagation and final rapture. Though crack initiations are too small to observe one can get an indication of the initiation point by observing the early crack development. The first observable cracks were most often propagating from underneath the washer of the top three threaded bars or adjacent to these threaded bars as seen in Figure 59. There were some instanced where the first visible cracks were between the threaded bars, quickly followed by cracks propagating from underneath the washers. This gives the indication that most of the crack initiation is close to or at the threaded bars. From this observation it is important to consider the implication of the threaded bars as a means to fulfill correct boundary conditions. The addition of threaded bars in the specimen may lead to a different crack pattern or a higher crack development. For dynamic test specimens it was observed a higher number of cracks than for static tests.

Figure 59: Early crack development for dynamically loaded specimens.

During the crack propagation phase, it is important to note that there was observed a pumping effect of water in the cracks. This cyclic pumping was observed due to dust particles being washed out from the cracks. When inspecting the specimen after fracture it was noted that dynamically loaded specimens had a high rate of erosion damage in the cracks that was not present for statically loaded specimens. The erosion damage is due to the cyclic loading, though it is believed that the pumping effect from water is increasing the erosion damage. During the crack propagation it was observed that cracks would grow untill they coaless with neibhouring cracks creating a dominant crack that would often be part of the main crack leading to failure. Some specimens show several dominant cracks leading to more than one potential main crack.

The three types of specimens behaved quite simmilar during fatigue loading, though it was observed that specimen type A had less erotion and smuldering in the lower part of the v-shaped cracks. For specimen type C cracking was observed earlyer and more severe than the other specimens. This was especially evident for specimen C5, where severe cracking normaly seen at the later stages of dynamic loading was observed at 300 to 400 cycles which acounts for approximately 20% of the fatigue life (see Figure 60).

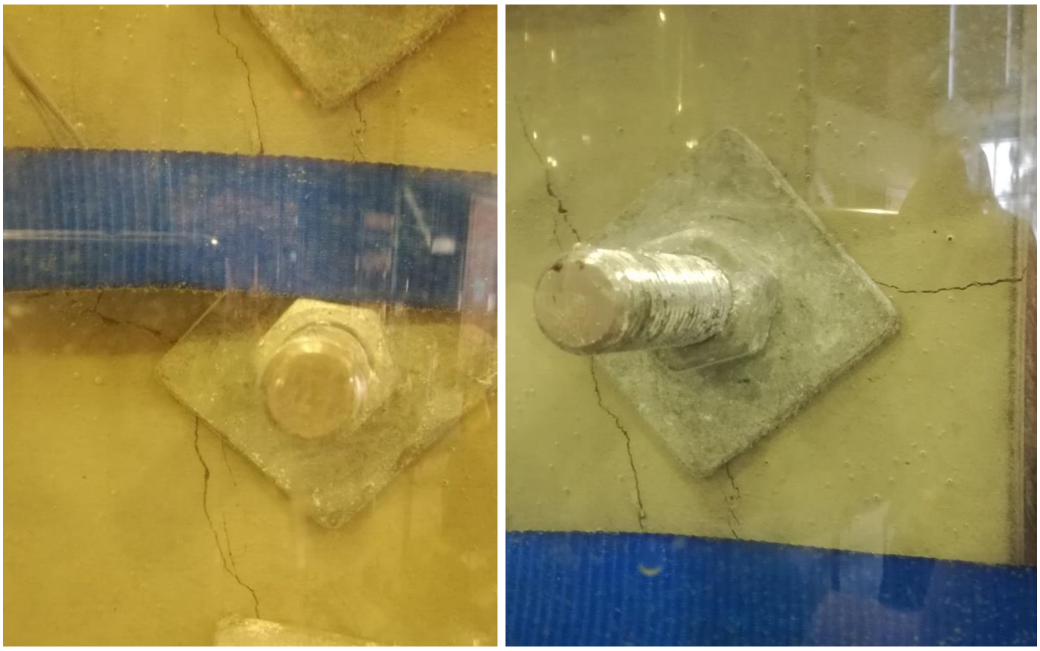

Figure 60: Early crack development (ca. 20% of life) for specimen C5

Specimen B4 was the first specimen tested with dynamic loading. As mentioned in 4.2 the loading plate started to slant towards one side during testing, and from Figure 61 one can clearly see that one side of the loaded area has suffered from severely crushing while the other side is almost unscathed. Though other specimens also experienced slanted loading area to some extent, no other test specimen came close to B4. Due to the change in hinge orientation after this occurrence it is uncertain if this would be a one-time phenomenon or a norm, however with a similar setup Bognøy et.al. experienced at least one such incident with their 17th specimen. It is believed that local weakness or a slight initial eccentricity would be the cause of a slanting load surface, and the eccentricity caused by the hinge orientation would amplify this leading to the state observed for B4. If so, then changing hinge orientation did prevent this large change in angle of load plane from occurring in several specimen tests.

Figure 61: Local crushing on one side under loaded area for specimen B4.

The angle of the main crack for specimen B4 is significantly different than the other specimens, propagating above the second threaded bar quickly making it to the side with a much higher angle. This has most likely to do with the slanted loading plate increasing stresses in this area.

8 Conclusion

This thesis is based on experimental data from 18 test specimens looking at the difference in static and dynamic capacities for unreinforced, minimum reinforced and steel fiber reinforced concrete (SFRC). The specimens were submerged in water and subjected to partially loaded areas and the following is our main findings:

8.1 Static tests

- Unreinforced concrete subjected to a partially loaded area show an increase of 6% (± 7%) compared to the capacity of the loaded area. However, due to brittle failure it would not be advisable to utilize this capacity increase for design.
- For concrete with a minimum reinforcement, the effect of a partially loaded area will give a capacity increase of approximately 11% (± 4%) above to the capacity of the loaded area, and steel fiber reinforced concrete with a residual tensile stress of 1.32Mpa show an increase of 20% (± 5%) for a partially loaded area.
- Steel fiber reinforcement in concrete gives a more ductile behavior than concrete with a minimum reinforcement, and seams to change the elasticity modulus for the concrete mix.

8.2 Dynamic tests

In their standard for offshore concrete structures DNV-OS-C502 section M, DNV GL provides verification of fatigue life according to equation given below. The C_1 factor takes climate into account and for structures submerged in water C_1=10.

$$logN = C_1 \frac{\left(1 - \frac{\sigma_{c.max}}{f_{rd}}\right)}{\left(1 - \frac{\sigma_{c.min}}{f_{rd}}\right)}$$

- Results from this investigation show that the formula from DNV-OS-C502 with C1 factor of 10 gives an accurate prediction of fatigue life for unreinforced concrete subjected to cyclic compressive forces submerged in water, and there is clear indication that partially loaded area of unreinforced concrete gives no increase in fatigue life.
- Partially loaded areas with minimum cover reinforcement gives a higher fatigue life than unreinforced concrete, with a suggested C_1 factor of 11.4 (± 0.65). Partially loaded areas with minimum cover reinforcement also gives higher fatigue life than partially loaded areas with sufficient splitting reinforcement, though within the margin of error.
- For steel fiber reinforced concrete (SFRC) with partially loaded areas the increased fatigue life compared to unreinforced concrete suggests a C_1 factor of 11.22 (± 1.02). Partially loaded areas with SFRC also gives higher fatigue life than partially loaded areas with sufficient splitting reinforcement, though within the margin of error.

- Partially loaded areas with minimum cover reinforcement and partially loaded areas with SFRC give approximately the same increase of fatigue life, though SFRC gives a larger uncertainty.
- There is no significant difference in deformation over lifetime between unreinforced, minimum reinforced or fiber reinforced concrete.
- For specimens with protruding threaded bars, bars in compression zone are likely a source for crack initiation which may lead to change in crack patterns or unusually high crack development.
- For dynamically loaded specimens increased erosion occurs due to a cyclic pumping effect from the cracks opening and closing. This pumping effect also leads to dust particles being washed out from the cracks.
- For SFRC specimens cracking is observed earlier in the fatigue life than for unreinforced concrete or concrete reinforced with minimum cover reinforcement.

8.3 Further work

- This thesis gives an indication of potential increase in capacity for fiber concrete and minimum reinforced specimens. To validate theses results for practical application a more comprehensive study needs to be conducted with a higher number of tests with different stress levels covering both high and low cycle fatigue.
- Dynamic loading introduces cracks in the structure. Combined with the pumping effect in the cracks due to water the corrosion of reinforcement should be investigated for environments with high chloride concentration. This should especially be investigated for steel fiber reinforced concrete.
- Compared to the results from Bognøy et.al. this thesis shows an increase in fatigue life for a cross-section with less reinforcement. An investigative study should be conducted to conclude if a reduction of fatigue life due to higher amounts of reinforcement is a fact, or if this indication is due to a low number of data.
- Crack propagation during fatigue loading indicates crack initiation at or close to the threaded bars. It would be important to study the implication of the threaded bars as a means to fulfill correct boundary conditions and their impact on the specimens.

9 References

Almar-Næss, A., 2009. *utmatting-teknikk.* [Online]
Available at: https://snl.no/utmatting_-_teknikk

Betongelementforeningen, 2010. *Betongelementboken Bind B: Elementer og knutepunkter.* Oslo: Betongelementforeningen.

Bognøy, E., Mo, T. M. S. & Vee, V., 2014. *Fatigue Capacity of partially loaded Areas in Concrete Structures submerged in Water,* Trondheim: NTNU.

Bratfos, H. A., n.d. *Universitetet i Oslo.* [Online]
Available at: https://www.uio.no/studier/emner/matnat/math/nedlagte-emner/MEK4520/h06/undervisningsmateriale/kapittel%202%20-%20line%C3%A6r-elastisk%20bruddmekanikk.pdf
[Accessed Søndag Mars 2019].

CEB, 1988. *Fatigue of concrete structures: state of the art report,* s.l.: CEB.

fib, 2013. *fib Model Code for Concrete Structures 2010,* s.l.: fédération internationale du béton.

Furnes, A. & Hauge, O. M., 2011. *Fatigue capacity of partially loaded areas in concrete structures,* Trondheim: NTNU.

Galloway, J. W., Harding, H. M. & Raithby, K. D., 1979. *Effects of moisture changes on flexural and fatigue strength of concrete.,* s.l.: Crowthorne.

Grzybowski, M. & Meyer, C., 1993. Damage accumulation in concrete with and without fiber reinforcement. *Material Journal*, 1 11, pp. 594-604.

HANJARI, K. Z., 2006. *Evaluation of WST Method as a Fatigue,* Göteborg: CHALMERS UNIVERSITY OF TECHNOLOGY .

Hanjari, K. Z., 2006. *Evaluation of WST Method as a Fatigue Test for Plain and Fiber-reinforced Concrete,* Göteborg: CHALMERS UNIVERSITY OF TECHNOLOGY .

Hiatt, J., 2016. *What is an SN-curve..* [Online]
Available at: https://community.plm.automation.siemens.com/t5/Testing-Knowledge-Base/What-is-a-SN-Curve/ta-p/355935
[Accessed Februar 2019].

Hilsdorf, H. K. & Kesler, C. E., 1966. *Fatigue strength of concrete under varying flexural stresses,* s.l.: ACI Journal, Proceedings Vol. 63, No 10.

Holmen, J. O., 1979. *Fatigue of concrete by constant and variable amplitude loading,* Trondheim: Division of Concrete Structures, Norwegian Institute of Technology, University of Trondheim.

Home, T. C.-. C. E., 2019. *theconstructor.org.* [Online]
Available at: https://theconstructor.org/concrete/fiber-reinforced-concrete/150/

Hooi, T. T., 2000. *Effects of passive confinement on fatigue properties of concrete,* s.l.: Magazine of Concrete Research.

Kanstad, T., Juvik, D. A. & Vatnar, A., 2011. *Forslag til retnigslinjer for dimensjonering, utførelse of kontroll av fiberarmerte betongkonstruksjoner,* s.l.: SINTEF.

Kanstad, T., Juvik, D. A. & Vatnar, A., 2011. *Forslag til retningslinjer for dimensjonering, utførelse og kontroll av fiberarmerte betongkonstruksjoner,* s.l.: SINTEF.

Kanstad, T. et al., 2011. *Forslag til retningslinjer for dimensjonering, utførelse og konstroll av fiberarmerte betongkonstruksjoner,* s.l.: COIN-Concrete innovation center.

Kasper, T. et al., 2014. *DESIGN GUIDELINE FOR STRUCTURAL APPLICATIONS OF STEEL FIBER REINFORCED CONCRETE,* s.l.: SFRC Consortium.

Leung, D. Y. & Yang, Y., 2011. *Wind energy development and its environmental impact: A review,* s.l.: Elsevier Ltd..

Löfgren, I., 2005. *Fibre-reinforced Concrete for industrial constructions ,* Göteborg: Chalmers University of Technology.

Murdock, J. & Kesler, C. E., 1960. *The Mechanism of Fatigue in Cement Paste and Plain Concrete,* s.l.: No. 587, University of Illinois.

Norge, S., 2008. *Eurokode 2: Prosjektering av betongkonstruksjoner Del 1-1: Almenne regler og regler for bygninger. ,* s.l.: Standard Norge.

Ohlsson, U., Daerga, P. A. & Elfgren, L., 1990. *Fracture energy and fatigue strength of unreinforced concrete beams at normal and low temperatures,* s.l.: Engineering Fracture Mechanics Vol. 1990(35), No 1, 2, 3, pp. 195-203 .

Per.Kr.Larsen, 2010. *Dimensjonering av stålkonstruksjoner.* 2.utg. ed. Trondheim: Fagbokforlaget.

Petkovic, G., 1991. *Properties of concrete related to fatigue damage : with emphasis on high strength concrete,* Trondheim: Division of Concrete Structures, Norwegian Institute of Technology, University of Trondheim.

Shin, M. & Andrawes, B., 2010. *Experimental investigation of actively confined concrete using shape memory alloys,* s.l.: Engineering Structures, Vol. 32 (3), pp. 656-664.

Stavanger, U. i., n.d. [Online]
Available at: http://www.ux.uis.no/~hirpa/6KdB/ME/S-N%20diagram.pdf?fbclid=IwAR1NQPaValjBKbglcY6KyXQgUcpE20dHU4TfVkWjdlarG7zEytqfFWkTn7Y
[Accessed 25. 05. 2019].

Tepfers, R., Gørling, J. & Samuelsson, T., 1973. *Concrete subjected to pulsating load and pulsating deformation of different pulse waveforms.,* s.l.: Nordisk betong Vol. No 4.

Thomas Telfjord Service Ltd, 1991. *CEB-FIB-MODEl CODE 1990,* London: COMITE EURO-INTERNATIONAL DU BETON.

Tomislav, Markic, T., Kaufmann , W. & Amin , A., 2018. *Stressfield solution for strip loaded reinforced concrete blocks.,* Zürich: Elsevier.

Torrenti, J., Pijaudier-Cabot, G. & Reynouard, J., 2013. *Mechanical Behavior of Concrete.* s.l.:John Wiley & Sons, Inc..

Van_Leeuwen, J. & Siemes, A. J. M., 1979. *Miner's rule with respect to plain concrete.,* s.l.: Heron Vol. 24, No 1.

veritas, D. n., 2010. *Offshore concrete structures,* s.l.: Det norske veritas.

wang, H. L. & Song, Y. P., 2010. *Fatigue capacity of plain concrete under fatigue loading with constant confined stress,* s.l.: RILEM 2010.

Zhang, J., 1998. *Fatigue fracture of fibre reinforced concrete: An expirimental and theoretical study,* Copenhagen: Tecnical Univarsity of Denmark.

Zhan, M. Y., 2016. *Multilevel Modeling of Fiber-Reinforced Concrete and Applications to Numerical Simulations of Tunnel Lining Segments,* Bochum : Ruhr University Bochum.

10 Appendix

Appendix A: Static calculations

A1: Static capacity of specimen type A and B at 28 days

A2: Static capacity of specimen type C at 28 days

Appendix B: Dynamic calculations

B1: Dynamic capacity of specimen type A

B2: Dynamic capacity of specimen type B

B3: Dynamic capacity of specimen type C

B4: SN-curve of different formulas

Appendix C: Reinforcement layout

C1: Reinforcement layout in specimen type A

C2: Reinforcement layout in specimen type B

C3: Reinforcement layout in specimen type C

Appendix D: Test-results

D1: Strength of test cubes

D2: Crack propagation in specimen type A: Minimum reinforcement

D3: Crack propagation in specimen type B: Unreinforced

D4: Crack propagation in specimen type C: Fiber-reinforced

Appendix E: Various documentation

E1: Concrete receipt of fiber-reinforced concrete

E2: Concrete receipt of normal concrete

Appendix A: Static calculations

A1: Static capacity of specimen A & B at 28 days

Due to the placement of minimum reinforcement in specimen A it will not be acounted for when calculating the splitting capacity of the speciment. Therefore the static capacity of speciment A and B will be calculated in the same manner.

In the effort of obtaining the most exact fracture load, all calculations are based on mean concrete strength, and safety factors are neglected. The original subscripts are being used in a large extent to prevent confusion between formulas listed in chapter 2: Literature review.

Input:

$f_{cm.28} := 36.80 \ MPa \qquad f_{tm.28} := 2.8 \ MPa$

Capacity due to load distribution from partially loaded area:

Area distribution:

$d_1 := 210 \ mm \qquad b_1 := 70 \ mm$

$d_2 := 210 \ mm \qquad b_2 := 210 \ mm$

$A_{c0} := d_1 \cdot b_1 = 0.015 \ m^2$

$A_{c1} := d_2 \cdot b_2 = 0.044 \ m^2$

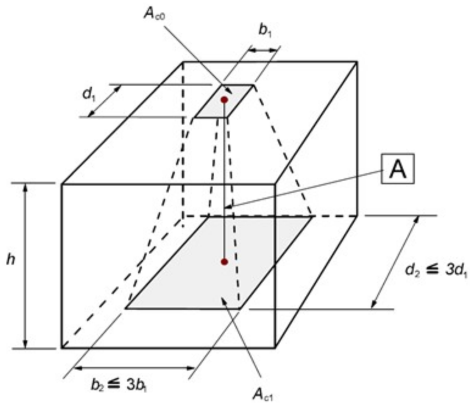

Compressive capacity acording to Eurocode 2 & Modelcode 2010:

$$F_{Rdu.Ec2} := A_{c0} \cdot f_{cm.28} \cdot \sqrt{\frac{A_{c1}}{A_{c0}}} = 936.97 \ kN \quad \leq \ 3 \ f_{cm.28} \cdot A_{c0} = 1622.88 \ kN \quad \text{OK}$$

Compressive capacity acording to DNV-OS-502:

$$F_{Rdu.DNV} := A_{c0} \cdot f_{cm.28} \cdot \sqrt[3]{\frac{A_{c1}}{A_{c0}}} = 780.2 \ kN \quad \leq \ 3 \ f_{cm.28} \cdot A_{c0} = 1622.88 \ kN \quad \text{OK}$$

Tensile capacity according to Model Code 1990:

EC2 gives no guidance when there is insufficient or no reinforcement in the tie. Model Code 90 suggests that the force is resisted by the tensile strength of concrete in the tention zone acordingly:

$h := 0.6\ b_2 \qquad b := d_2 \qquad A := h \cdot b$

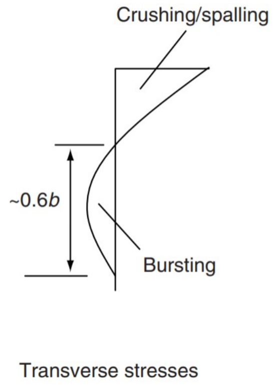

$T := A \cdot f_{tm.28} = 74.1\ kN$

$$F_{ctd} := 4\ T\ \frac{b_2}{b_2 - b_1} = 444.53\ kN$$

Capacity due to load distibution from partially loaded area:

$F_{Ac1} := min\left(F_{Rdu.Ec2}, F_{Rdu.DNV}, F_{ctd}\right) = 444.528\ kN$

Capacity of loaded area of concrete:

$F_{Ac0} := f_{cm.28} \cdot A_{c0} = 540.96\ kN$

Static capacity of specimen A & B:

$F_{max} := \max\left(F_{Ac0}, F_{Ac1}\right) = 540.96\ kN$

A2: Static capacity of specimen C at 28 days

In the effort of obtaining the most exact fracture load, all calculations are based on mean concrete strength, and safety factors are neglected. The original subscripts are being used in a large extent to prevent confusion between formulas listed in chapter 2: Literature review.

Input:

$f_{cm.28} := 34.53\ MPa$ $\qquad f_{ctm.28} := 2.7\ MPa$ $\qquad f_{ftk.res.2.5} := 1.32\ MPa$

Capacity due to load distribution from partially loaded area:

Area distribution:

$d_1 := 210\ mm \qquad b_1 := 70\ mm$

$d_2 := 210\ mm \qquad b_2 := 210\ mm$

$A_{c0} := d_1 \cdot b_1 = \left(1.47 \cdot 10^4\right)\ mm^2$

$A_{c1} := d_2 \cdot b_2 = \left(4.41 \cdot 10^4\right)\ mm^2$

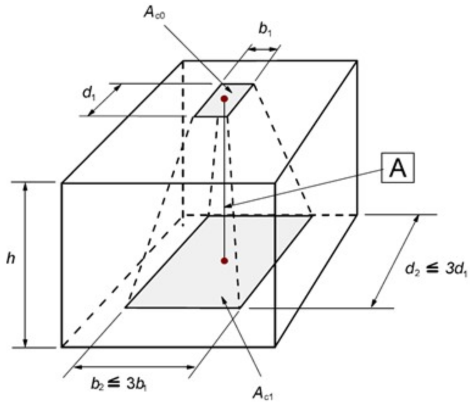

Compressive capacity acording to Eurocode 2 and Modal Code 2010:

$$F_{Rdu} := A_{c0} \cdot f_{cm.28} \cdot \sqrt{\frac{A_{c1}}{A_{c0}}} = 879.17\ kN \quad \le\ 3 \cdot f_{cm.28} \cdot A_{c0} = 1522.773\ kN \qquad \text{OK}$$

Compressive capacity acording to DNV-OS-502:

$$F_{Rdu} := A_{c0} \cdot f_{cm.28} \cdot \sqrt[3]{\frac{A_{c1}}{A_{c0}}} = 732.073\ kN \ \le\ 3 \cdot f_{cm.28} \cdot A_{c0} = 1522.773\ kN \qquad \text{OK}$$

Tensile capacity:

- Capacity from concretes tensile strength according to Model Code 1990:

EC2 gives no guidance when there is insufficient or no reinforcement in the tie. Model Code 1990 sugests that the force is resisted by the tensile strength of concrete in the tention zone acordingly:

$h := 0.6\ b_2$ $\quad b := d_2$ $\quad A := h \cdot b$

$T := A \cdot f_{ctm.28} = 71.4\ kN$

$F_{ctd.concrete} := 4\ T\ \dfrac{b_2}{b_2 - b_1} = 428.65\ kN$

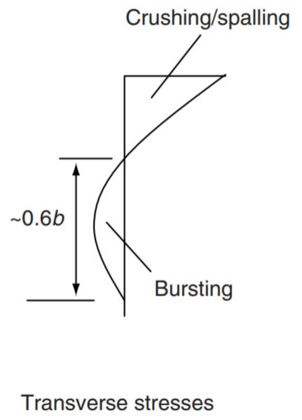

- Capacity from residual tensile strength according to SFRC Constrium:
SFRC Consortium gives a guidance in the design guideline for structural aplications of SFRC for calculating the tie force for a cracked crossection with SFRC acordingly:

$h := d_2$
$b := b_2$

$A := 0.8\ h \cdot b$
$f_{res.2.5} := 1.5\ MPa$

$T := A \cdot f_{res.2.5} = 52.92\ kN$

$F_{ctd.2.5} := 4\ T\ \dfrac{b_2}{b_2 - b_1} = 317.52\ kN$

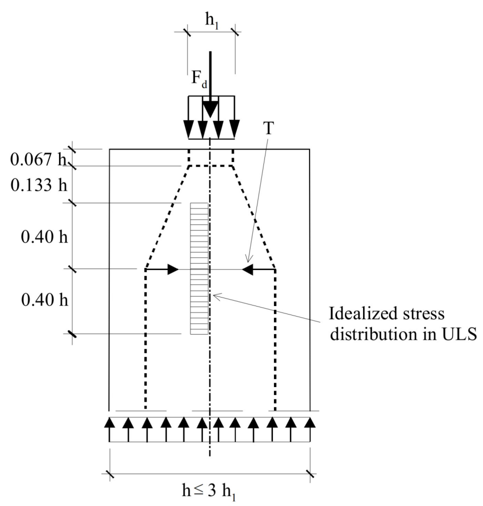

- Tensile capacity:

$F_{ctd} := \max\left(F_{ctd.concrete}, F_{ctd.2.5}\right) = 428.652\ kN$

Capacity due to load distibution from partially loaded area:

$F_{Ac1} := min\left(F_{Rdu}, F_{ctd.concrete}\right) = 428.652\ kN$

Capacity of loaded area of concrete:

$F_{Ac0} := f_{cm.28} \cdot A_{c0} = 507.591\ kN$

Static capacity of specimen A & B:

$F_{max} := \max\left(F_{Ac0}, F_{Ac1}\right) = 507.591\ kN$

Appendix B: Dynamic calculations

B1: Calculation and plot of SN-curves from different formulas 28 days

For simplicity the calculation bases concrete strength f_{ck} on the results from testing, and is expressed as maximum force F_{max} divided by load area A_{c0}. The stresses $\sigma_{c.max}$ and $\sigma_{c.min}$ are expressed as the applied force divided by loaded area.

In the effort of obtaining the most exact fracture load, all calculations are based on mean concrete strength, and safety factors are neglected. The original subscripts are being used in a large extent to prevent confusion between formulas listed in chapter 2: Literature review.

Input:

$F_{max} := 540.96 \cdot \boldsymbol{kN}$ $\qquad F_{load.max} := 0.7 \cdot F_{max}$ $\qquad F_{load.min} := 0.1 \cdot F_{max}$

Data:

In order to plott the number of cycles to failure N over the stress level S, the number of cycles N are calculated for all stresses from $\sigma_{c.min}$ to f_{ck} with an interval of 0.1. The minimum stress $\sigma_{c.min}$ will be set equal to $0.1 \cdot f_{ck}$.

$A_{c0} := 210\ \boldsymbol{mm} \cdot 70\ \boldsymbol{mm} = 0.015\ \boldsymbol{m}^2$ $\qquad f_{ck} := \dfrac{F_{max}}{A_{c0}} = 36.8\ \boldsymbol{MPa}$

$$\sigma_{c.max} := 0.11\ f_{ck}, 0.12\ f_{ck} .. f_{ck} = \begin{bmatrix} 4.048 \\ 4.416 \\ \vdots \end{bmatrix} \boldsymbol{MPa} \qquad \sigma_{c.min} := 0.1\ f_{ck}$$

Fatigue capacity acording to Model Code 2010

- Characteristic fatigue reference strength:

$s := 3.8$ $\qquad t := 28$ $\qquad \beta_{c.sus} := 1.0$

$$\beta_{cc} := \exp\left(s \cdot \left(1 - \left(\frac{28}{t}\right)^{0.5}\right)\right) = 1$$

$$f_{ck.fat} := \beta_{cc} \cdot \beta_{c.sus} \cdot f_{ck} \cdot \left(1 - \frac{f_{ck}}{400\ \boldsymbol{MPa}}\right) = 33.414\ \boldsymbol{MPa}$$

- Minimum and maximum compressive stress levels:

By asuming a constant stress field $\dfrac{\sigma_{c1}}{\sigma_{c2}} = 1$ giving:

$\eta_c := \dfrac{1}{1.5 - 0.5 \cdot 1} = 1$ $\qquad \gamma_{Ed} := 1.0$

$$S_{cd.max.MC} := \frac{\gamma_{Ed} \cdot \sigma_{c.max} \cdot \eta_c}{f_{ck.fat}} = \begin{bmatrix} 0.121 \\ \vdots \end{bmatrix} \qquad S_{cd.min.MC} := \frac{\gamma_{Ed} \cdot \sigma_{c.min} \cdot \eta_c}{f_{ck.fat}} = 0.11$$

- Number of cycles to failure:

$$Y := \frac{0.45 + 1.8 \cdot S_{cd.min.MC}}{1 + 1.8 \cdot S_{cd.min.MC} - 0.3\ S_{cd.min.MC}^{\ 2}} = 0.543$$

$$logN := \frac{8}{Y - 1} \cdot \left(S_{cd.max.MC} - 1\right)$$

$$N_{MC} := 10^{logN}$$

$$N_{MC.water} := N_{MC}^{\ 0.8}$$

Model Code does not account for short cycle fatigue with $N < 10^4$ cycles and is therefor not plotted in this region.

Fatigue capacity acording to DNV-OS-C502

- Number of cycles to failure for concrete in air:

$$c_{1.air} := 12 \qquad S_{cd.max.DNV} := \frac{\sigma_{c.max}}{f_{ck}} \qquad S_{cd.min.DNV} := \frac{\sigma_{c.min}}{f_{ck}} = 0.1$$

$$logN_{DNV} := c_{1.air} \cdot \frac{\left(1 - S_{cd.max.DNV}\right)}{\left(1 - S_{cd.min.DNV}\right)} \qquad N_{DNV.air} := 10^{logN_{DNV}}$$

- Number of cycles to failure for concrete in water:

$$c_{1.water} := 10$$

$$logN_{DNV.water} := c_{1.water} \cdot \frac{\left(1 - S_{cd.max.DNV}\right)}{\left(1 - S_{cd.min.DNV}\right)} \qquad N_{DNV.water} := 10^{logN_{DNV.water}}$$

-Potential increase in number of cycles:

$$X := \frac{c_{1.air}}{\left(1 - \left(\frac{\sigma_{c.min}}{f_{ck}}\right) + 0.1 \cdot c_{1.air}\right)} = 5.714$$ => No increase in capacity for N < $10^{5.3}$

Fatigue capacity according to Aas-Jakobsens formula

$$\beta := 0.0685 \qquad R := \frac{\sigma_{c.min}}{\sigma_{c.max}}$$

$$logN_{AaJ} := \frac{1 - \frac{\sigma_{c.max}}{f_{ck}}}{\beta - \beta \cdot R} \qquad N_{AaJ} := 10^{logN_{AaJ}}$$

Fatigue capacity according to Ove Holmens formula

$$S_{cd.max} := \frac{\sigma_{c.max}}{f_{ck}} = \begin{bmatrix} 0.11 \\ 0.12 \\ \vdots \end{bmatrix} \qquad S_{cd.min} := \frac{\sigma_{c.min}}{f_{ck}} = 0.1$$

$$logN_{OH} := \left(1 - S_{cd.max}\right) \cdot \left(12 + 16\ S_{cd.min} + 8\ S_{cd.min}^{\ 2}\right)$$

$$N_{OH} := 10^{logN_{OH}}$$

Fatigue capacity according to Bognøy et. al.

$$lnN_{Bog} := \frac{1 - S_{cd.max}}{0.038} \qquad N_{Bog} := e^{lnN_{Bog}}$$

Plotting of SN-curve

Model Code does not account for short cycle fatigue with $N < 10^4$ cycles and is therefor not plotted in this region.

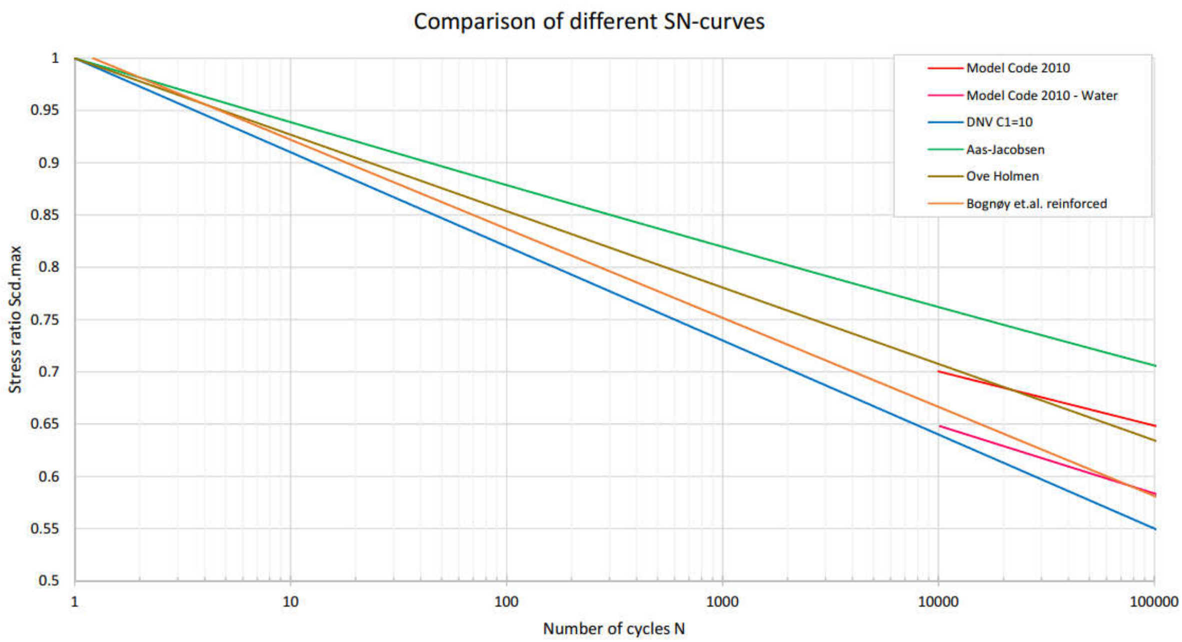

B2: Dynamic capacity of specimen A

For simplicity the calculation bases its strength f_{ck} on the results from testing, and is expressed as maximum force F_{max} divided by load area A_{c0}. The stresses $\sigma_{c.max}$ and $\sigma_{c.min}$ are expressed as the applied force divided by loaded area.

In the effort of obtaining the most exact fracture load, all calculations are based on mean concrete strength, and safety factors are neglected. The original subscripts are being used in a large extent to prevent confusion between formulas listed in chapter 2: Literature review.

Input:

$F_{max} := 638.35 \cdot kN$ $\quad F_{load.max} := 0.7 \cdot F_{max}$ $\quad F_{load.min} := 0.1 \cdot F_{max}$

- Standard deviation: $F_{SD} := 22.86\ kN$

Data:

$$A_{c0} := 210\ mm \cdot 70\ mm = 0.015\ m^2 \qquad f_{ck} := \frac{F_{max}}{A_{c0}} = 43.425\ MPa$$

$$\sigma_{c.max} := \frac{F_{load.max}}{A_{c0}} = 30.398\ MPa \qquad \sigma_{c.min} := \frac{F_{load.min}}{A_{c0}} = 4.343\ MPa$$

Fatigue capacity acording to DNV-OS-C502

- Stress levels:

$$S_{cd.max} := \frac{\sigma_{c.max}}{f_{ck}} = 0.7 \qquad S_{cd.min} := \frac{\sigma_{c.min}}{f_{ck}} = 0.1$$

- Upper and lower limit of $S_{cd.max}$:

$$S_{cd.max.upper} := \frac{F_{load.max}}{F_{max} - F_{SD}} = 0.73 \qquad S_{cd.max.lower} := \frac{F_{load.max}}{F_{max} + F_{SD}} = 0.68$$

- Number of cycles to failure:

$$c_1 := 10$$

$$logN := c_1 \cdot \frac{\left(1 - S_{cd.max}\right)}{\left(1 - S_{cd.min}\right)} = 3.333 \qquad N_{DNV} := 10^{logN} = 2154$$

-Potential increase in number of cycles:

$$X := \frac{c_1}{\left(1 - \left(\frac{\sigma_{c.min}}{f_{ck}}\right) + 0.1 \cdot c_1\right)} = 5.263$$

$$c_2 := 1 + 0.2\ (logN - X) = 0.614$$ < 1.0 No increase in capacity.

- Upper limit of cycles to failure:

$$logN_{upper} := c_1 \cdot \frac{(1 - S_{cd.max.lower})}{(1 - S_{cd.min})}$$

$$N_{DNV.upper} := 10^{logN_{upper}} = 4002$$

-Lower limit of cycles to failure:

$$logN_{lower} := c_1 \cdot \frac{(1 - S_{cd.max.upper})}{(1 - S_{cd.min})}$$

$$N_{DNV.lower} := 10^{logN_{lower}} = 1108$$

-Expected fatigue life acording to DNV-OS-C502:

$$N_{DNV} = 2154$$

$$N_{DNV.upper} = 4002$$

$$N_{DNV.lower} = 1108$$

B3 - Dynamic capacity of specimen B

For simplicity the calculation bases its strength f_{ck} on the results from testing, and is expressed as maximum force F_{max} divided by load area A_{c0}. The stresses $\sigma_{c.max}$ and $\sigma_{c.min}$ are expressed as the applied force divided by loaded area.

In the effort of obtaining the most exact fracture load, all calculations are based on mean concrete strength, and safety factors are neglected. The original subscripts are being used in a large extent to prevent confusion between formulas listed in chapter 2: Literature review.

Input:

$F_{max} := 621.57 \cdot kN$ $\quad F_{load.max} := 0.7 \cdot F_{max}$ $\quad F_{load.min} := 0.1 \cdot F_{max}$

- Standard deviation: $F_{SD} := 22.16\ kN$

Data:

$A_{c0} := 210\ mm \cdot 70\ mm = 0.015\ m^2$ $\quad f_{ck} := \dfrac{F_{max}}{A_{c0}} = 42.284\ MPa$

$\sigma_{c.max} := \dfrac{F_{load.max}}{A_{c0}} = 29.599\ MPa$ $\quad \sigma_{c.min} := \dfrac{F_{load.min}}{A_{c0}} = 4.228\ MPa$

Fatigue capacity acording to DNV-OS-C502

- Stress levels:

$S_{cd.max} := \dfrac{\sigma_{c.max}}{f_{ck}} = 0.7$ $\quad S_{cd.min} := \dfrac{\sigma_{c.min}}{f_{ck}} = 0.1$

- Upper and lower limit of $S_{cd.max}$:

$S_{cd.max.upper} := \dfrac{F_{load.max}}{F_{max} - F_{SD}} = 0.73$ $\quad S_{cd.max.lower} := \dfrac{F_{load.max}}{F_{max} + F_{SD}} = 0.68$

- Number of cycles to failure:

$c_1 := 10$

$logN := c_1 \cdot \dfrac{(1 - S_{cd.max})}{(1 - S_{cd.min})} = 3.333$ $\quad N_{DNV} := 10^{logN} = 2154$

-Potential increase in number of cycles:

$$X := \frac{c_1}{\left(1 - \left(\frac{\sigma_{c.min}}{f_{ck}}\right) + 0.1 \cdot c_1\right)} = 5.263$$

$c_2 := 1 + 0.2\left(logN - X\right) = 0.614$ < 1.0 No increase in capacity.

- Upper limit of cycles to failure:

$$logN_{upper} := c_1 \cdot \frac{\left(1 - S_{cd.max.lower}\right)}{\left(1 - S_{cd.min}\right)}$$

$$N_{DNV.upper} := 10^{logN_{upper}} = 3991$$

-Lower limit of cycles to failure:

$$logN_{lower} := c_1 \cdot \frac{\left(1 - S_{cd.max.upper}\right)}{\left(1 - S_{cd.min}\right)}$$

$$N_{DNV.lower} := 10^{logN_{lower}} = 1111$$

-Expected fatigue life acording to DNV-OS-C502:

$$N_{DNV} = 2154$$

$$N_{DNV.upper} = 3991$$

$$N_{DNV.lower} = 1111$$

B4: Dynamic capacity of specimen C

For simplicity the calculation bases its strength f_{ck} on the results from testing, and is expressed as maximum force F_{max} divided by load area A_{c0}. The stresses $\sigma_{c.max}$ and $\sigma_{c.min}$ are expressed as the applied force divided by loaded area.

In the effort of obtaining the most exact fracture load, all calculations are based on mean concrete strength, and safety factors are neglected. The original subscripts are being used in a large extent to prevent confusion between formulas listed in chapter 2: Literature review.

Input:

$F_{max} := 634.75 \cdot kN$ $\quad F_{load.max} := 0.7 \cdot F_{max}$ $\quad F_{load.min} := 0.1 \cdot F_{max}$

- Standard deviation: $F_{SD} := 27.55\ kN$

Data:

$$A_{c0} := 210\ mm \cdot 70\ mm = 0.015\ m^2 \qquad f_{ck} := \frac{F_{max}}{A_{c0}} = 43.18\ MPa$$

$$\sigma_{c.max} := \frac{F_{load.max}}{A_{c0}} = 30.226\ MPa \qquad \sigma_{c.min} := \frac{F_{load.min}}{A_{c0}} = 4.318\ MPa$$

Fatigue capacity acording to DNV-OS-C502

- Stress levels:

$$S_{cd.max} := \frac{\sigma_{c.max}}{f_{ck}} = 0.7 \qquad S_{cd.min} := \frac{\sigma_{c.min}}{f_{ck}} = 0.1$$

- Upper and lower limit of $S_{cd.max}$:

$$S_{cd.max.upper} := \frac{F_{load.max}}{F_{max} - F_{SD}} = 0.73 \qquad S_{cd.max.lower} := \frac{F_{load.max}}{F_{max} + F_{SD}} = 0.67$$

- Number of cycles to failure:

$$c_1 := 10$$

$$logN := c_1 \cdot \frac{\left(1 - S_{cd.max}\right)}{\left(1 - S_{cd.min}\right)} = 3.333 \qquad N_{DNV} := 10^{logN} = 2154$$

-Potential increase in number of cycles:

$$X := \frac{c_1}{\left(1-\left(\frac{\sigma_{c.min}}{f_{ck}}\right)+0.1 \cdot c_1\right)} = 5.263$$

$c_2 := 1 + 0.2\,(logN - X) = 0.614$ < 1.0 No increase in capacity.

- Upper limit of cycles to failure:

$$logN_{upper} := c_1 \cdot \frac{\left(1-S_{cd.max.lower}\right)}{\left(1-S_{cd.min}\right)}$$

$$N_{DNV.upper} := 10^{logN_{upper}} = 4538$$

-Lower limit of cycles to failure:

$$logN_{lower} := c_1 \cdot \frac{\left(1-S_{cd.max.upper}\right)}{\left(1-S_{cd.min}\right)}$$

$$N_{DNV.lower} := 10^{logN_{lower}} = 956$$

-Expected fatigue life acording to DNV-OS-C502:

$N_{DNV} = 2154$

$N_{DNV.upper} = 4538$

$N_{DNV.lower} = 956$

Appendix C: Reinforcement layout

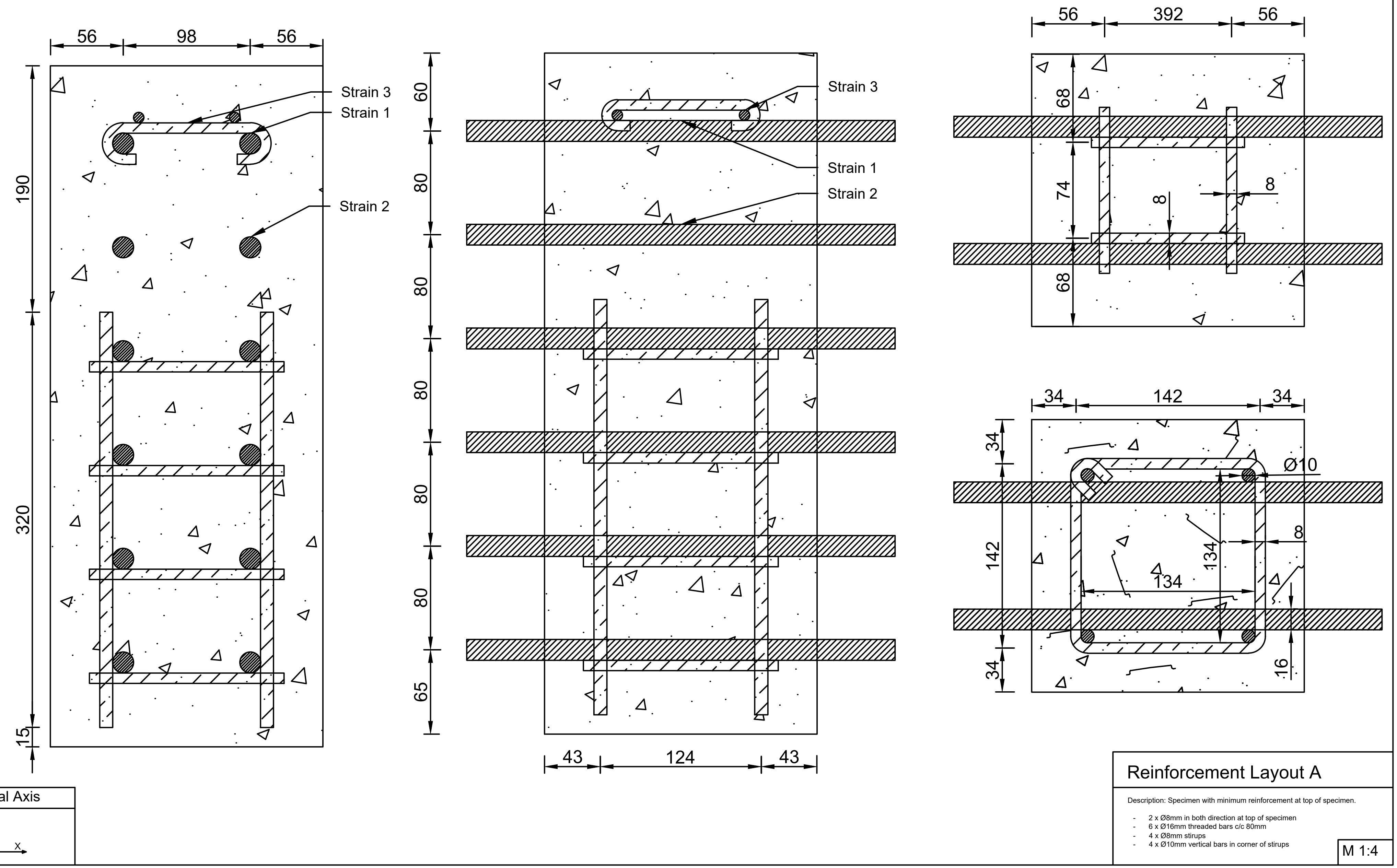

Reinforcement Layout A

Description: Specimen with minimum reinforcement at top of specimen.

- 2 x Ø8mm in both direction at top of specimen
- 6 x Ø16mm threaded bars c/c 80mm
- 4 x Ø8mm stirups
- 4 x Ø10mm vertical bars in corner of stirups

M 1:4

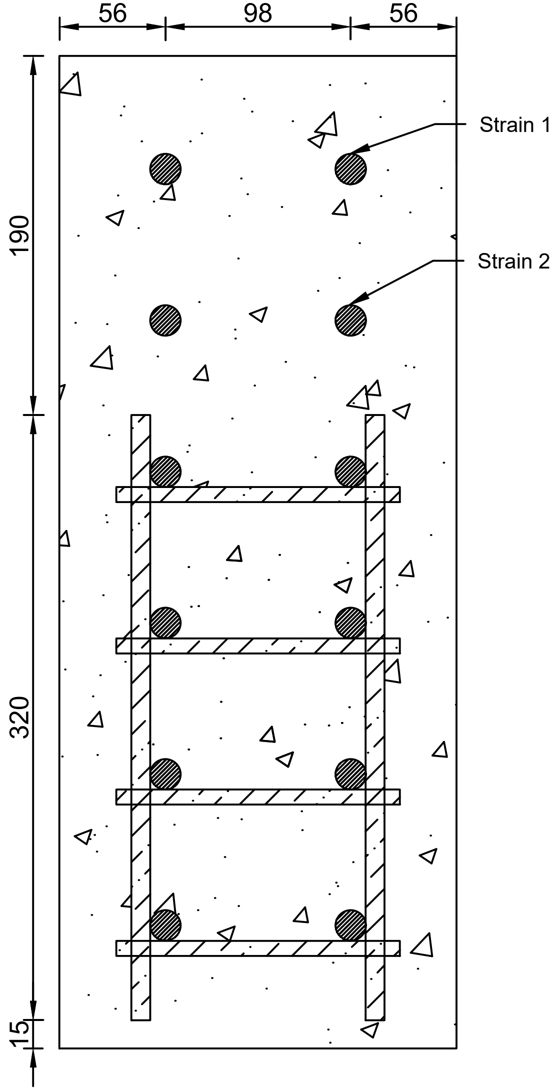

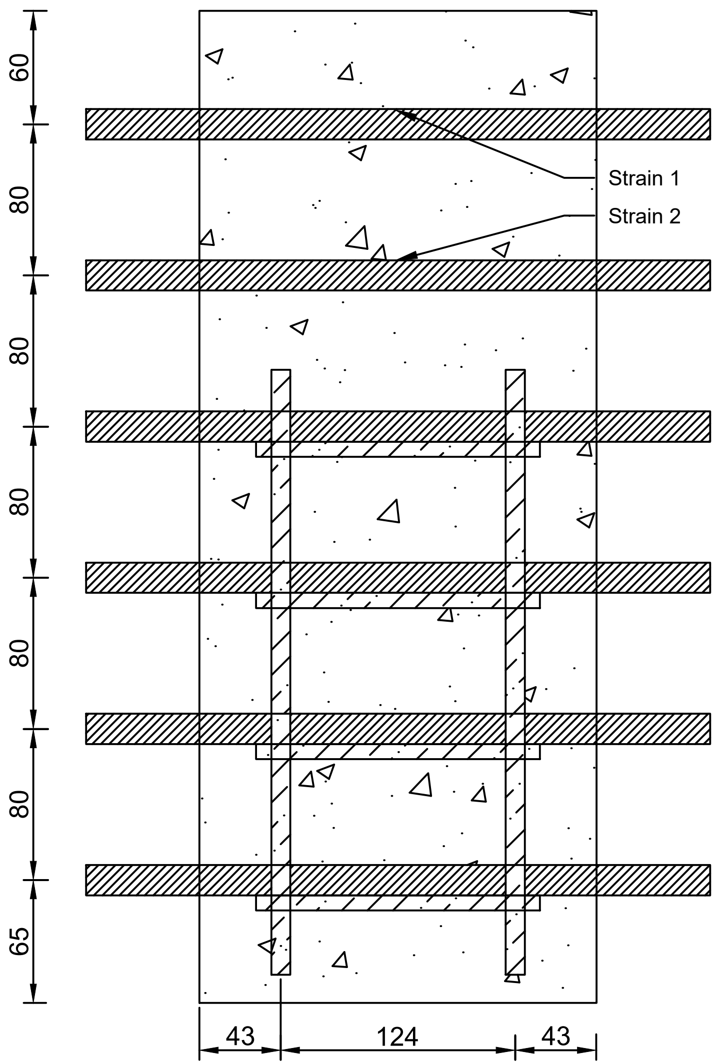

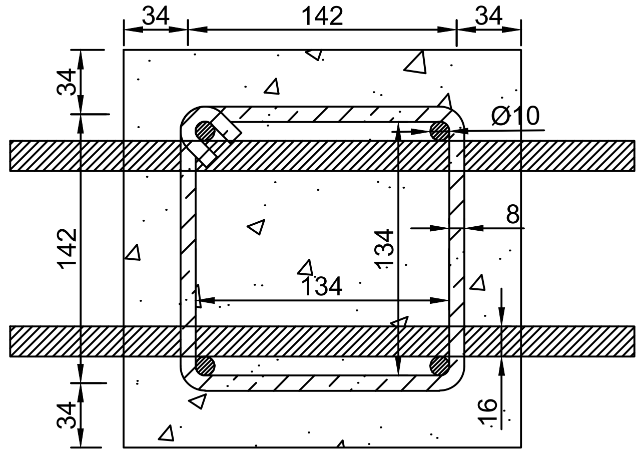

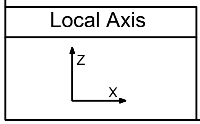

Reinforcement Layout B

Description: Specimen with no reinforcement at top of specimen

- 6 x Ø16mm threaded bars c/c 80mm
- 4 x Ø8mm stirups
- 4 x Ø10mm bars in corner of stirups

M 1:4

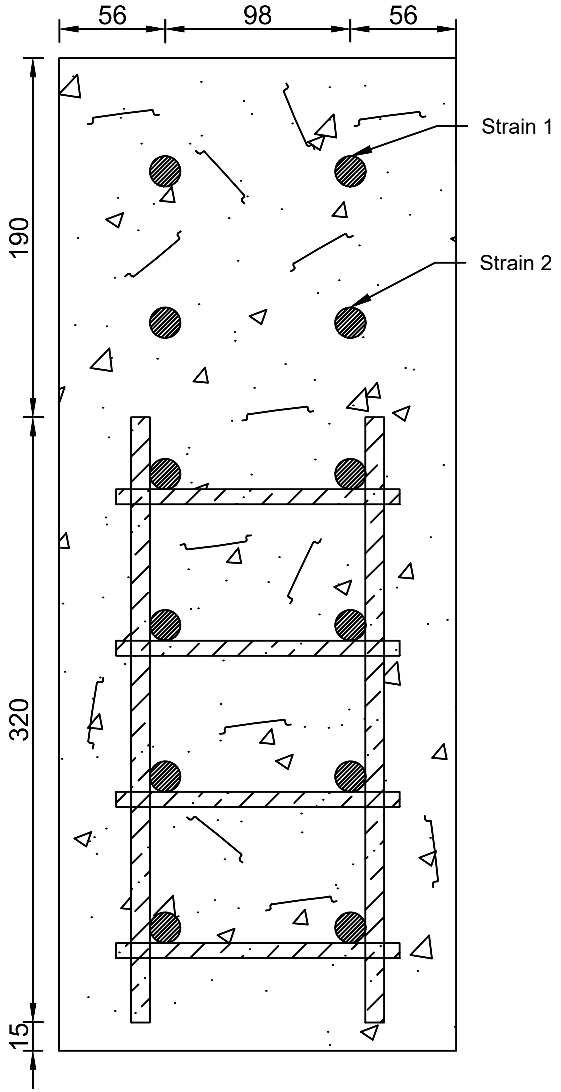

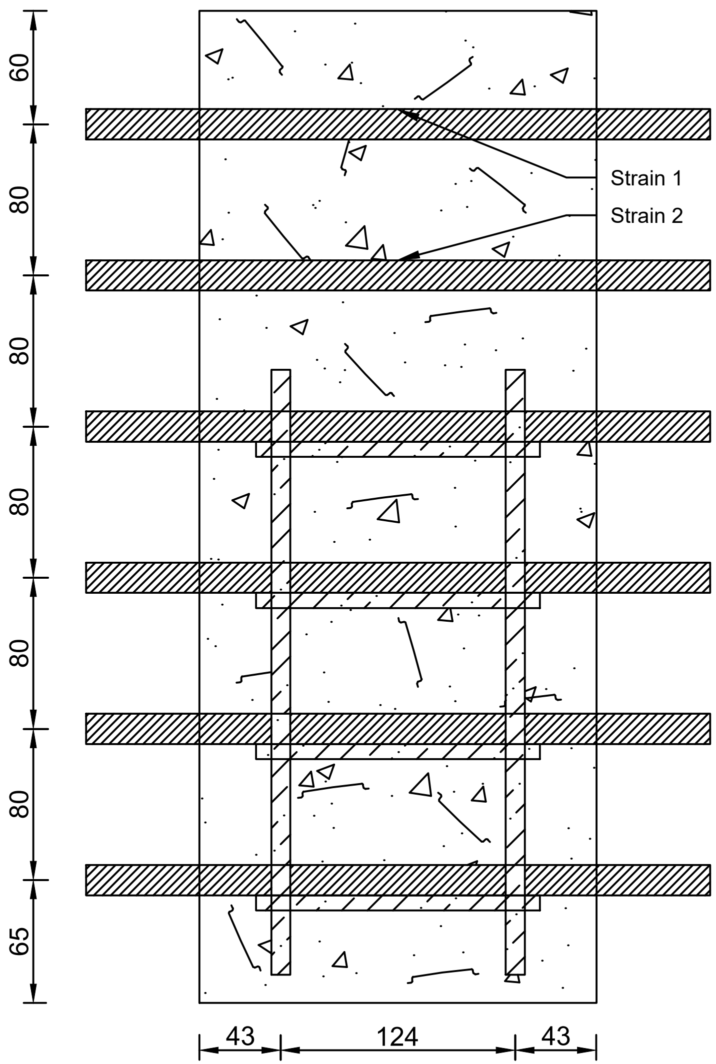

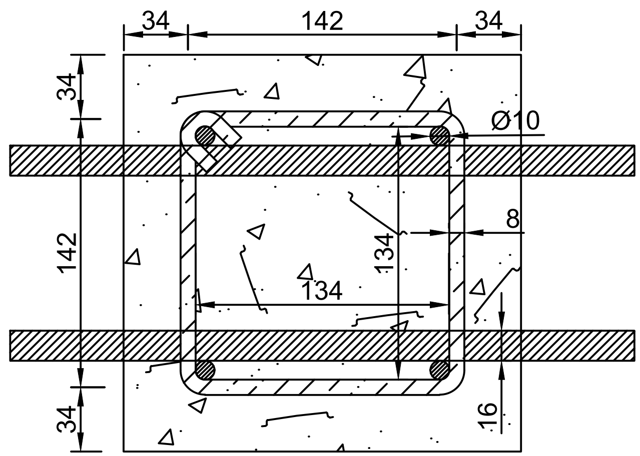

Local Axis

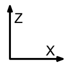

Reinforcement Layout C

Description: Specimen with no reinforcement at top of specimen and fiber reinforced concrete.

- 6 x Ø16mm threaded bars c/c 80mm
- 4 x Ø8mm stirups
- 4 x Ø10mm bars in corner of stirups
- Fiber reinforced concrete 20kg/m^2

M 1:4

Appendix D: Test results

D1: Strength of test cubes

Concrete strenght of normal concrete				
Cube nr.	**Date**	**Days since casting**	**Cube strength [MPa]**	**Cylinder stength [MPa]**
1.1	14.03.2019	28	46,31	37,05
1.2	14.03.2019	28	45,76	36,61
1.3	14.03.2019	28	45,93	36,74
2.1	21.03.2019	35	47,58	38,06
2.2	21.03.2019	35	49,22	39,38
2.3	21.03.2019	35	49,31	39,45
3.1	25.04.2019	39	49,49	39,59
3.2	25.04.2019	39	49,24	39,39
3.3	25.04.2019	39	49,70	39,76
4.1	26.04.2019	40	49,79	39,83
4.2	26.04.2019	40	49,49	39,59
4.3	26.04.2019	40	49,79	39,83
5.1	28.04.2019	42	49,66	39,73
5.2	28.04.2019	42	50,75	40,60
5.3	28.04.2019	42	50,05	40,04
6.1	29.04.2019	43	49,58	39,66
6.2	29.04.2019	43	50,11	40,09
6.3	29.04.2019	43	49,84	39,87

Concrete strenght of fiber reinforced concrete				
Cube nr.	**Date**	**Days since casting**	**Cube strength [MPa]**	**Cylinder stength [MPa]**
1.1	14.03.2019	28	42,61	34,09
1.2	14.03.2019	28	42,68	34,14
1.3	14.03.2019	28	44,20	35,36
2.1	20.03.2019	36	44,20	35,36
2.2	20.03.2019	36	44,72	35,78
2.3	20.03.2019	36	45,86	36,69
3.1	01.04.2019	46	47,14	37,71
3.2	01.04.2019	46	47,59	38,07
3.3	01.04.2019	46	48,22	38,58
4.1	02.04.2019	47	47,98	38,38
4.2	02.04.2019	47	47,28	37,82
4.3	02.04.2019	47	46,75	37,40
5.1	03.04.2019	48	48,05	38,44
5.2	03.04.2019	48	49,37	39,50
5.3	03.04.2019	48	47,91	38,33

D2: Crack propagation in specimen type A: Minimum reinforcement

Static tested specimens

A1

A2

A3

Dynamic tested specimens

A4

A5

A6

D3: Crack propagation in specimen type B: Unreinforced

Static tested specimens

B1

B2

B3

Dynamic tested specimens

B4

B5

B6

D4: Crack propagation in specimen type C: Fiber-reinforced

Static tested specimens

C1

C2

C3

Dynamic tested specimens

C4

C5

C6

Appendix E: Various documentation

E1: Concrete receipt of fiber-reinforced concrete

Receipt	**25300 ~ B25 M90 D16 Std-Fa Cl 0,1**		
Consistency [mm]	220	V/(c+ks)-ratio	0.63
Air content [%]	2.0	Equiv. cement [kg]	297
Cement paste volume [L]	287	Free water [Effective]	187
V/p - ratio	0.49	Matrix volume exl. Air [L]	318
Akalas [kg/m^3]	4.5 d	Clorides [% of cement]	0.07
Amount of react. rocks [%]	76.0	Silika k-value	1.00
Concrete composition	**kg/m^3**	**Reference standard**	**NS206**
Aggregate 8-16 mm	851.75	Durability class	M90
Aggregate 0-8 mm	969.49	Strength class	B25
Aggregate 0-2 mm	51.58	Chloride class	CL 0.10
Norcem Std FA	291.41	Aggregate size D, [mm]	16
Silica	5.95	Exposure class	X0
Water	185.62		
Dynamon SX-23	2.23	***Measured slump [mm]***	***225***
Mapetard R	0.00	***Measured air content [%]***	***1.3***
Projected density	2342.60	***Measured density [kg/m^3]***	***2372,26***

E2: Concrete receipt of concrete without fibers

Receipt	**25300 ~ B25 M90 D16 Std-Fa Cl 0,1**		
Consistency [mm]	200	v/(c+ks)-ratio	0.63
Air content [%]	2.0	Equiv. cement [kg]	292
Cement paste volume [L]	287	Free water [Effective]	184
v/p - ratio	0.49	Matrix volume exl. Air [L]	314
Akalies [kg/m^3]	4.4	Clorides [% of cement]	0.07
Amount of react. rocks (%)	76.1	Silica k-value	1.00
Concrete composition	**kg/m^3**	**Reference standard**	**NS206**
Agregate 8-16 mm	853.39	Durability class	M90
Agregate 0-8 mm	986.18	Strength class	B25
Agregate 0-2 mm	47.24	Cloride class	CL 0.10
Norcem Std FA	286.22	Agregate size D, [mm]	16
Silica	5.84	Exposure class	X0
Water	182.43		
Dynamon SX-23	2.04	***Measured slump [mm]***	***235***
Mapetard R	0.00	***Measured air content [%]***	***1.9***
Projected density	2348.14	***Measured density [kg/m^3]***	***2381,24***

Fatigue capacity of partially loaded areas for fiber reinforced concrete structures submerged in water

Elvestad & Fosse

NTNU
Kunnskap for ei betre verd

DNV·GL